ANTENNA PATTERNS FOR DETECTING SLOWLY MOVING TARGETS IN TWO CHANNEL GMTI PROCESSING

A THESIS SUBMITTED TO
THE GRADUATE SCHOOL OF NATURAL AND APPLIED SCIENCES
OF
MIDDLE EAST TECHNICAL UNIVERSITY

BY

GÖKHAN YILDIRIM

IN PARTIAL FULFILLMENT OF THE REQUIREMENTS
FOR
THE DEGREE OF MASTER OF SCIENCE
IN
ELECTRICAL AND ELECTRONICS ENGINEERING

JUNE 2010

Approval of the thesis:

ANTENNA PATTERNS FOR DETECTING SLOWLY MOVING TARGETS IN TWO CHANNEL GMTI PROCESSING

submitted by **GÖKHAN YILDIRIM** in partial fulfillment of the requirements for the degree of **Master of Science in Electrical and Electronics Engineering Department, Middle East Technical University** by,

Prof. Dr. Canan ÖZGEN _____
Dean, Graduate School of **Natural and Applied Sciences, METU**

Prof. Dr. İsmet ERKMEN _____
Head of Deparment, **Electrical and Electronics Engineering, METU**

Assoc. Prof. Dr. Seyit Sencer KOÇ _____
Supervisor, **Electrical and Electronics Engineering, METU**

Examining Committee Members

Prof. Dr. Yalçın TANIK _____
Electrical and Electronics Engineering, METU

Assoc. Prof. Dr. Seyit Sencer KOÇ _____
Electrical and Electronics Engineering, METU

Prof. Dr. Mete SEVERCAN _____
Electrical and Electronics Engineering, METU

Assist. Prof. Dr. Çağatay CANDAN _____
Electrical and Electronics Engineering, METU

Dr. Ülkü ÇİLEK DOYURAN _____
Design Leader, ASELSAN

Date: 28/06/2010

I hereby declare that all information in this document has been obtained and presented in accordance with academic rules and ethical conduct. I also declare that, as required by these rules and conduct, I have fully cited and referenced all material and results that are not original to this work.

Name, Last Name: **Gökhan YILDIRIM**

Signature:

ABSTRACT

ANTENNA PATTERNS FOR DETECTING SLOWLY MOVING TARGETS IN TWO CHANNEL GMTI PROCESSING

Yıldırım, Gökhan

M.Sc., Department of Electrical and Electronics Engineering

Supervisor: Assoc. Prof. Dr. Seyit Sencer Koç

June 2010, 104 pages

Ground Moving Target Indicator (GMTI) is a well-known and widely used signal processing method in airborne and spaceborne radars. In airborne radar and GMTI literature, many radar designs and signal processing techniques have been developed to increase the detection and estimation performance under heavy interference conditions. The motion of the aircraft on which the radar is mounted, high altitudes and ranges, targets with low radar cross sections and slowly moving targets complicates the problem of localization and observation of moving targets on a huge area of interest. In order to overcome these problems, engineers developed more complex radar hardwares with many receiver channels and signal processing algorithms. Multi-channel receiver provides adaptive digital beam-forming and adaptive Doppler processing capabilities. However, designing a cost efficient and light multi-channel receiver and a signal

processing unit, which can handle a huge amount of received data from multi channels, is a difficult task to accomplish. Therefore, this thesis aims to propose non-adaptive antenna beams to reduce the number of channels to two in GMTI processing. This reduction yields a simplification both in receiver structure and signal processing unit. The measure of excellence of these propositions will be the ability to detect slowly moving targets with nearly optimum performance.

Keywords: GMTI, STAP, Eigen-Beam, Endo-Clutter, Two Channel, Karhunen-Leove Expansion

ÖZ

İKİ KANAL GMTI İŞLEMEDE YAVAŞ HEDEFLERİN TESPİTİ İÇİN ANTEN ÖRÜNTÜLERİ

Yıldırım, Gökhan
Yüksek Lisans., Elektrik-Elektronik Mühendisliği Bölümü
Tez Yöneticisi: Doç. Dr. Seyit Sencer Koç

Haziran 2010, 104 sayfa

Hareketli Yer Hedeflerinin Tespiti (GMTI), oldukça bilinen ve hava ve uzay platformu radarlarında geniş ölçüde kullanılan bir yöntemdir. Hava platformu radar ve GMTI literatüründe, ağır girişim koşullarında tespit ve kestirim performansını arttırmak için birçok radar tasarımı ve sinyal işleme tekniği geliştirilmiştir. Radarın bulunduğu platformun hareketi, yüksek irtifa ve menziller, düşük radar kesit alanlı ve yavaş hareket eden hedefler, hareketli hedeflerin büyük bir ilgi alanında gözlemlenmesini ve konumunun belirlenmesini zorlaştırmaktadır. Mühendisler bu sorunların üstesinden gelmek için çok kanallı almaç içeren karmaşık radar donanımları ve sinyal işleme algoritmaları geliştirmiştir. Çok kanallı almaç, uyarlamalı huzme biçimlendirme ve uyarlamalı Doppler işleme yeteneği sağlamaktadır. Ancak, uygun maliyetli ve hafif bir çok kanallı almaç ile bu almaçlardan gelen yüksek miktardaki veriyi yönetebilecek bir sinyal işleme birimi tasarlamak zorlayıcı bir iştir. Bu nedenle bu tez, uyarlanabilir

olmayan anten huzmeleri önererek GMTI sisteminde kanal sayısını azaltmayı amaçlamaktadır. Bu azaltma almaç yapısında ve sinyal işleme biriminde sadeleşme sağlamaktadır. Önerilen anten huzmelerinin başarımları, yavaş hedefleri optimuma yakın bir performansla tespit etme yetenekleri ile ölçülecektir.

Anathar Kelimeler: GMTI, STAP, Eigen-Huzme, Kargaşa İçi, İki Kanal, Karhunen-Leove Açılımı

To My Family

ACKNOWLEDGEMENTS

I have completed my thesis with the great assistance of various people, who helped me during my research and synthesis periods.

First, I would like to thank my supervisor Assoc. Prof. Dr. Seyit Sencer Koç for his guidance, encouragement and objective views which helped me stay concentrated in every working hour I spent on my thesis.

I would like to express my deepest gratitude to my lovely family for their support and trust they have given to me.

I would like to thank TÜBİTAK for her financial support throughout my thesis.

Finally, I would like to indicate my appreciation to ASELSAN Inc. for her opportunities and supports during the completion of my thesis.

TABLE OF CONTENTS

LIST OF TABLES

TABLES

LIST OF FIGURES

FIGURES

CHAPTER 1

INTRODUCTION

1.1. Radar and GMTI History

Object detection with radar was first used by Christian Hülsmeyer, who illustrated the possibility of detection under non-visible conditions, in 1904. In 1917, Nikola Tesla enhanced the radar principle by stating the feasibility of intentionally transmitting and receiving electromagnetic waves to detect the relative position of a target. Several developments have been made on radar concepts by scientists and engineers up to World War II.

In the World War II, British Army used the ground stationed radars (which are called Chain Home) effectively against the German Air Forces (Luftwaffe) to locate the bomber aircrafts of German Army. However, after locating the bomber aircrafts, the pilots of the anti-bomber aircrafts of British Air Forces had to see the German aircrafts in order to eliminate them. As a precaution, Luftwaffe started to fly at night and in bad weather conditions, in order to avoid the enemy. British Air Forces had to take a counter measure in order to see the enemy aircrafts while flying, during the nights and bad weather conditions.

Airborne radar idea was first proposed by Scottish inventor Robert Wattson-Watt; his idea was realized by miniaturizing the radar systems to the sizes which are suitable for aircrafts, by increasing the operating frequency of the radar and resultantly, ability to decrease the antenna size. These radars

were able to end the German night and bad weather bombing tactics during the war, [1]. These radars were intended to be used in Air-to-Air Detection or Air Moving Target Indication (AMTI).

Ground Moving Target Indication (GMTI) ideas arose because of the Cold War requirements starting from 1970s. Several developments were made in the course of the Cold War up to the contract of Joint STARS (Surveillance Target and Attack Radar System) with Grumman/Norden and Motorola in 1985. The system had to have a GMTI mode and an imaging mode called Synthetic Aperture Radar (SAR) in order to be used against Warsaw Pact's armored follow-on forces, before they arrive to NATO's defenses. After the cold war, GMTI was used during the Post Cold War era, in Gulf War, in Kosovo and Afghanistan, [2].

1.2. Thesis Motivation and Objective

In airborne radar and GMTI literature, many radar designs and signal processing techniques have been developed to increase the detection and estimation performance under heavy interference conditions. The motion of the aircraft on which the radar is mounted, high altitudes and ranges, targets with low radar cross sections and slowly moving targets complicates the problem of localization and observation of moving targets on a huge are of interest. In order to overcome these problems, engineers developed more complex radar hardwares with many receiver channels and signal processing algorithms. Multi-channel receiver provides adaptive digital beam-forming and adaptive Doppler processing capabilities. However, designing a cost efficient and light multi-channel receiver and a signal processing unit, which can handle a huge amount of received data from multi-channels, are difficult tasks to accomplish.

Therefore, the main motivation of work in this thesis is to propose good non-adaptive antenna beams to reduce the number of channels to two in

GMTI processing. This reduction yields a simplification both in receiver structure and signal processing unit. The measure of excellence of the propositions will be the ability to detect slowly moving targets with nearly optimum performance. In order to support the proposition, there are certain objectives that will be mentioned throughout the thesis:

- Explaining the main principle of airborne radar
- Investigating the optimum multi-channel GMTI signal processing technique
- Deriving and investigating the sub-optimum signal processing techniques with reduced number of channels and/or pulses
- Determining the advantages and disadvantages of sub-optimum techniques
- Proposing some good reduced channel (sub-optimum) solutions and supporting these solutions with logical bases

1.3. Thesis Outline

Chapter 1 mentioned the history of radar and GMTI concepts and outlines the work done throughout the thesis. Chapter 2 will familiarize with the basic principles of airborne radar, GMTI and Space-Time Adaptive Processing (STAP) and introduce the data collection and signal models. Chapter 3 will investigate the performance of optimum and sub-optimum (reduced rank) STAP approaches, their advantages and disadvantages and cover the subspace and subspace processing concepts. Chapter 4 will state the main problem that the thesis aims to overcome, indicate the assumptions and constraints, propose good solutions and investigate their performances.

CHAPTER 2

RADAR, GMTI AND SPACE TIME ADAPTIVE PROCESSING CONCEPTS

2.1. Radar Background

The term RADAR is an acronym for “Radio Detection and Ranging”. The main purpose of radar is to detect existence of a target by transmitting electromagnetic waves and receiving the reflections of these waves from the targets. In addition to the existence of a target, manipulation of the transmitted and received waves will basically give the following information:

- Range (how far away the target is from the radar) of the target by measuring the time difference between transmitted and received waves
- Velocity (radial or along the range vector) of the target by measuring the frequency difference between transmitted and received waves (which will also be referred as Doppler phenomenon or Doppler shift)

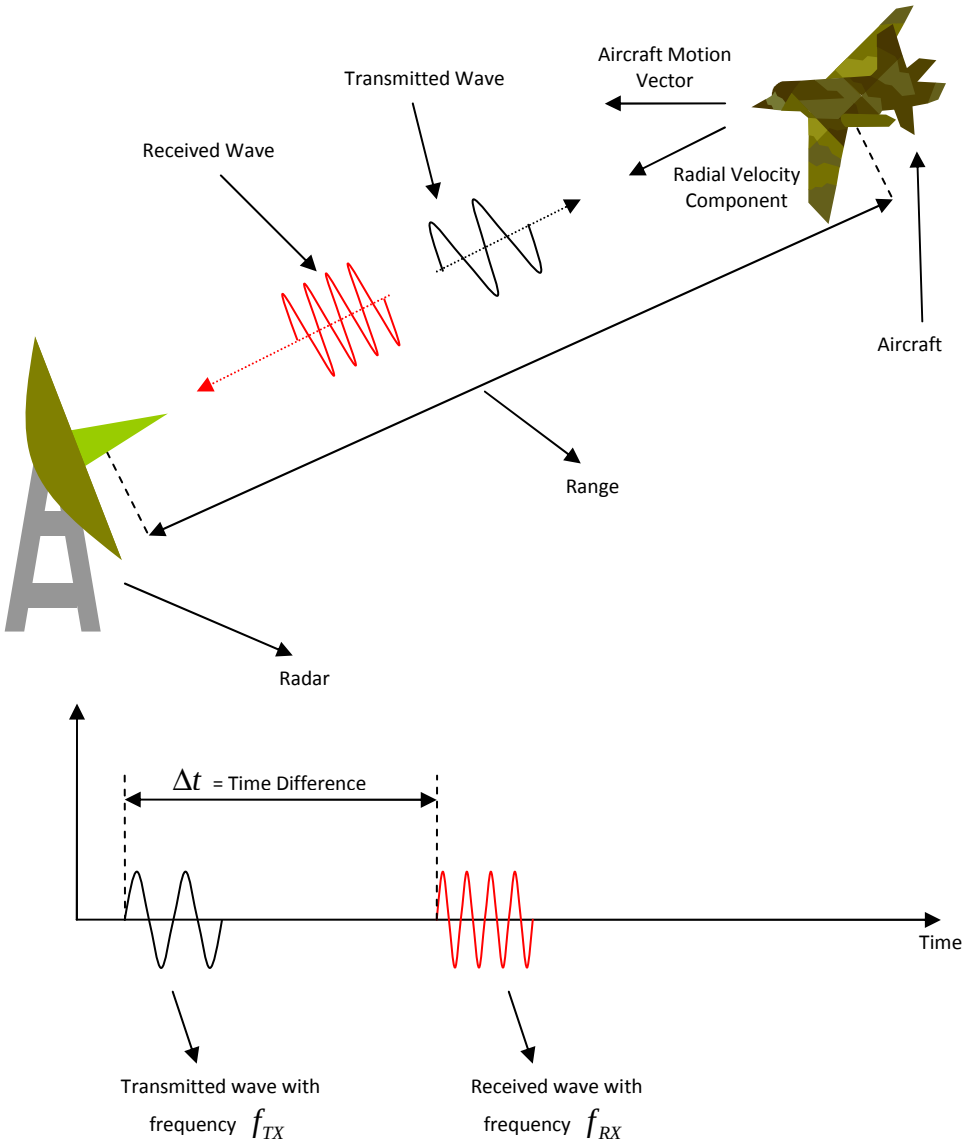

Figure 2-1 Radar detection

Since electromagnetic waves travels with the speed of light ($c = 2.998x10^8 m/s$) and as it can be seen from Figure 2-1 that the electromagnetic wave travels two times the distance between radar and the target, the range of the target can be found using (2-1):

$$R = \frac{c\Delta t}{2}. \tag{2-1}$$

The radial velocity of the target is related to the Doppler shift between the transmitted and received waves. The amount of the Doppler shift is measured by using (2-2):

$$f_D = f_{TX} - f_{RX} \,. \tag{2-2}$$

Here f_D is represents the Doppler shift. The shift depends on how fast the range between the radar and the aircraft changes within the cycles of the electromagnetic wave. The distance traveled by the electromagnetic wave can be represented as a function of time as in the (2-3):

$$d(t) = 2R - \frac{2V_R t}{c} \,. \tag{2-3}$$

Here V_R is the radial velocity component of the moving target. This range corresponds to a time varying phase change, which is represented in (2-4):

$$\phi(t) = 2\pi f_{TX}\left(2R - \frac{2V_R t}{c}\right). \tag{2-4}$$

Since the frequency is the derivative of phase, then:

$$f_D = \frac{1}{2\pi}\frac{d\phi}{dt} = -f_{TX}\frac{2V_R}{c} = -\frac{2V_R}{\lambda} \,. \tag{2-5}$$

Here, λ represents the wavelength of the transmitted electromagnetic wave. Resultantly we have:

$$f_D = f_{TX} - f_{RX} = -\frac{2V_R}{\lambda} \,, \tag{2-6}$$

$$V_R = \frac{\lambda(f_{RX} - f_{TX})}{2} \,. \tag{2-7}$$

Eqn. (2-6) shows that the measurable Doppler shift is a result of radial velocity of the target and a function of operational wavelength (or frequency). It is obvious that, if the radar is mounted on a moving platform,

the effective or the relative radial motion between the radar and the moving target determines the Doppler shift.

2.2. GMTI Background

Ground Moving Target Indicator (GMTI) is the general name for an ability of radar systems or algorithms which can detect moving targets on the ground. The main challenge of GMTI is to detect the targets which are buried under heavy ground reflection signals, which, from now on will be referred to as clutter. Classical airborne radar systems with GMTI have the basic structure of a side looking airborne radar (SLAR) as illustrated in Figure 2-2:

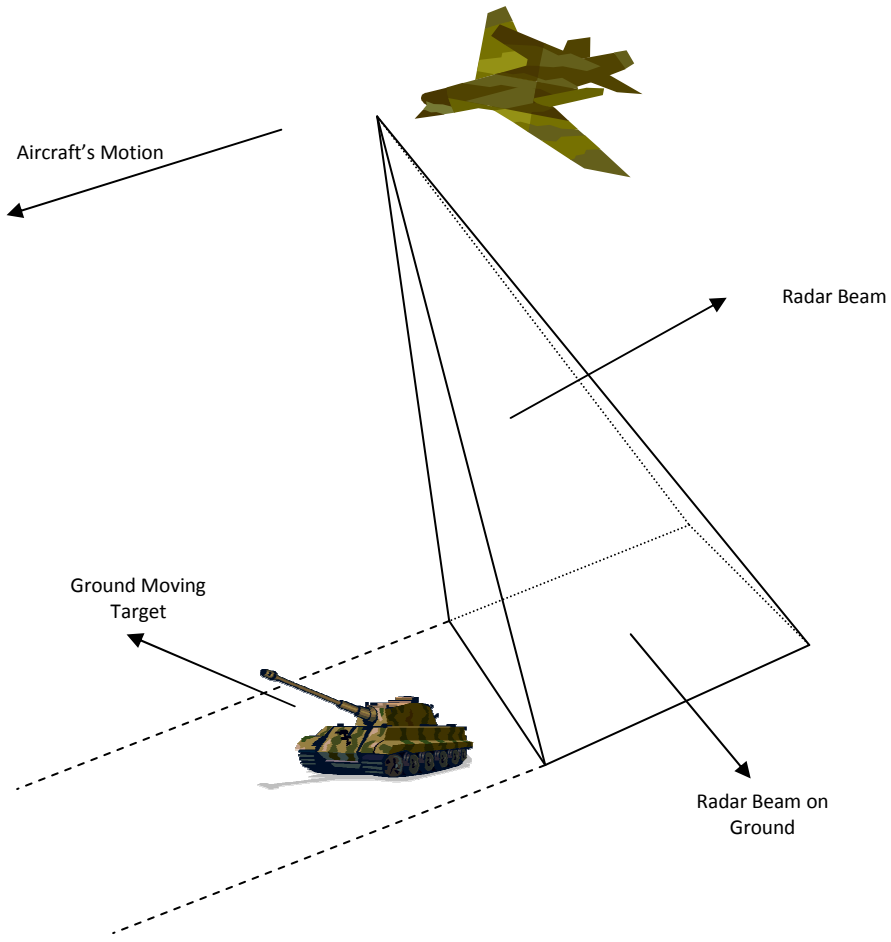

Figure 2-2 GMTI operation

In GMTI operation, a side looking radar antenna sweeps the surface by illuminating it with electromagnetic pulses with pre-defined waveform properties. Detection can be done if the target is illuminated for a certain amount of time (observation time) or by a certain number of pulses. Several signal processing techniques have been used to reveal ground moving targets.

2.3. GMTI Techniques

Throughout the course of GMTI history, different techniques were used to reveal the moving ground targets. The well-known and widely used techniques are mentioned in the following subsections.

2.3.1. Displaced Phase Center Antenna (DPCA) Technique

DPCA is the most basic GMTI technique, which was widely used in early GMTI systems, [3]. Its fundamental principle is to eliminate the unwanted reflections and to reveal the moving targets on ground by looking at the same area from the same point in space, but at a different time.

The data collection geometry can be seen in Figure 2-3:

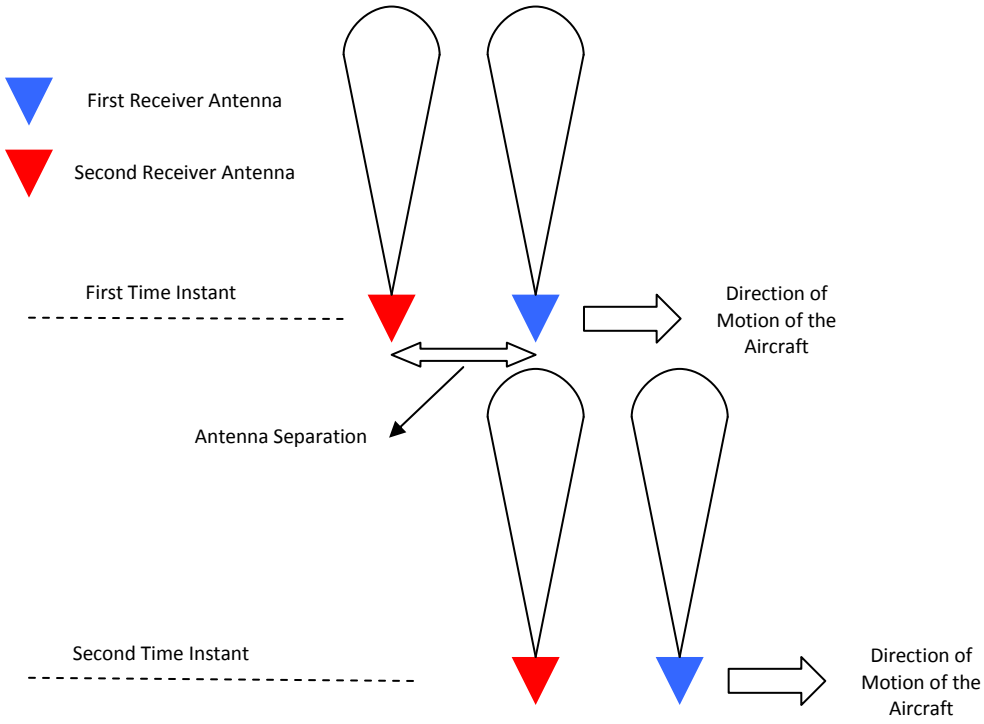

Figure 2-3 DPCA data collection geometry

In principle, radar transmits and receives one pulse in the first time instant (first pulse). In the second time instant (second pulse), the aircraft moves forward, exactly the amount of separation between the two receiver antennae and again the radar transmits and receives (Figure 2-3). The received signal of the first receiver in the first pulse and the received signal of the second receiver in the second pulse are taken from the same surface on the ground. Theoretically, it can be said that the returns from non-moving ground objects (also called clutter) are same. However, returns from moving ground objects will differ because of the motion of the ground target. DPCA technique uses the fact that the moving target can be revealed by subtracting these two pulses.

The performance of DPCA is very good if the aircraft's velocity is adjusted precisely to match the antenna separation distance on each pulse. However, due to the practical factors like air turbulence, inaccurate velocity measurement devices, unstable pulse repetitions and channel mismatches, DPCA technique's performance degrades and can be enhanced by using adaptive processing for better clutter suppression, [4].

2.3.2. Adaptive Displaced Phase Center Antenna (ADPCA) Technique

ADPCA technique was developed in order to cope with the practical problems like unwanted aircraft motion, erroneous velocity measurements, inconsistent pulse repetitions and non-ideal receiver channels. The term "adaptive" implies that the received data are used to estimate and correct the errors, which are caused by practical problems mentioned above. The ADPCA data collection geometry is illustrated in Figure 2-4:

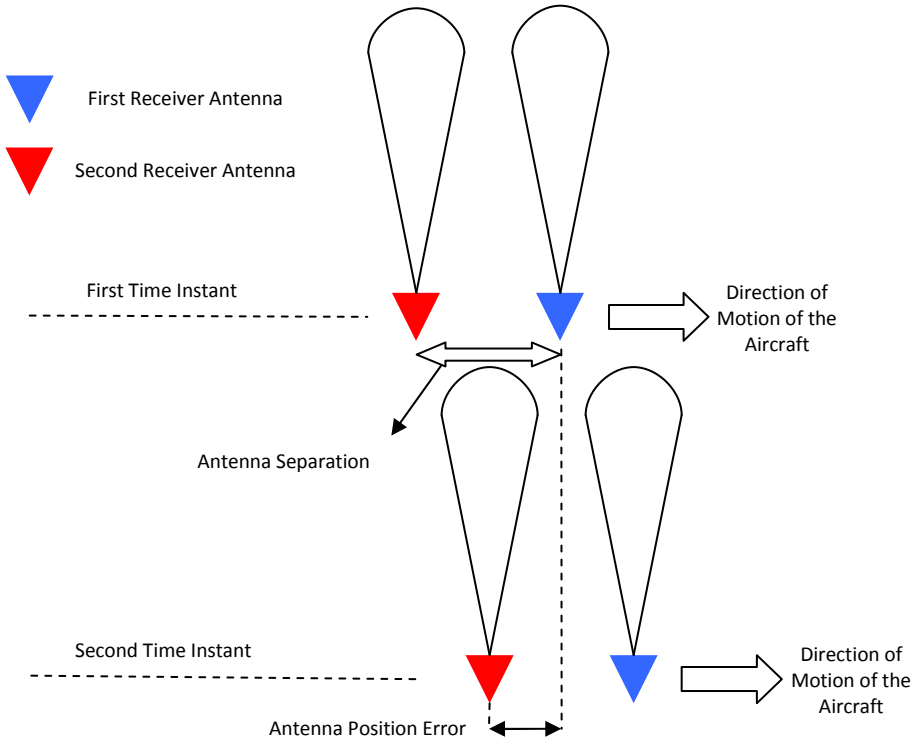

Figure 2-4 ADPCA data collection geometry

There are two different ADPCA techniques in the literature to perform detection operation. The first technique is mentioned in [4] and the main steps in this ADPCA technique are as follows:

- Estimate the antenna position error using the received data
- Calculate the phase shift caused by this error
- Correct the received data with the calculated phase shift
- Conduct the subtraction operation as in the DPCA case.
- Detect the moving targets

The second technique is introduced in [5] and it is using a detector similar to the one which will be derived in section 3.1. Throughout the thesis, the second ADPCA technique will be considered.

The performance of ADPCA technique is better as far as the practical problems are concerned, [5]. However, DPCA and ADPCA techniques are able to detect relatively fast moving targets because of the clutter spread due to the aircraft motion, [5].

2.4. Endo-Clutter and Exo-Clutter Targets

Ideally, if the radar is stationary and transmits electromagnetic pulses to the surface with the same angle, the signals reflected from the clutter will not have a Doppler spread. However, in practice, the following items can cause clutter spread:

- The motion of the platform, on which the radar is mounted
- The motion introduced by wind to ground objects and sea surface (Internal Clutter Motion)
- The change in aspect angle of the clutter patch

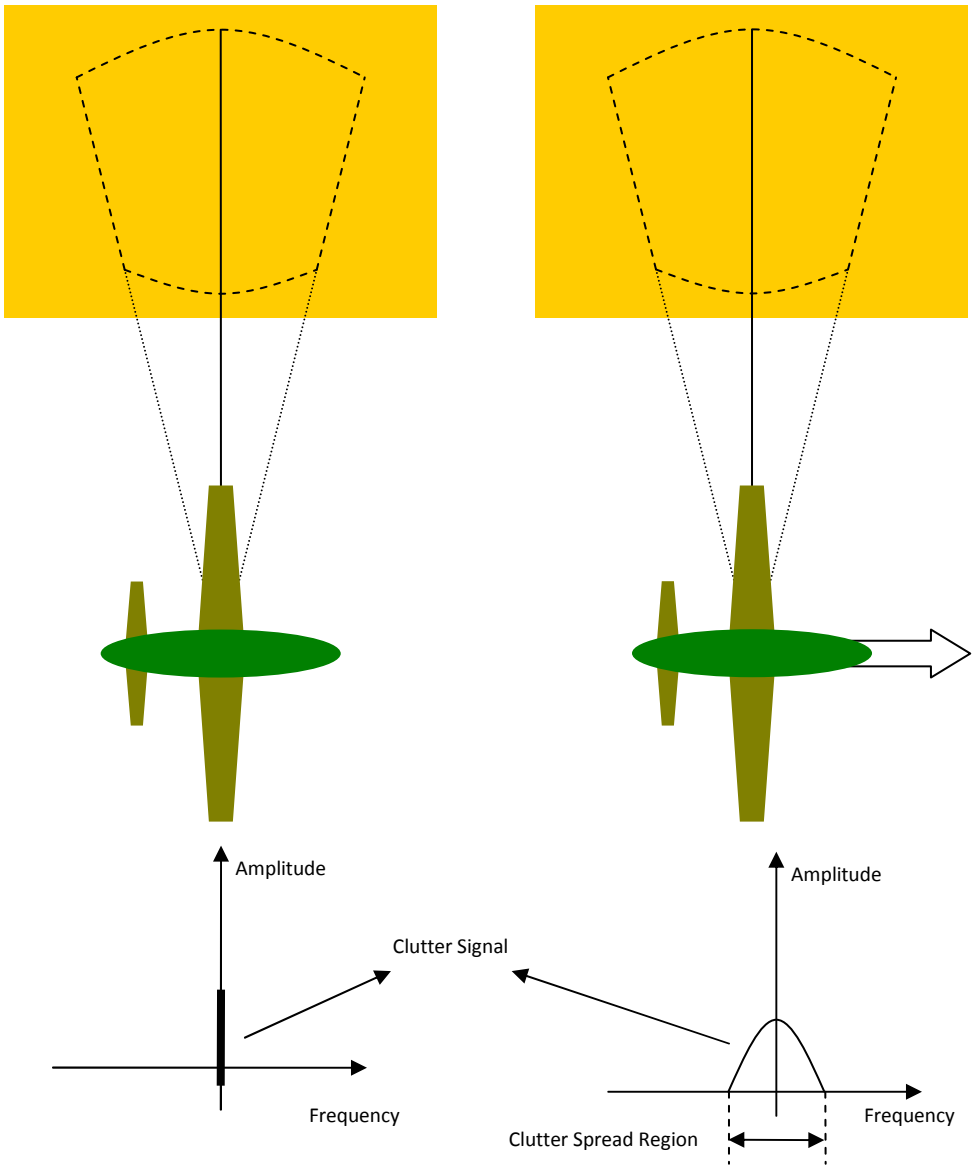

Figure 2-5 Clutter frequency spectrum in non-moving and moving aircraft cases

The DPCA and ADPCA techniques are successful to detect the targets outside or at the edge of the clutter spread region (Figure 2-5). These types of targets are called “Exo-clutter Targets”. Exo-clutter targets have higher Doppler shifts which means they move relatively fast.

Main challenging problem is to detect the targets inside the clutter spread region, which are called “Endo-clutter Targets” as shown in Figure

2-6. The detection of these targets is difficult since they are buried under a high clutter power because of their low Doppler shifts.

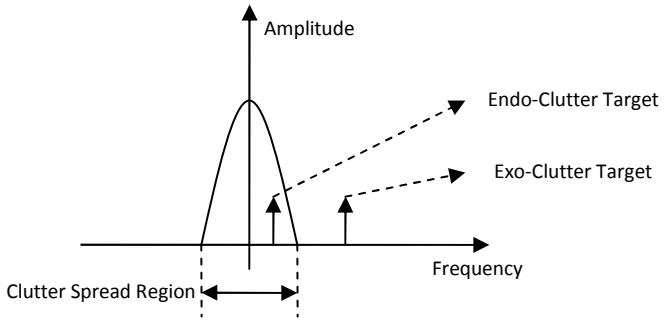

Figure 2-6 Endo-Clutter and Exo-Clutter targets

The DPCA and ADPCA techniques can also detect the endo-clutter targets; however, a more general approach to the solution of detection problem may enhance the endo-clutter detection performance significantly. This approach leads us to the Space-Time Adaptive Processing (STAP), which is the general solution of detection problem and it gives optimum detection performance.

2.5. Motivations to STAP and STAP Data Collection Geometry

In GMTI data collection, the received signals are taken from different antennae (spatial domain) at different times (temporal domain). Widely used GMTI techniques like DPCA and ADPCA is not optimum in detecting the slowly moving targets or in other words endo-clutter targets, because they are using the correlation between space and time. However, since all the signals received from all channels in different times are not independent generally, an optimum signal processing scheme has to be 2-D adaptive processing, [6].

Space-Time Adaptive Processing (STAP) gives the opportunity to take advantage of the correlation between space and time domains in an adaptive manner; thus, it will provide the optimum performance in

detection of endo-clutter targets. Exo-clutter targets can be detected with a nearly optimum performance with non-adaptive and 1-D processing methods, since exo-clutter performance only depends on noise component, which is an independent variable in space and time domains. The STAP technique is the optimum processing technique, which offers a 2D adaptive signal processing both in space (beam-forming) and time (Doppler processing).

Full STAP data collection geometry is illustrated in Figure 2-7:

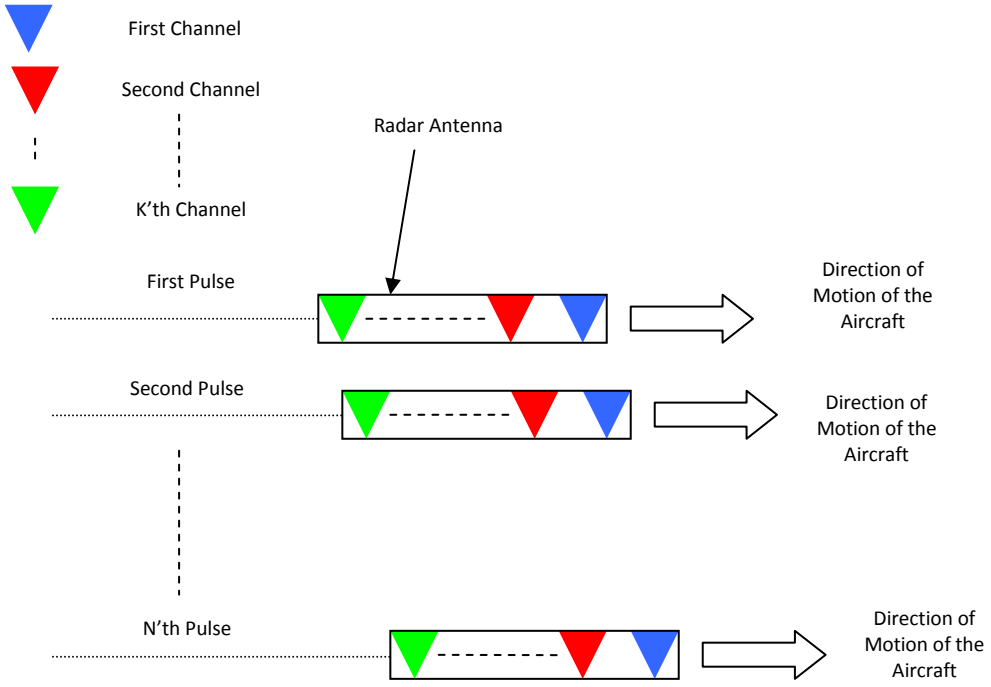

Figure 2-7 STAP data collection geometry

In STAP, a number of channels (K many) and a number of pulses (N many) can be used to operate. The number of channels and pulses provide KN many degrees of freedoms (DoFs) which can be used to suppress the clutter and detect endo-clutter targets.

2.6. Signal and Statistics Models in STAP

There are mainly four types of signals in STAP terminology. These are target, clutter, interference and thermal noise signals. The interfering signals are not in the scope of this thesis and will not be investigated. The remaining signals and their statistical models are explained in the subsections 2.6.1, 2.6.2 and 2.6.3.

2.6.1. Target Signal Model

Target signal can be expressed as the signals reflected from the moving targets back to the radar channels. The target signal has two main components; space and time. The received signal in time depends on the velocities of target and aircraft, and the azimuth angle of the target.

Target signal parameters are shown in Figure 2-8:

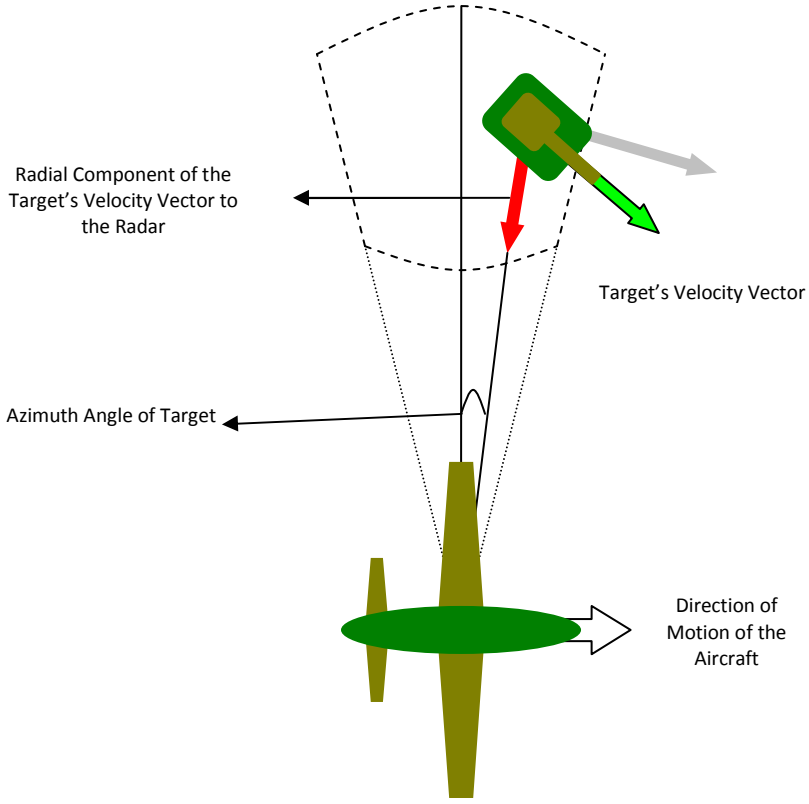

Figure 2-8 Target signal parameters

Let the target's radial velocity component be V_R, aircraft velocity be V_A, azimuth angle of the target be θ_T and the wavelength of the transmitted pulse be λ. The Doppler shift of the target can be found from (2-8):

$$f_D = \frac{2V_R}{\lambda} + \frac{2V_A \sin(\theta_T)}{\lambda}. \tag{2-8}$$

Let the pulse repetition interval (PRI) of the radar be T_p. Then in every T_p, the phase of the received signal from one channel differs by $f_D T_p$. The received signal from the target for one received channel and N pulses can be written as in (2-9):

$$\mathbf{p_t} = \begin{bmatrix} \exp(-j2\pi f_D T_p(0)) \\ \exp(-j2\pi f_D T_p(1)) \\ \vdots \\ \exp(-j2\pi f_D T_p(N-1)) \end{bmatrix}. \tag{2-9}$$

$\mathbf{p_t}$ denotes the received target signal vector in time domain. Target signal in space domain depends on the azimuth angle of the target and channel separation as illustrated in Figure 2-9:

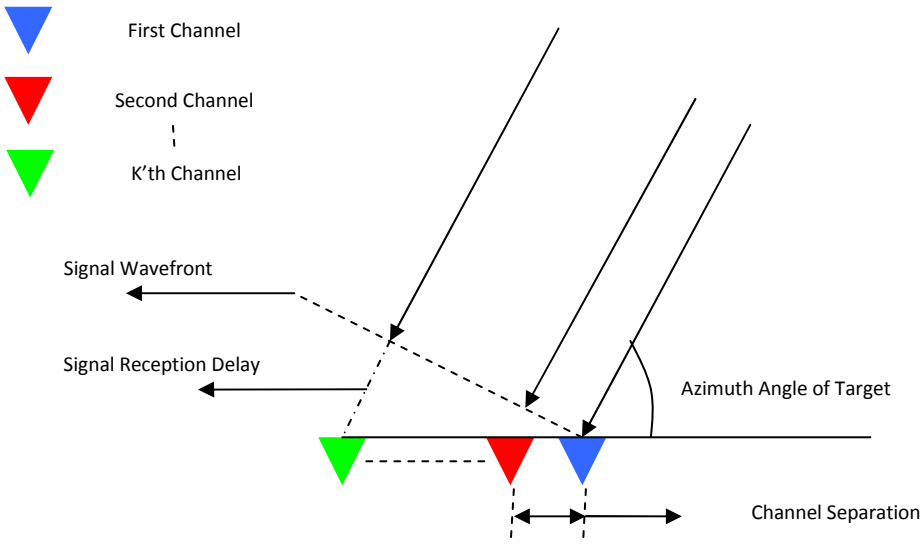

Figure 2-9 Target signal reception in space domain

The phase of the signal which is received from a channel depends on its signal reception delay. The delay for Kth channel can be written as in (2-10):

$$D_K = (K-1)d\sin(\theta_T). \tag{2-10}$$

Here d is the channel separation. This separation in space causes the change in phase represented in (2-11):

$$\phi_K = \frac{(K-1)d\sin(\theta_T)}{\lambda}. \tag{2-11}$$

In the analysis, it is assumed that all the channels have unity antenna gain and isotropic antenna patterns.

Consequently, the target signal vector in space can be written as in (2-12):

$$\mathbf{p_s} = \begin{bmatrix} \exp\left(j2\pi\frac{(0)d\sin(\theta_T)}{\lambda}\right) \\ \exp\left(j2\pi\frac{(1)d\sin(\theta_T)}{\lambda}\right) \\ \vdots \\ \exp\left(j2\pi\frac{(K-1)d\sin(\theta_T)}{\lambda}\right) \end{bmatrix}. \tag{2-12}$$

The space-time signal received from the target is the Kronecker product of space and time signals defined in (2-14):

$$\mathbf{p} = \mathbf{p_t} \otimes \mathbf{p_s}, \tag{2-13}$$

$$\mathbf{p} = \begin{bmatrix} \mathbf{p_1} \\ \mathbf{p_2} \\ \vdots \\ \mathbf{p_N} \end{bmatrix}. \tag{2-14}$$

Here $\otimes$ means the Kronecker product operation. Every $\mathbf{p_i}$ represents the Kx1 channel response of i'th pulse and $\mathbf{p}$ is a KNx1 vector. The total space-time response $\mathbf{p}$ is multiplied by a random complex coefficient

which includes the reflected power of the target because of its reflectivity, orientation with respect to radar, range and other system parameters. The complex coefficient can be modeled as in (2-15):

$$\alpha = \alpha_I + j\alpha_Q \,, \tag{2-15}$$

where α_I and α_Q are assumed to be independent identically distributed random variables with zero mean Gaussian distribution with a variance of $\frac{\sigma_t^2}{2}$, where σ_t^2 is assumed to be known. This model is referred to as Gaussian Fluctuating Signal Swerling-1 target model, in which the coefficient is constant in one space-time response (coherent processing interval) but will differ in another space-time response.

2.6.2. Clutter Signal Model

Clutter signal includes the reflected electromagnetic waves from all ground obstacles (but not the electromagnetic wave sources like jammers).

Consider an infinitesimal ground clutter patch as shown in Figure 2-10:

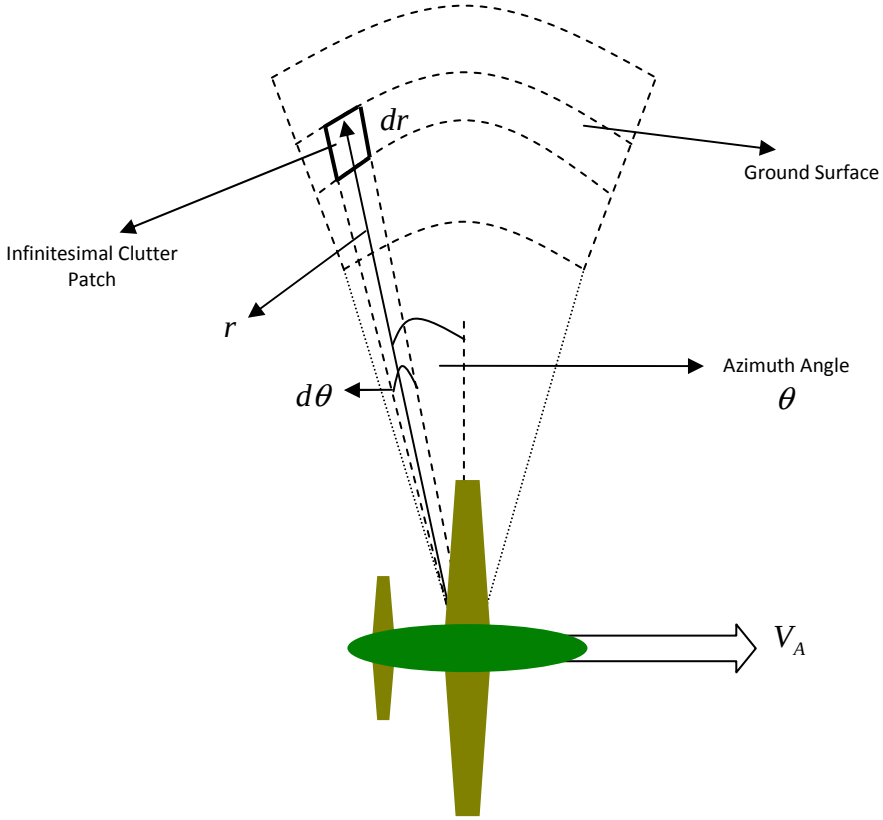

Figure 2-10 Clutter signal collection

Received signal from the ground clutter patch depends on the following parameters:

- Angular distribution of clutter on that particular azimuth angle → $c(\theta)$ (random)
- Transmit antenna voltage pattern gain on that particular azimuth angle → $G_T(\theta)$ (known, deterministic)
- Pulse repetition interval → T_p (known, deterministic)
- Doppler shift for stationary ground clutter patch which can be calculated from (2-16) (known, deterministic):

$$f_D = \frac{2V_A \sin(\theta)}{\lambda}. \tag{2-16}$$

- Phase shift due to the azimuth angle of the ground clutter patch which is determined from (2-17) (known, deterministic):

$$\phi_i = \frac{id \sin(\theta)}{\lambda}. \tag{2-17}$$

Total response received from i'th channel and in n'th pulse can be written as in (2-18):

$$c_{ni}(\theta) = c(\theta) G_T(\theta) \exp(-j2\pi f_D T_p n) \exp(j2\pi\phi_i), \tag{2-18}$$

Covariance of any channel at any time instant can be found with an expectation operation which is given in (2-19):

$$\mathbf{R}_\mathbf{c}(i+nK, m+kK) = E\{c_{ni}(\theta) c_{km}^*(\theta)\}. \tag{2-19}$$

Consequently, covariance matrix can be written as in (2-20) (full derivation can be found in APPENDIX A), derivation is based on the works in [14]):

$$\mathbf{R}_\mathbf{c} = \sigma_c^2 \int |G_T(\theta)|^2 \exp\left(-j2\pi \frac{2\Delta x(n-k) - (i-m)d}{\lambda} \sin(\theta)\right) d\theta. \tag{2-20}$$

The clutter covariance matrix $\mathbf{R}_\mathbf{c}$ is a KNxKN Hermitian matrix. Here in equation (2-20) a uniform clutter is assumed. By using the clutter covariance matrix, we can generate clutter realizations as follows, [7]:

$$\mathbf{R}_\mathbf{c} = E\{\mathbf{c}\mathbf{c}^\mathbf{H}\}, \tag{2-21}$$

$$\mathbf{R}_\mathbf{c} = \mathbf{D}\mathbf{D}^\mathbf{H}, \tag{2-22}$$

$$\mathbf{c} = \mathbf{D}\mathbf{n}, \tag{2-23}$$

$$E\{\mathbf{c}\mathbf{c}^\mathbf{H}\} = E\{\mathbf{D}\mathbf{n}\mathbf{n}^\mathbf{H}\mathbf{D}^H\} = \mathbf{D}E\{\mathbf{n}\mathbf{n}^\mathbf{H}\}\mathbf{D}^\mathbf{H} = \mathbf{D}\mathbf{D}^\mathbf{H} = \mathbf{R}_\mathbf{c}. \tag{2-24}$$

The matrix $\mathbf{D}$ can be obtained by Karhunen-Leove Expansion as illustrated in (2-26):

$$\mathbf{R_c} = \sum_{i=1}^{KN} \lambda_i^c \mathbf{e_i} \mathbf{e_i^H}, \tag{2-25}$$

$$\mathbf{D} = \sum_{i=1}^{KN} \sqrt{\lambda_i^c}\, \mathbf{e_i} \mathbf{e_i^H}. \tag{2-26}$$

The clutter realization will have the form in (2-27):

$$\mathbf{c} = \begin{bmatrix} \mathbf{c_1} \\ \mathbf{c_2} \\ \vdots \\ \mathbf{c_N} \end{bmatrix}. \tag{2-27}$$

Every $\mathbf{c_i}$ represents the Kx1 channel response of i'th pulse and $\mathbf{c}$ is a KNx1 vector. The vector $\mathbf{c}$ is the clutter realization vector and $\mathbf{n}$ represents an independent complex Gaussian distributed realization with an identity covariance matrix. Thus, the clutter is assumed to be Gaussian clutter with covariance matrix $\mathbf{R_c}$.

2.6.3. Noise Signal Model

The noise is assumed to be independent and identically distributed complex Gaussian random vector; thus, noise signal can be written as:

$$\mathbf{n} = \mathbf{n_I} + j\mathbf{n_Q}, \tag{2-28}$$

$$E\{\mathbf{n}\mathbf{n^H}\} = \sigma_n^2 \mathbf{I_{KNxKN}}. \tag{2-29}$$

where $\mathbf{I_{KNxKN}}$ is an identity matrix of size KNxKN.

2.6.4. Received Signal and Hypotheses

The total received signal in different hypotheses can be represented as in (2-30) and (2-31):

$$\mathbf{r} = \mathbf{c} + \mathbf{n} + \alpha\mathbf{p} \quad : H_1 , \tag{2-30}$$

$$\mathbf{r} = \mathbf{c} + \mathbf{n} \quad : H_0 . \tag{2-31}$$

H_1 represents the hypothesis in which the target exists. Otherwise H_0 is used. The total covariance matrices of given hypothesis are given by (2-32) and (2-33):

$$\mathbf{R_1} = E\{\mathbf{r}\mathbf{r}^{\mathbf{H}}\} = \mathbf{R_c} + \sigma_n^2\mathbf{I} + \sigma_t^2\mathbf{p}\mathbf{p}^{\mathbf{H}} = \mathbf{R} + \sigma_t^2\mathbf{p}\mathbf{p}^{\mathbf{H}} \quad : H_1 , \tag{2-32}$$

$$\mathbf{R}_0 = E\{\mathbf{r}\mathbf{r}^{\mathbf{H}}\} = \mathbf{R_c} + \sigma_n^2\mathbf{I} = \mathbf{R} \quad : H_0 . \tag{2-33}$$

Note that covariance matrices of different hypotheses are different.

CHAPTER 3

FULL RANK STAP, REDUCED RANK STAP AND SUBSPACE CONCEPTS

Full rank STAP is the optimum signal processing scheme in which the data from all the channels and pulses are used simultaneously in a 2-D adaptive signal processing operation. Reduced rank STAP, however, applies a reduction operation on the received data before conducting adaptive processing, in order to simplify the STAP operation at the cost of reduced detection performance. There are several rank reduction techniques (channel wise, pulse wise or both) which can be applied depending on the trade-off between complexity and performance of radar. In the following subsections, full rank and reduced rank STAP techniques will be analyzed. Subsequently, subspace concept will be introduced to have an understanding of subspace processing idea.

3.1. Full Rank STAP Detection and Performance

Full rank STAP detection can be thought as binary hypotheses testing problem with the following hypotheses in (3-1) and (3-2):

$$\mathbf{r} = \mathbf{c} + \mathbf{n} + \alpha\mathbf{p} \quad : H_1 , \tag{3-1}$$

$$\mathbf{r} = \mathbf{c} + \mathbf{n} \quad : H_0 . \tag{3-2}$$

Here the received signal is of the form represented in (3-3):

$$\mathbf{r} = \begin{bmatrix} \mathbf{r_1} \\ \mathbf{r_2} \\ \vdots \\ \mathbf{r_N} \end{bmatrix}. \tag{3-3}$$

Every $\mathbf{r_i}$ represents the Kx1 channel response of i'th pulse and $\mathbf{r}$ is a KNx1 vector.

In the sections 2.6.2 and 2.6.3, it was stated that the clutter and noise signals are assumed to be independent and complex Gaussian distributed random vectors with different covariance matrices. Thus the probability distribution of received signal $\mathbf{r}$ can be written as a joint Gaussian distribution. The optimum detector is given in (3-4) (Full derivation can be found in APPENDIX B):

$$\left|\mathbf{p^H R^{-1} r}\right|^2 \gtrless \xi''' \tag{3-4}$$

$$\mathbf{w^H} = \mathbf{p^H R^{-1}} \tag{3-5}$$

$$\left|\mathbf{w^H r}\right|^2 \gtrless \xi''' \tag{3-6}$$

Here $\mathbf{w}$ is the optimum weight vector and $\mathbf{R} = \mathbf{R_c} + \sigma_n^2\mathbf{I}$ is the clutter-plus-noise covariance matrix. This weight applies on target, clutter and the noise terms. If we write the target signal to clutter-plus-noise ratio (SCNR), we get (3-7) (Full derivation can be found in APPENDIX C):

$$SCNR = \frac{\sigma_t^2\left|\mathbf{w^H p}\right|^2}{\mathbf{w^H R w}}. \tag{3-7}$$

We can manipulate (3-7) in order to find a bound to SCNR using Schwarz inequality (Full derivation can be found in APPENDIX C):

$$SCNR \leq \sigma_t^2 \mathbf{p}^{\mathbf{H}} \mathbf{R}^{-1} \mathbf{p} \,. \tag{3-8}$$

In order to check the consistency, assume that there is no clutter and the target is buried under the noise. Then the signal-to-noise ratio (SNR) bound is determined by (3-9):

$$SNR \leq \sigma_t^2 \mathbf{p}^{\mathbf{H}} \left(\sigma_n^2 \mathbf{I}\right)^{-1} \mathbf{p} \,, \tag{3-9}$$

$$SNR \leq \frac{\sigma_t^2 \mathbf{p}^{\mathbf{H}} \mathbf{p}}{\sigma_n^2} \,, \tag{3-10}$$

$$SNR \leq KN \frac{\sigma_t^2}{\sigma_n^2} \,. \tag{3-11}$$

It can be observed that, pre-processed SNR is improved by a factor of KN after the weighting operation. This is an expected result under white noise conditions because we have KN many samples of target to be used.

The SCNR bound represented in (3-8) is important, because it will be used several times in the analyses in Chapter 4.

3.2. Rank Reduction Techniques

The size of the detection problem can be inferred from the Degrees of Freedoms (DoF) or the rank of the covariance matrix $\mathbf{R}$. Rank reduction techniques are signal processing operations which reduces the DoFs and generally the rank of the covariance matrix. A very good taxonomy of rank reduction techniques is given in [6] as illustrated in Figure 3-1:

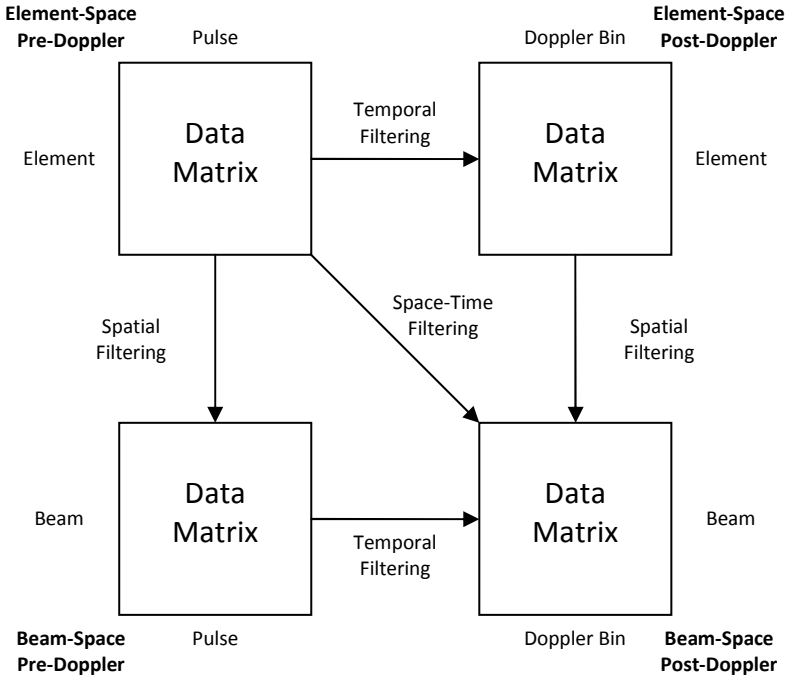

Figure 3-1 Taxonomy of rank reduction techniques

The rank reduction techniques will be mentioned in 3.2.1, 3.2.2 and 3.2.3.

3.2.1. Beam-Space Rank Reduction

The idea behind the beam-space rank reduction is to form beam or beams before Doppler processing.

Remember (3-3) the received signal is of the form:

$$\mathbf{r} = \begin{bmatrix} \mathbf{r}_1 \\ \mathbf{r}_2 \\ \vdots \\ \mathbf{r}_N \end{bmatrix}. \qquad (3\text{-}12)$$

Each $\mathbf{r}_i$ represents the K channel response in one pulse.

In beam-space rank reduction, we will combine the elements of $\mathbf{r}_i$ with beam-forming weights to conduct the rank reduction operation which can be seen in Figure 3-2:

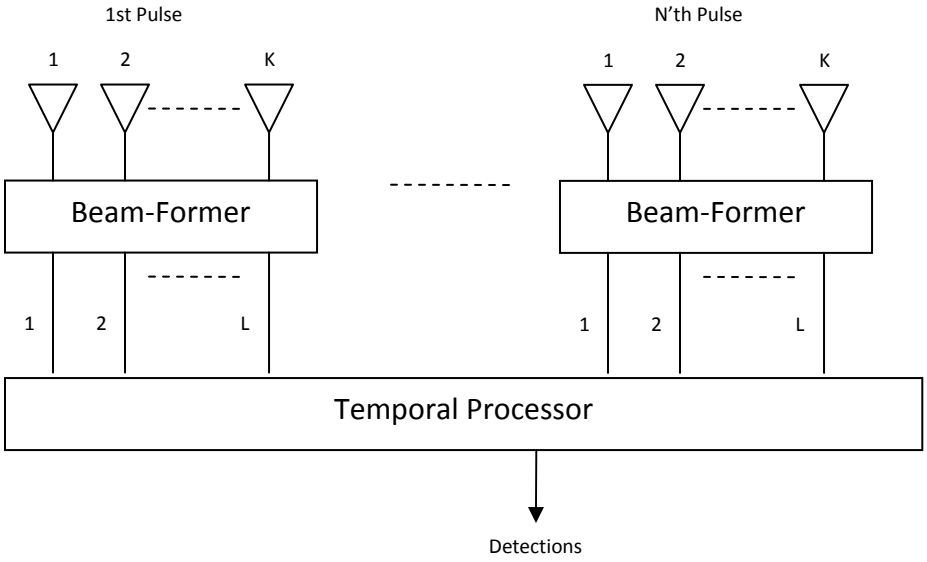

Figure 3-2 Beam-space rank reduction

Define a rank reducer matrix as follows:

$$\mathbf{B}=\begin{bmatrix} \mathbf{w}_{11} & \mathbf{w}_{21} & \cdots & \mathbf{w}_{L1} & & \mathbf{0}_{Kx1} & \cdots & \cdots & \mathbf{0}_{Kx1} \\ \mathbf{0}_{Kx1} & \cdots & \cdots & \mathbf{0}_{Kx1} & \cdots & \vdots & & & \vdots \\ \vdots & & & \vdots & & \mathbf{0}_{Kx1} & \cdots & \cdots & \mathbf{0}_{Kx1} \\ \mathbf{0}_{Kx1} & \cdots & \cdots & \mathbf{0}_{Kx1} & & \mathbf{w}_{1N} & \mathbf{w}_{2N} & \cdots & \mathbf{w}_{LN} \end{bmatrix} \tag{3-13}$$

The rank reducer matrix $\mathbf{B}$ is a KNxLN matrix which constitutes L many beams for each pulse. In order to have a rank reduction operation, L<K must be satisfied. The $\mathbf{w}_{ij}$ vectors are the beam-forming weights of size Kx1. Applying the rank reducing matrix will yield received signal vectors and covariance matrix given in (3-14), (3-15) and (3-16):

$$\mathbf{r}_B = \mathbf{B}^H \mathbf{r}\,, \tag{3-14}$$

$$\mathbf{R_B} = E\left\{\mathbf{r_B r_B^H}\right\} = E\left\{\mathbf{B^H r r^H B}\right\} = \mathbf{B^H} E\left\{\mathbf{r r^H}\right\}\mathbf{B} = \mathbf{B^H R B}, \tag{3-15}$$

$$\mathbf{p_B} = \mathbf{B^H p}. \tag{3-16}$$

Then the SCNR bound formula in (3-8) will be modified as in (3-18):

$$SCNR \le \sigma_t^2 \mathbf{p_B^H R_B^{-1} p_B}, \tag{3-17}$$

$$SCNR \le \sigma_t^2 \mathbf{p^H B}\left(\mathbf{B^H R B}\right)^{-1}\mathbf{B^H p}. \tag{3-18}$$

3.2.2. Post-Doppler Rank Reduction

The method of post-Doppler rank reduction is to apply a Discrete Fourier Transform to the data and then to process the received signals from each element to form beams. Post-Doppler rank reduction techniques can be classified in terms of the number of Doppler bins used to form beams. The rank reduction operation in this method is illustrated in Figure 3-3:

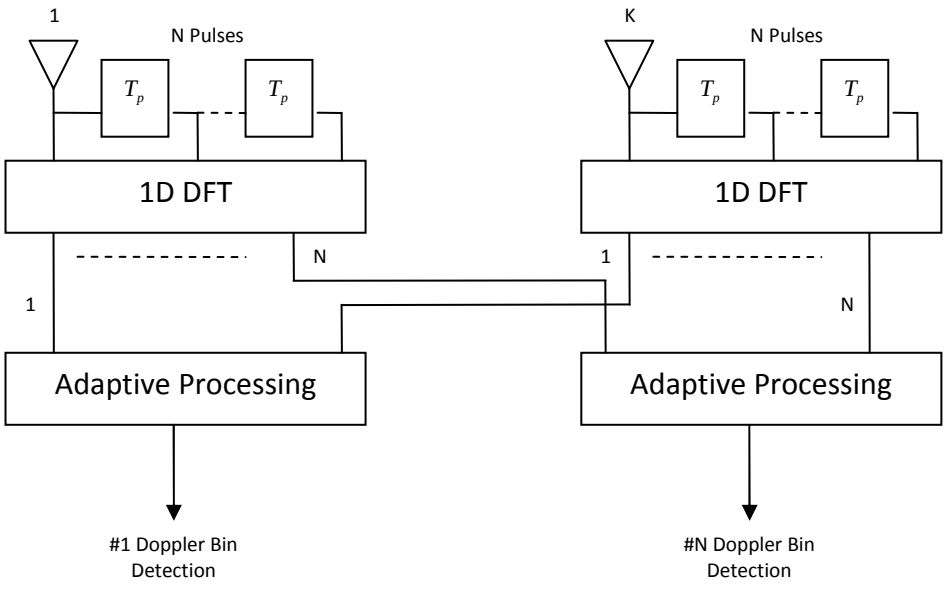

Figure 3-3 Post-Doppler single Doppler bin rank reduction

The rank reducer matrix (for single Doppler bin) will be as in (3-19):

$$\mathbf{D_n} = \begin{bmatrix} \mathbf{I_{KxK}} \\ w_n^1 \mathbf{I_{KxK}} \\ \vdots \\ w_n^{N-1} \mathbf{I_{KxK}} \end{bmatrix}. \tag{3-19}$$

Here, $\mathbf{D_n}$ represents the collection of n'th Doppler bin steering vectors to get n'th bin rank reduction and it is a KNxN matrix. $w_n^i = \exp\left(j2\pi i f_n T_p\right)$ is the Discrete Fourier Transform complex coefficient at n'th Doppler bin for i'th pulse. Applying the rank reducing matrix will yield following received signal vectors and covariance matrix shown in (3-20), (3-21) and (3-22):

$$\mathbf{r_{Dn}} = \mathbf{D_n^H r}\,, \tag{3-20}$$

$$\mathbf{R_{Dn}} = E\left\{\mathbf{r_{Dn} r_{Dn}^H}\right\} = E\left\{\mathbf{D_n^H r r^H D_n}\right\} = \mathbf{D_n^H} E\left\{\mathbf{r r^H}\right\}\mathbf{D_n} = \mathbf{D_n^H R D_n}\,, \tag{3-21}$$

$$\mathbf{p_{Dn}} = \mathbf{D_n^H p}\,. \tag{3-22}$$

Then the SCNR bound formula will be modified as in (3-24):

$$SCNR \le \sigma_t^2 \mathbf{p_{Dn}^H R_{Dn}^{-1} p_{Dn}}\,, \tag{3-23}$$

$$SCNR \le \sigma_t^2 \mathbf{p^H D_n} \left(\mathbf{D_n^H R D_n}\right)^{-1} \mathbf{D_n^H p}\,. \tag{3-24}$$

In Post-Doppler rank reduction, computational advantage arises only if we use number of Doppler bins less than N. Otherwise, if we use all Doppler bins, the Post-Doppler technique does not reduce the rank and gives optimum result, since DFT is a revertible operation.

3.2.3. Beam-Space Post-Doppler Rank Reduction

Beam-Space Post-Doppler rank reduction is a technique which reduces the rank twice by combining the beam-space and post-Doppler rank reduction methods.

The reduction operation can be shown in Figure 3-4:

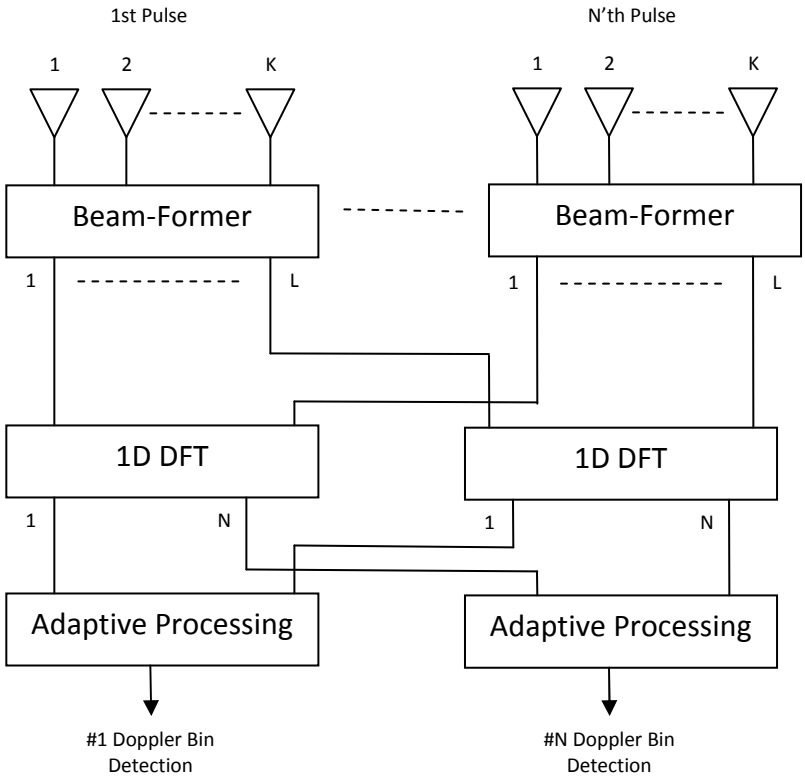

Figure 3-4 Beam-space Post-Doppler rank reduction

Rank reducer matrix can be represented as in (3-25), in terms of the matrices in (3-13) and (3-19):

$$\mathbf{B_D} = \mathbf{B}\mathbf{D_n}\,. \tag{3-25}$$

Since we first apply beam-forming, then the Post-Doppler technique, SCNR bound formula can be determined as (3-30):

$$\mathbf{r_{BD}} = \mathbf{B_D^H r}\,, \tag{3-26}$$

$$\mathbf{R_{BD}} = E\left\{\mathbf{r_{BD}}\mathbf{r_{BD}^H}\right\} = E\left\{\mathbf{B_D^H}\mathbf{r}\mathbf{r^H}\mathbf{B_D}\right\} = \mathbf{B_D^H}E\left\{\mathbf{r}\mathbf{r^H}\right\}\mathbf{B_D} = \mathbf{B_D^H}\mathbf{R}\mathbf{B_D}\,, \tag{3-27}$$

$$\mathbf{p_{BD}} = \mathbf{B_D^H p}\,, \tag{3-28}$$

$$SCNR \le \sigma_t^2 \mathbf{p_{BD}^H}\mathbf{R_{BD}^{-1}}\mathbf{p_{BD}}\,, \tag{3-29}$$

$$SCNR \le \sigma_t^2 \mathbf{p}^{\mathbf{H}} \mathbf{B}_{\mathbf{D}} \left(\mathbf{B}_{\mathbf{D}}^{\mathbf{H}} \mathbf{R} \mathbf{B}_{\mathbf{D}} \right)^{-1} \mathbf{B}_{\mathbf{D}}^{\mathbf{H}} \mathbf{p} \,. \tag{3-30}$$

3.3. Advantages and Disadvantages of Rank Reduction

Rank reduction techniques provide a trade-off between detection performance and practical implementation in the GMTI systems. Main advantages and disadvantages of rank reduction techniques can be summarized as follows:

Table 3-1 Advantages and disadvantages of rank reduction

	Advantages	Disadvantages
Full STAP	1. Optimum detection performance 2. Provides full adaptability to external factors	1. The antenna element and feed network is complicated and expensive 2. The amount of data to be processed is huge 3. Practical problems like channel calibration with many channels is a difficult problem to solve.
Beam-Space	1. Reduced number of beams provides data reduction and focused operation 2. Forming beams with RF hardware is less expensive than constituting a multi-channel system.	1. Non-adaptive beam-forming reduces the DoFs without the knowledge of the environment.
Post-Doppler	1. Reduced number of data and matrix sizes facilitate the matrix operations	1. Using less number of bins degrades the performance, using more bins do not provide simplification in computation.
Beam-Space Post-Doppler	1. Reduced number of channels and data and provides a very simple processing solution	1. Reduction in DoF is very significant, which may degrade the performance to unwanted levels.

3.4. Clutter, Noise and Target Subspaces

Subspace concept is an approach in GMTI processing and interference suppression, which takes advantage of the dimensionality and orthogonality concepts.

In a full STAP system, we have K many elements and N many pulses, which provides KN many DoFs. Analogously, we are working in a KN dimensional space. Subspace concept's purpose can be listed as follows:

1) Determine the subspace (and its dimensions) which the clutter is in
2) Determine the subspace (and its dimensions) which the target signal is in
3) Carefully process the data which spread in these subspaces to reveal the target signal buried under the clutter signal.

3.4.1. Clutter Subspace

Clutter subspace will be our main subspace to be observed. Clutter is modeled in section 2.6.2 as colored signal with Gaussian distribution. This model causes correlation between clutter samples and this correlation results a reduction in dimension. Thus, we will state that the clutter is not spread along all KN dimensions.

Consider a data collection scenario in which the aircraft moves forward to a distance which is an integer multiple of antenna separation as illustrated in Figure 3-5:

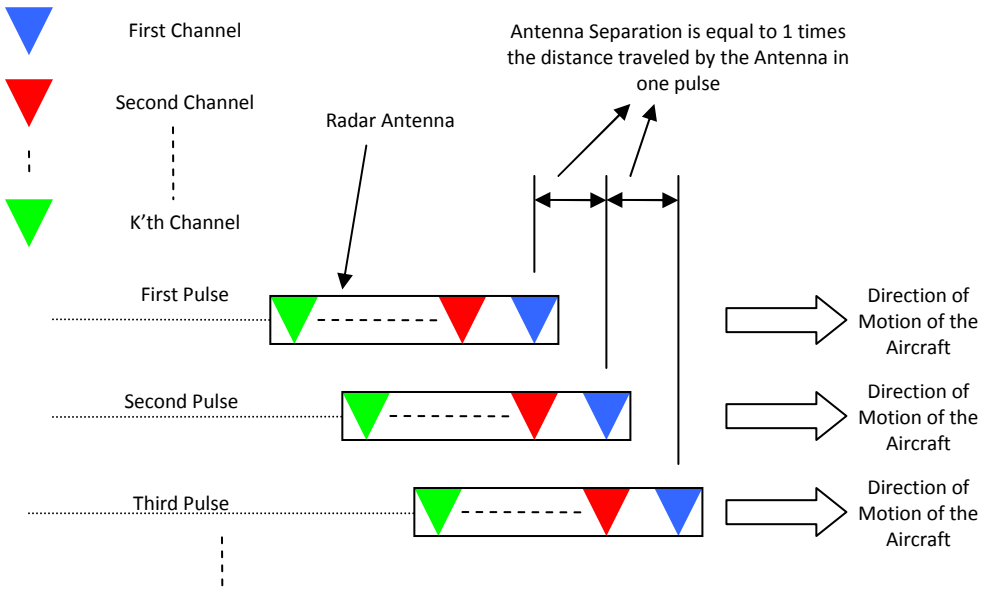

Figure 3-5 Data collection scenario

In this scenario, responses from K many channels in N many pulses are collected to form space-time response (KNx1 vector).

Remember the received clutter signal form from (2-27):

$$\mathbf{c} = \begin{bmatrix} \mathbf{c}_1 \\ \mathbf{c}_2 \\ \vdots \\ \mathbf{c}_N \end{bmatrix}. \tag{3-31}$$

We can generate a new representation to received clutter as in (3-32):

$$\mathbf{C} = \begin{bmatrix} \mathbf{c}_1^{\mathbf{T}} \\ \mathbf{c}_2^{\mathbf{T}} \\ \vdots \\ \mathbf{c}_N^{\mathbf{T}} \end{bmatrix}. \tag{3-32}$$

New representation in (3-32) is a matrix of size NxK. The first dimension of the matrix is constituted from temporal response and the second dimension is constituted from spatial response.

Taking the Fourier Transform of that matrix in both dimensions can give the temporal and spatial spectral distribution of clutter in a 2D fashion as illustrated in Figure 3-6:

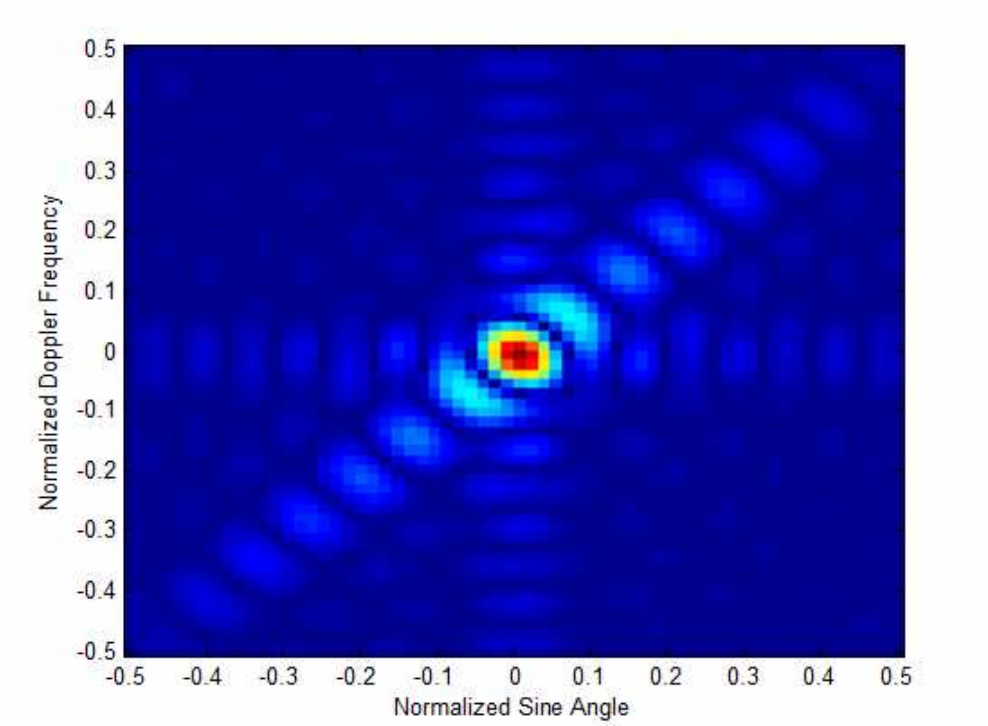

Figure 3-6 2D (temporal and spatial) spectrial distribution of clutter

Normalized sine angle represents the azimuth angle of the antenna between -90 and 90 degrees with a sine operation; because, clutter spectral distribution is proportional to the sine of the azimuth angle,

which can be seen in (2-20). Normalized Doppler frequency indicates the frequency spectra normalized with the pulse repetition frequency.

It can be seen from Figure 3-6 that the clutter is accumulated around a certain line. This line is called "clutter ridge", [5], [6]. Define the "clutter ridge" parameter as in (3-33):

$$\beta = \frac{2V_A T_P}{d}. \tag{3-33}$$

The parameter β is called the slope of the clutter ridge, and it represents the slope between spatial and temporal frequencies. If β is an integer value, the rank of the clutter covariance matrix can be determined as follows:

$$rank\{\mathbf{R}_c\} = K + (N-1)\beta. \tag{3-34}$$

This idea is first stated in [8], but the proof can be found in [9]. From (3-34), we can observe that clutter signal is spread along $K + (N-1)\beta$ many dimensions. Clutter ridges are the 2D Fourier Transform of the matrix stated in (3-32), which is generated by using the parameters in Table 3-2 and the clutter realization technique mention in section 2.6.2. The covariance matrices are generated by using (2-20) with the parameters in Table 3-2:

Table 3-2 Demonstration parameters

Parameter Name	Value
Number of Antenna Elements (K)	16
Number of Pulses (N)	16
Platform Velocity (V_A)	100 m/s
Pulse Repetition Interval (T_P)	Depends on the figure
Antenna Separation (d)	0.02 m
Clutter Ridge (β)	Depends on the figure
Number of DoFs	16x16 = 256

Figure 3-7, Figure 3-8, Figure 3-9 and Figure 3-10 demonstrate some examples of clutter ridge slope and rank of covariance matrices:

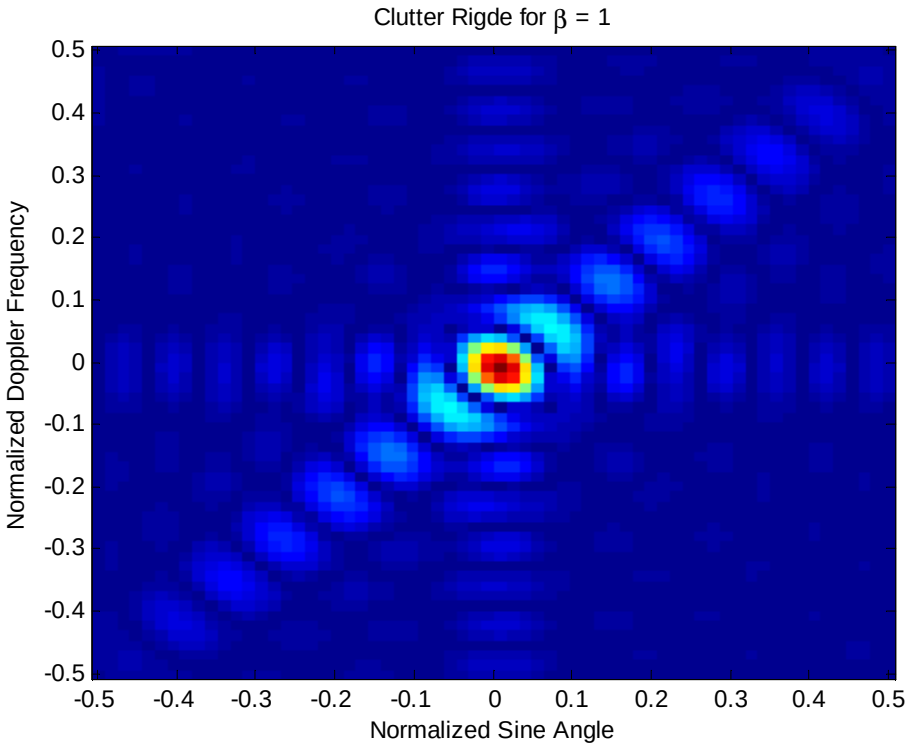

Figure 3-7 Clutter Ridge for $\beta = 1$

For $\beta = 1$, rank of the clutter covariance matrix is

$rank\{\mathbf{R}_c\} = 16 + (16-1)1 = 31.$

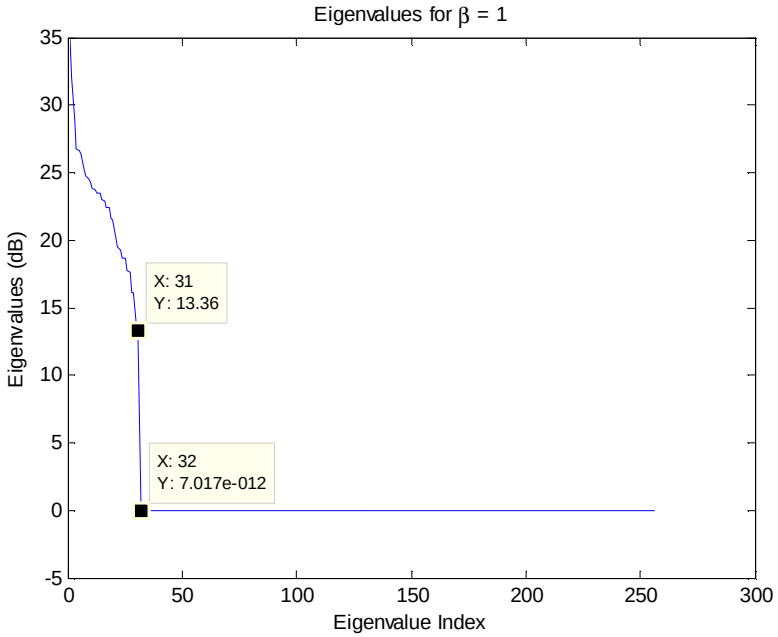

Figure 3-8 Eigenvalues for $\beta = 1$

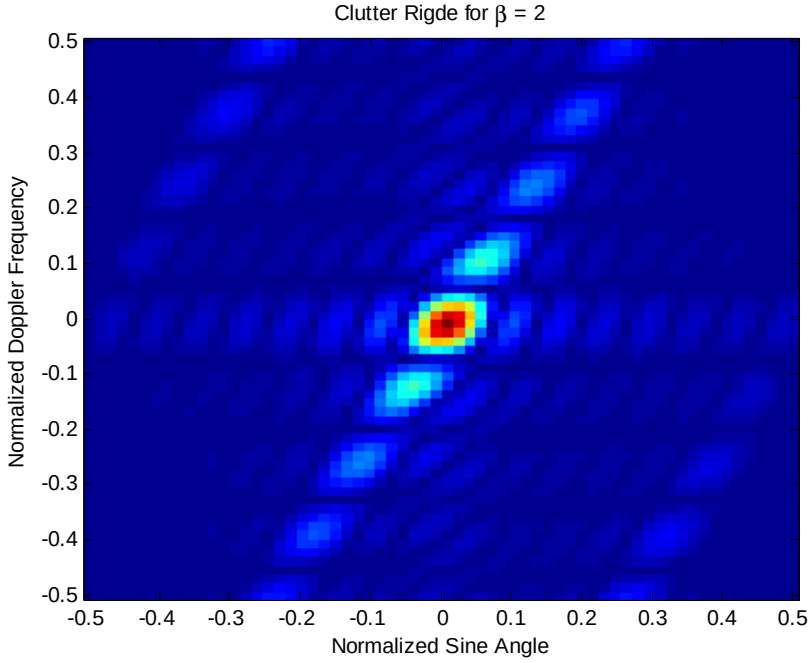

Figure 3-9 Clutter Ridge for $\beta = 2$

For $\beta = 2$, rank of the clutter covariance matrix is

$rank\{\mathbf{R_c}\} = 16 + (16-1)2 = 46$.

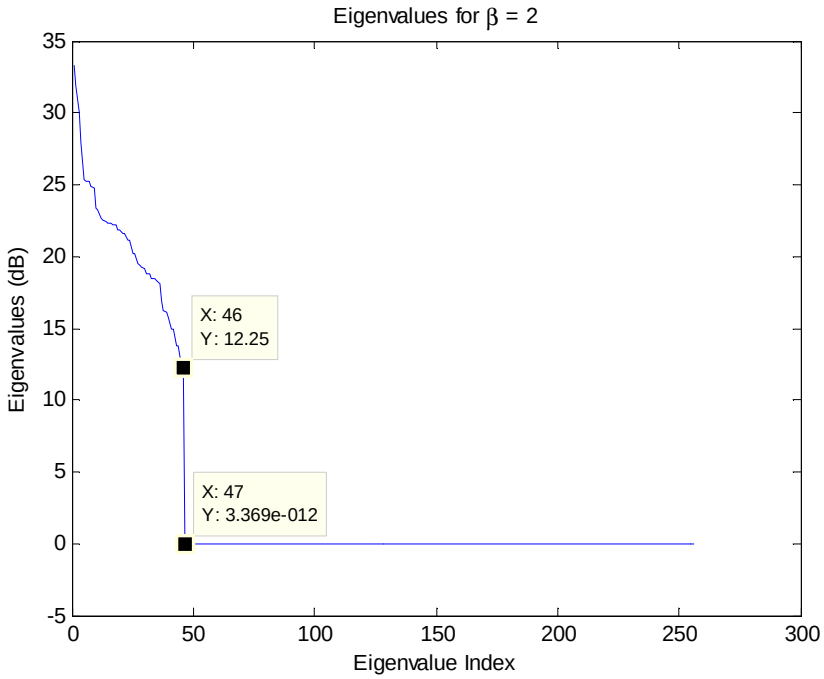

Figure 3-10 Eigenvalues for $\beta = 2$

For K=16 and N = 16 the results are as expected; the numbers of eigenvalues are exactly the same with the rank formula given in (3-34).

3.4.2. Noise Subspace

The noise is assumed to be a white signal with Gaussian distribution in section 2.6.3. Since noise is white, it has to be spread along each dimension with equal power. Consider the covariance matrix of the noise:

$$\mathbf{R_n} = \sigma_n^2 \mathbf{I}. \tag{3-35}$$

Since it is identity matrix, it is full rank (i.e. KN dimensional) and all the eigenvalues are equal to σ_n^2.

3.4.3. Target Subspace

Target signal spreads along one dimension only with respect to its basis. The only vector in the basis of the target signal is equal to its target signal vector omitting the constant terms as in (3-36):

$$\mathbf{p} = \begin{bmatrix} \mathbf{p}_1 \\ \mathbf{p}_2 \\ \vdots \\ \mathbf{p}_N \end{bmatrix}. \tag{3-36}$$

Clutter subspace has a basis with $rank\{\mathbf{R}_c\}$ many basis vectors. Generally, target and clutter subspaces do not have a common basis vector. Thus, as far as the basis of clutter subspace is concerned, the target signal has components in multiple dimensions. The main purpose will be to get the target signal components in different dimensions and combine them coherently to obtain a good performance.

3.5. Subspace Processing and Eigen-Beam Concepts

The aim of subspace processing is to solve the detection problem in orthogonal dimensions and combine them to get an ultimate performance which is close to the theoretical SCNR bound. For the sake of simplicity, consider a one pulse case (N=1). Then our problem reduces to K dimensions which are the channels of our antenna. We can write the eigenvalue decomposition of total covariance matrix as in (3-37):

$$\mathbf{R} = \mathbf{U}\Psi\mathbf{U}^{\mathbf{H}}. \tag{3-37}$$

Here, $\mathbf{U}$ is a unitary matrix which is a collection of eigenvectors of matrix $\mathbf{R}$. Ψ is a diagonal matrix in which the diagonal entries are the eigenvalues of matrix $\mathbf{R}$. Inspecting matrix $\mathbf{U}$:

$$\mathbf{U} = \begin{bmatrix} \mathbf{e}_1 & \mathbf{e}_2 & \cdots & \mathbf{e}_K \end{bmatrix}. \tag{3-38}$$

Each $\mathbf{e_i}$ is an eigenvector of $\mathbf{R}$. Consider a beam-space rank reduction by selecting the eigenvectors as the beam-forming weights. We will call that beams as eigen-beams, which is a beam-forming technique used in communication and direction finding (DF) systems, [12], [13].

We can get the SCNR bound in (3-45) by using eigen-beams for one pulse case as follows:

$$\mathbf{B} = \mathbf{U}\,, \tag{3-39}$$

$$SCNR \le \sigma_t^2 \mathbf{p^H B}\left(\mathbf{B^H R B}\right)^{-1}\mathbf{B^H p}\,, \tag{3-40}$$

$$SCNR \le \sigma_t^2 \mathbf{p^H B}\left(\mathbf{B^H U \Psi U^H B}\right)^{-1}\mathbf{B^H p}\,, \tag{3-41}$$

$$SCNR \le \sigma_t^2 \mathbf{p^H B \Psi^{-1} B^H p}\,, \tag{3-42}$$

$$\Psi^{-1} = \begin{bmatrix} 1/\lambda_1 & 0 & \cdots & 0 \\ 0 & 1/\lambda_2 & \ddots & \vdots \\ \vdots & \ddots & \ddots & 0 \\ 0 & \cdots & 0 & 1/\lambda_K \end{bmatrix}, \tag{3-43}$$

$$\mathbf{B^H p} = \begin{bmatrix} \mathbf{e_1^H} \\ \mathbf{e_2^H} \\ \vdots \\ \mathbf{e_K^H} \end{bmatrix}\mathbf{p} = \begin{bmatrix} \mathbf{e_1^H p} \\ \mathbf{e_2^H p} \\ \vdots \\ \mathbf{e_K^H p} \end{bmatrix} = \begin{bmatrix} G_1 \\ G_2 \\ \vdots \\ G_K \end{bmatrix}, \tag{3-44}$$

$$SCNR \le \sigma_t^2 \sum_{i=1}^{K} \frac{|G_i|^2}{\lambda_i}\,. \tag{3-45}$$

In (3-45), it can be observed that the SCNR is bounded by the sum of contributions of every dimension. By defining the contribution ratio as $\frac{|G_i|^2}{\lambda_i}$, for a case K = 32, we will have the following contribution ratios:

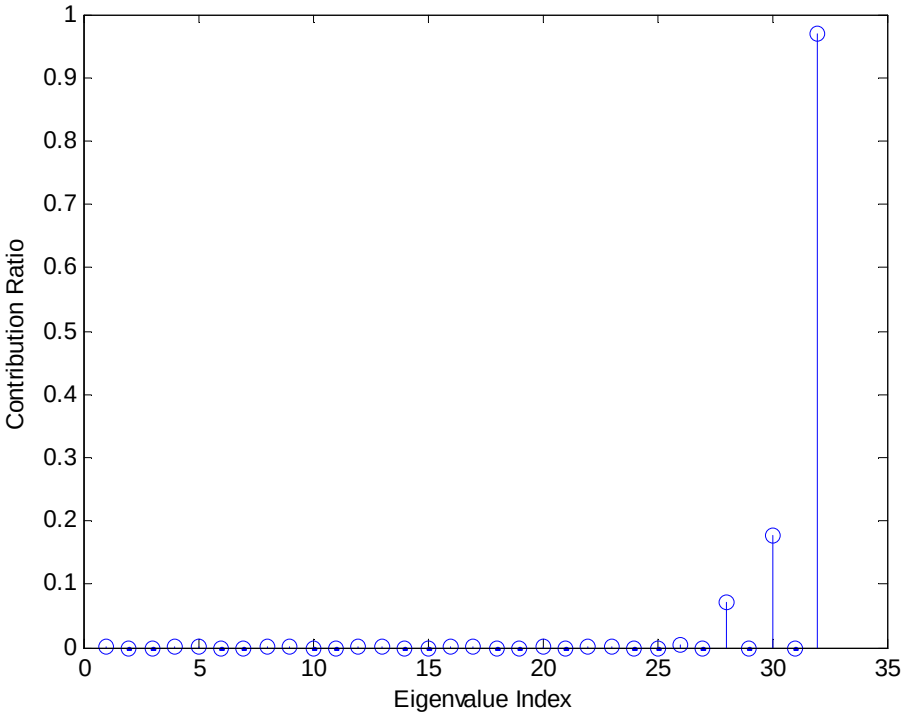

Figure 3-11 Contribution ratios

In one pulse case, most of the contributions to the SCNR value come from 28^{th}, 30^{th} and 32^{nd} dimensions. The corresponding eigen-beams are shown in Figure 3-12, Figure 3-13 and Figure 3-14:

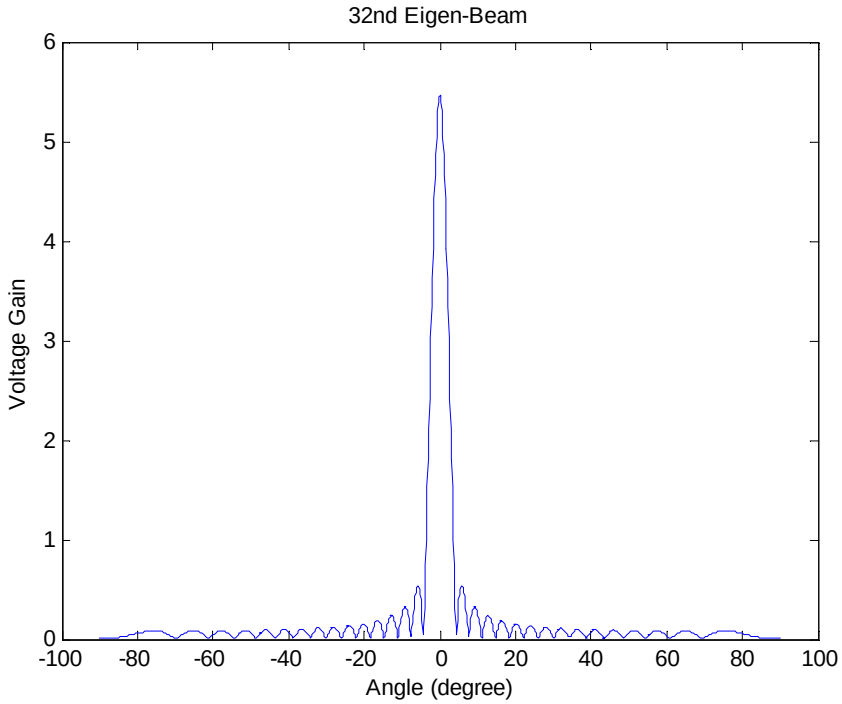

Figure 3-12 32nd eigen-beam

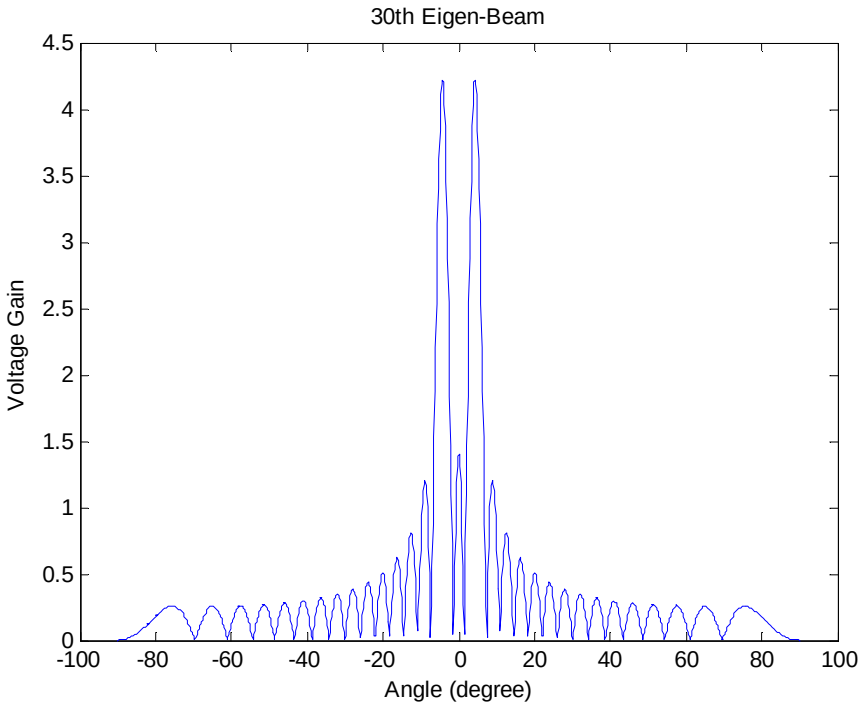

Figure 3-13 30th eigen-beam

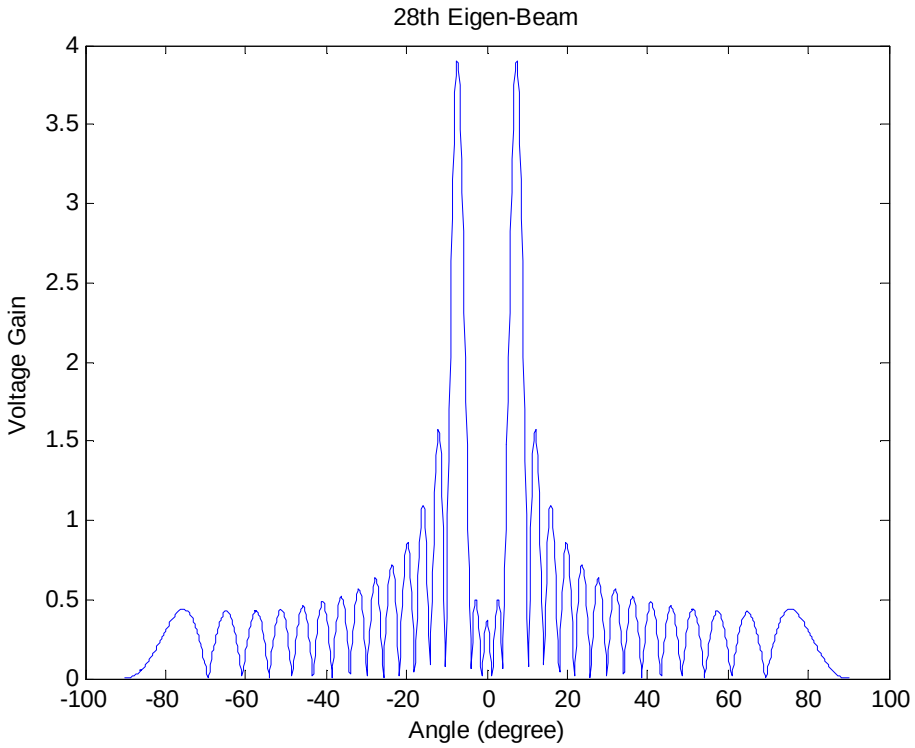

Figure 3-14 28th eigen-beam

In the one pulse case, the detection problem can be solved as independent problems in K dimensions and then can be added to get a better result. Depending on the performance needs, the number of eigen-beams that have to be used can be determined by (3-45). However, the analysis is valid for only one pulse case. For multi pulse case, since there is a correlation between space and time signals, an analytic derivation is not available. Instead, eigen-beam idea will be transferred to multi pulse case and analyzed numerically.

CHAPTER 4

OPTIMIZING ANTENNA PATTERNS WITH BEAM-SPACE APPROACH

4.1. Problem Statement

The main problem this thesis aims to solve is to propose beam-space rank reduction solutions down to two channels, while keeping the endo-clutter target detection performance in GMTI processing at an acceptable level. The beam-space rank reduction solutions is constrained to have two signal-independent beams (which means the beams are formed with passive hardware elements like couplers and beam-forming operation does not have a feedback from the received signal). Good endo-clutter target performance will be measured with closeness of SCNR bound value of that beam-space solution to the optimum STAP SCNR bound value for low target velocities.

4.2. Assumptions, Constraints and Performance Loss Metrics

There are certain assumptions that have been made to get a solution.

The receiver structure of the beam-space solution is considered as illustrated in Figure 4-1:

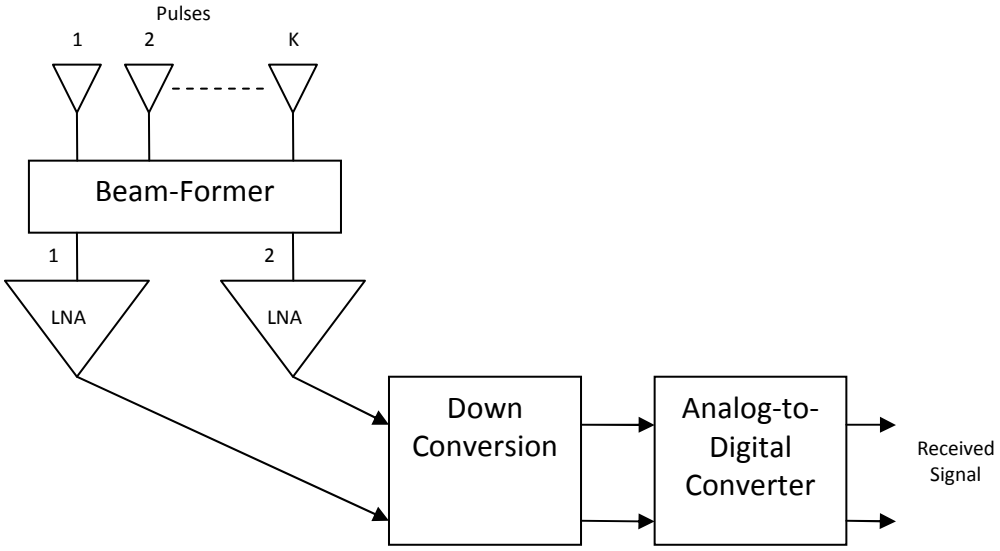

Figure 4-1 Two beam receiver structure

In the receiver structure, the signals coming from the outside world (clutter, target and external noise) are combined in the beam-former to get two output beams. Then these beams are passed through a Low-Noise Amplifier (LNA) which adds a thermal noise component to the received signal. Assume that the external noise is very small compared to the other signals. This received structure will give the received signal at the output of the analog-to-digital converter represented in (4-1):

$$\mathbf{r_B} = \mathbf{B^H c} + \alpha \mathbf{B^H p} + \mathbf{n}\,. \tag{4-1}$$

Here $\mathbf{B}$ is the beam-former matrix, $\mathbf{c}$ is the clutter signal received from all K elements, α is the complex amplitude of the target signal, $\mathbf{p}$ is the target signal received from all K elements and $\mathbf{n}$ is the thermal noise signal added to the beams after LNA.

The clutter probability distribution is assumed to be a zero mean multivariate complex Gaussian distribution with covariance matrix $\mathbf{R}_c$. Noise components are independent from each other, have a zero mean white Gaussian distribution for each beam and have a covariance matrix $\sigma_n^2\mathbf{I}$ where σ_n^2 represents the noise power. All signal components are independent from each other (clutter, noise and target).

The overall covariance matrix of the received signal without the target signal can be found as in (4-3):

$$\mathbf{R}_\mathbf{B} = E\left\{(\mathbf{r}_\mathbf{B} - E\{\mathbf{r}_\mathbf{B}\})(\mathbf{r}_\mathbf{B} - E\{\mathbf{r}_\mathbf{B}\})^\mathbf{H}\right\} = \mathbf{B}^\mathbf{H} E\{\mathbf{c}\mathbf{c}^\mathbf{H}\}\mathbf{B} + E\{\mathbf{n}\mathbf{n}^\mathbf{H}\}, \tag{4-2}$$

$$\mathbf{R}_\mathbf{B} = \mathbf{B}^\mathbf{H}\mathbf{R}_\mathbf{c}\mathbf{B} + \sigma_n^2\mathbf{I}. \tag{4-3}$$

There are certain constraints applied in the analysis in order to compare the resultant beams fairly. In the beam-former matrix, there are two beam-former weight vectors which constitute the beams. These vectors are illustrated in Figure 4-2:

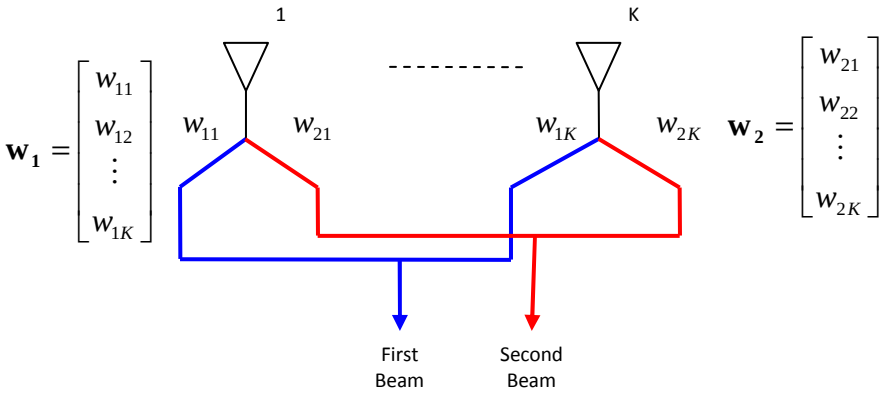

Figure 4-2 Beamforming operation

Here $\mathbf{w}_1$ and $\mathbf{w}_2$ are beam-former vectors and w_{1j}, w_{2j} are the elements of these vectors.

The power constraint of these vector elements can be represented as in Figure 4-3:

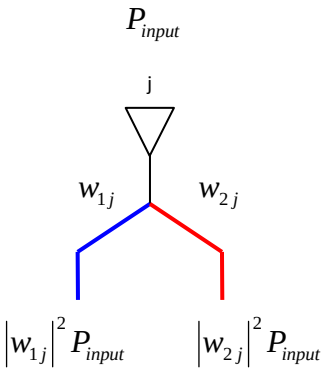

Figure 4-3 Power division in beamforming

Considering the power constraint, the suggestion in (4-5) can be made:

$$P_{input} \geq |w_{1j}|^2 P_{input} + |w_{2j}|^2 P_{input}, \tag{4-4}$$

$$1 \geq |w_{1j}|^2 + |w_{2j}|^2. \tag{4-5}$$

This inequality is the first constraint. For each element in beam-former vectors, this inequality must hold.

The SCNR bounds of optimum and sub-optimum (or beam-space reduced rank in this case) can be represented in (4-6) and (4-7), respectively, as follows:

$$SCNR_{optimum} \leq \sigma_t^2 \mathbf{p}^{\mathbf{H}} \left(\mathbf{R}_{\mathbf{c}} + \sigma_n^2 \mathbf{I} \right)^{-1} \mathbf{p}, \tag{4-6}$$

$$SCNR_{beam-space} \leq \sigma_t^2 \mathbf{p}^{\mathbf{H}} \mathbf{B} \left(\mathbf{B}^{\mathbf{H}} \mathbf{R}_{\mathbf{c}} \mathbf{B} + \sigma_n^2 \mathbf{I} \right)^{-1} \mathbf{B}^{\mathbf{H}} \mathbf{p}. \tag{4-7}$$

Since we know that optimum performance is always greater than or equal to beam-space performance, we can define a metric as in (4-12):

$$SCNR_{optimum} \geq SCNR_{beam-space}, \tag{4-8}$$

$$\sigma_t^2 \mathbf{p}^{\mathbf{H}} \left(\mathbf{R_c} + \sigma_n^2 \mathbf{I}\right)^{-1} \mathbf{p} \geq \sigma_t^2 \mathbf{p}^{\mathbf{H}} \mathbf{B} \left(\mathbf{B}^{\mathbf{H}} \mathbf{R_c} \mathbf{B} + \sigma_n^2 \mathbf{I}\right)^{-1} \mathbf{B}^{\mathbf{H}} \mathbf{p}, \tag{4-9}$$

$$\mathbf{p}^{\mathbf{H}} \left(\mathbf{R_c} + \sigma_n^2 \mathbf{I}\right)^{-1} \mathbf{p} - \mathbf{p}^{\mathbf{H}} \mathbf{B} \left(\mathbf{B}^{\mathbf{H}} \mathbf{R_c} \mathbf{B} + \sigma_n^2 \mathbf{I}\right)^{-1} \mathbf{B}^{\mathbf{H}} \mathbf{p} \geq 0, \tag{4-10}$$

$$\mathbf{p}^{\mathbf{H}} \mathbf{R}_{\mathbf{difference}} \ \mathbf{p} \geq 0, \tag{4-11}$$

$$\mathbf{R}_{\mathbf{difference}} = \left(\mathbf{R_c} + \sigma_n^2 \mathbf{I}\right)^{-1} - \mathbf{B} \left(\mathbf{B}^{\mathbf{H}} \mathbf{R_c} \mathbf{B} + \sigma_n^2 \mathbf{I}\right)^{-1} \mathbf{B}^{\mathbf{H}}. \tag{4-12}$$

Here we have defined a new matrix $\mathbf{R}_{\mathbf{difference}}$ called "Difference Matrix" which can be considered as a measure of the statistical difference in clutter and noise signals, between the optimum and beam-space solutions. The difference matrix must be a positive semi definite matrix (all eigenvalues are non-negative), in order to satisfy the inequality in (4-11). Second constraint is the positive semi-definiteness of difference matrix.

For good beam-space solutions, we want the value in (4-11) to be close to zero, for slow targets' $\mathbf{p}$ vectors, in order to get close to the optimum SCNR bound. From a different point of view, the matrix $\mathbf{B}\left(\mathbf{B}^{\mathbf{H}} \mathbf{R_c} \mathbf{B} + \sigma_n^2 \mathbf{I}\right)^{-1} \mathbf{B}$ can be treated as a matrix which cancels the eigenvalues of $\left(\mathbf{R_c} + \sigma_n^2 \mathbf{I}\right)^{-1}$ and the matrix $\mathbf{R}_{\mathbf{difference}}$ has minimum number of non-zero eigenvalues or the sum of its eigenvalues is minimized.

First of all, consider the difference matrix in noise only case (clutter has zero power) in (4-18):

$$\mathbf{R}_{\mathbf{difference}} = \left(\mathbf{R_c} + \sigma_n^2 \mathbf{I}\right)^{-1} - \mathbf{B} \left(\mathbf{B}^{\mathbf{H}} \mathbf{R_c} \mathbf{B} + \sigma_n^2 \mathbf{I}\right)^{-1} \mathbf{B}^{\mathbf{H}}, \tag{4-13}$$

$$\mathbf{R}_{\mathbf{difference}} = \left(\sigma_n^2 \mathbf{I}\right)^{-1} - \mathbf{B} \left(\sigma_n^2 \mathbf{I}\right)^{-1} \mathbf{B}^{\mathbf{H}}, \tag{4-14}$$

$$\mathbf{R}_{\mathbf{difference}} = \frac{\mathbf{I}}{\sigma_n^2} - \frac{\mathbf{BB}^{\mathbf{H}}}{\sigma_n^2}, \tag{4-15}$$

$$\mathbf{BB}^{\mathbf{H}} = \begin{bmatrix} \mathbf{w}_1 & \mathbf{w}_2 \cdots \mathbf{0}_{\mathbf{Kx1}} & \mathbf{0}_{\mathbf{Kx1}} \\ \mathbf{0}_{\mathbf{Kx1}} & \mathbf{0}_{\mathbf{Kx1}} \cdots \vdots & \vdots \\ \vdots & \vdots \cdots \mathbf{0}_{\mathbf{Kx1}} & \mathbf{0}_{\mathbf{Kx1}} \\ \mathbf{0}_{\mathbf{Kx1}} & \mathbf{0}_{\mathbf{Kx1}} \cdots \mathbf{w}_1 & \mathbf{w}_2 \end{bmatrix} \begin{bmatrix} \mathbf{w}_1^{\mathbf{H}} & \mathbf{0}_{\mathbf{Kx1}} \cdots \mathbf{0}_{\mathbf{Kx1}} & \mathbf{0}_{\mathbf{Kx1}} \\ \mathbf{w}_2^{\mathbf{H}} & \mathbf{0}_{\mathbf{Kx1}} \cdots \vdots & \vdots \\ \vdots & \vdots \cdots \mathbf{0}_{\mathbf{Kx1}} & \mathbf{w}_1^{\mathbf{H}} \\ \mathbf{0}_{\mathbf{Kx1}} & \mathbf{0}_{\mathbf{Kx1}} \cdots \mathbf{0}_{\mathbf{Kx1}} & \mathbf{w}_2^{\mathbf{H}} \end{bmatrix}, \tag{4-16}$$

$$\mathbf{BB}^{\mathbf{H}} = \begin{bmatrix} \mathbf{w}_1\mathbf{w}_1^{\mathbf{H}} + \mathbf{w}_2\mathbf{w}_2^{\mathbf{H}} & \mathbf{0}_{\mathbf{KxK}} & \cdots & \mathbf{0}_{\mathbf{KxK}} \\ \mathbf{0}_{\mathbf{KxK}} & \mathbf{w}_1\mathbf{w}_1^{\mathbf{H}} + \mathbf{w}_2\mathbf{w}_2^{\mathbf{H}} & \ddots & \vdots \\ \vdots & \ddots & \ddots & \mathbf{0}_{\mathbf{KxK}} \\ \mathbf{0}_{\mathbf{KxK}} & \cdots & \mathbf{0}_{\mathbf{KxK}} & \mathbf{w}_1\mathbf{w}_1^{\mathbf{H}} + \mathbf{w}_2\mathbf{w}_2^{\mathbf{H}} \end{bmatrix}, \tag{4-17}$$

$$\mathbf{R}_{\mathbf{difference}} = \frac{1}{\sigma_n^2} \begin{bmatrix} \mathbf{R}_{\mathbf{block}} & \mathbf{0}_{\mathbf{KxK}} & \cdots & \mathbf{0}_{\mathbf{KxK}} \\ \mathbf{0}_{\mathbf{KxK}} & \mathbf{R}_{\mathbf{block}} & \ddots & \vdots \\ \vdots & \ddots & \ddots & \mathbf{0}_{\mathbf{KxK}} \\ \mathbf{0}_{\mathbf{KxK}} & \cdots & \mathbf{0}_{\mathbf{KxK}} & \mathbf{R}_{\mathbf{block}} \end{bmatrix}. \tag{4-18}$$

The matrix $\mathbf{R}_{\mathbf{difference}}$ turns out to have a form of repeated block matrices. Thus, analysis of the eigenvalues of one block matrix in (4-19) will suffice:

$$\mathbf{R}_{\mathbf{block}} = \mathbf{I} - \mathbf{w}_1\mathbf{w}_1^{\mathbf{H}} - \mathbf{w}_2\mathbf{w}_2^{\mathbf{H}}. \tag{4-19}$$

Let $\mathbf{w}_1$ and $\mathbf{w}_2$ be two orthonormal vectors (i.e. $\|\mathbf{w}_1\|^2 = 1, \|\mathbf{w}_2\|^2 = 1, \mathbf{w}_1^{\mathbf{H}}\mathbf{w}_2 = 0$). Using Gram-Schmidt orthonormalization procedure, we can complete these vectors to K vectors by adding the set $\{\mathbf{e}_\mathbf{k}\}_{k=3}^{K}$. The set $\mathbf{w}_1, \mathbf{w}_2, \mathbf{e}_3, ..., \mathbf{e}_\mathbf{K}$ is a complete orthonormal set. We can find the eigenvalues corresponding to the vectors in the orthonormal set, we will get the results in (4-21), (4-22) and (4-24):

$$\lambda_{\mathbf{w1}} = \mathbf{w}_1^{\mathbf{H}}\mathbf{R}_{\mathbf{block}}\mathbf{w}_1 = \mathbf{w}_1^{\mathbf{H}}\mathbf{w}_1 - \mathbf{w}_1^{\mathbf{H}}\mathbf{w}_1\mathbf{w}_1^{\mathbf{H}}\mathbf{w}_1 - \mathbf{w}_1^{\mathbf{H}}\mathbf{w}_2\mathbf{w}_2^{\mathbf{H}}\mathbf{w}_1, \tag{4-20}$$

$$\lambda_{w1} = \mathbf{w}_1^{\mathbf{H}} \mathbf{R}_{\mathbf{block}} \mathbf{w}_1 = 1 - 1 - 0 = 0\,, \tag{4-21}$$

$$\lambda_{w2} = \mathbf{w}_2^{\mathbf{H}} \mathbf{R}_{\mathbf{block}} \mathbf{w}_2 = 1 - 1 - 0 = 0\,, \tag{4-22}$$

$$\lambda_{e3} = \mathbf{e}_3^{\mathbf{H}} \mathbf{R}_{\mathbf{block}} \mathbf{e}_3 = \mathbf{e}_3^{\mathbf{H}} \mathbf{e}_3 - \mathbf{e}_3^{\mathbf{H}} \mathbf{w}_1 \mathbf{w}_1^{\mathbf{H}} \mathbf{e}_3 - \mathbf{e}_3^{\mathbf{H}} \mathbf{w}_2 \mathbf{w}_2^{\mathbf{H}} \mathbf{e}_3\,, \tag{4-23}$$

$$\lambda_{e3} = \mathbf{e}_3^{\mathbf{H}} \mathbf{R}_{\mathbf{block}} \mathbf{e}_3 = 1 - 0 - 0 = 1. \tag{4-24}$$

The upper derivation shows that $\mathbf{w}_1$ and $\mathbf{w}_2$ are eigenvectors of $\mathbf{R}_{\mathbf{difference}}$ with 0 eigenvalue and these beam-former vectors will cancel the two eigenvalues of optimum STAP covariance matrix $\mathbf{R}_{\mathbf{c}} + \sigma_n^2 \mathbf{I}$ in noise (because of the normalization), independent from the number of pulses. Thus, we can define our third constraints as in (4-25) and (4-26):

$$\left\| \mathbf{w}_1 \right\|^2 = \mathbf{w}_1^{\mathbf{H}} \mathbf{w}_1 = 1\,, \tag{4-25}$$

$$\left\| \mathbf{w}_2 \right\|^2 = \mathbf{w}_2^{\mathbf{H}} \mathbf{w}_2 = 1. \tag{4-26}$$

4.3. Possible Good Beam-Space Solutions

We will use the orthonormalization beam-pattern idea presented in section 4.2 in combination with the eigen-beam approach in clutter plus noise case. In order to have an analytic solution, consider one pulse detection problem (N=1), where the covariance matrix of optimum STAP case is of size KxK and represented with Karhunen-Leove Expansion in (4-27) as follows:

$$\mathbf{R}_{\mathbf{c}} + \sigma_n^2 \mathbf{I} = \sum_{i=1}^{K} \lambda_i \mathbf{e}_{\mathbf{i}} \mathbf{e}_{\mathbf{i}}^{\mathbf{H}}\,. \tag{4-27}$$

Let λ_1 and λ_2 be the two largest eigenvalues of the covariance matrix and let beam-former vectors be $\mathbf{w_1} = \mathbf{e_1}$ and $\mathbf{w_2} = \mathbf{e_2}$.

Since $\mathbf{w_1}$ and $\mathbf{w_2}$ are orhonormal, we have the equality in (4-28):

$$\mathbf{B^H B} = \begin{bmatrix} \mathbf{w_1^H w_1} & \mathbf{w_1^H w_2} \\ \mathbf{w_2^H w_1} & \mathbf{w_2^H w_2} \end{bmatrix} = \begin{bmatrix} 1 & 0 \\ 0 & 1 \end{bmatrix} = \mathbf{I}. \tag{4-28}$$

The difference matrix of that case can be written as in (4-29) (full derivation can be found in APPENDIX D):

$$R_{difference} = \sum_{i=3}^{K} \frac{1}{\lambda_i} \mathbf{e_i e_i^H}. \tag{4-29}$$

As it can be seen from the Karhunen-Leove Expansion of difference matrix in (4-29), the two largest eigenvalues of the one-pulse covariance matrix of the optimum STAP case cancelled in the suboptimum case directly using the eigen-beams corresponding to that eigenvalues. Equivalently, the rank of difference matrix is minimized. The idea of eigen-beams corresponding to the two greatest eigenvalues of one-pulse covariance matrix will be extended and analyzed with respect to their performances in multi-pulsed cases in section 4.4.

4.4. Performance of Eigen-Beam Patterns

Performance analyses of two eigen-beam approach will be conducted under several conditions with different parameters.

These conditions are illustrated in Figure 4-4:

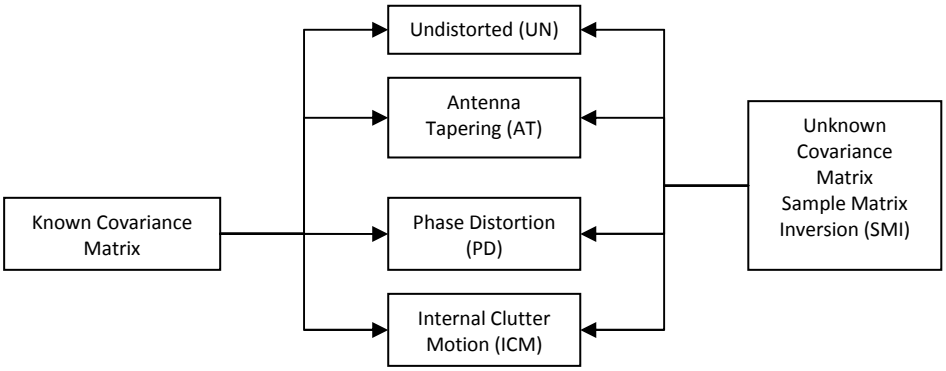

Figure 4-4 Performance analyses conditions

In addition to the cases mentioned above, performances of other cases (one eigen-beam, three eigen-beam and ADPCA) will also be compared with the two eigen-beam approach.

Parameters which are used to calculate the performances are listed below:

Table 4-1 Simulation parameters

Parameter Name	Value
Number of Antenna Elements	16
Number of Pulses	16
Platform Velocity	75 m/s
Pulse Repetition Interval	100 μs
Operating Wavelength	0.03 m
Antenna Separation	0.015 m
Clutter Ridge	1
Number of DoFs	16x16 = 256
SCR	-10 dB
SNR	0 dB

The clutter covariance matrix, which is given in (2-20) is repeated here for convenience:

$$R_c(i+nK, m+kK) = \sigma_c^2 \int |G_T(\theta)|^2 \exp\left(j2\pi \frac{2\Delta x(k-n)+(i-m)d}{\lambda} \sin(\theta) \right) d\theta \,. \quad (4\text{-}30)$$

Using the defined parameters, the clutter covariance matrix will be as in Figure 4-5:

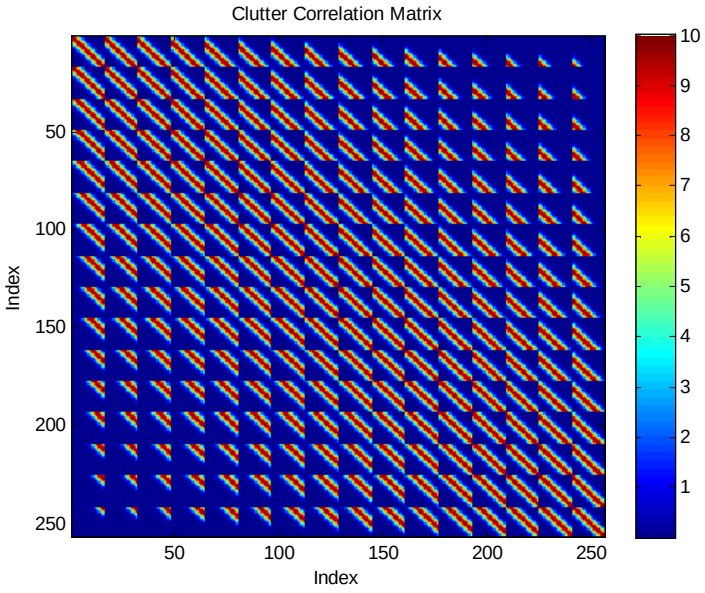

Figure 4-5 Space-time clutter covariance matrix

The patterns of two eigen-beams corresponding to the largest eigenvectors of greatest are shown in Figure 4-6:

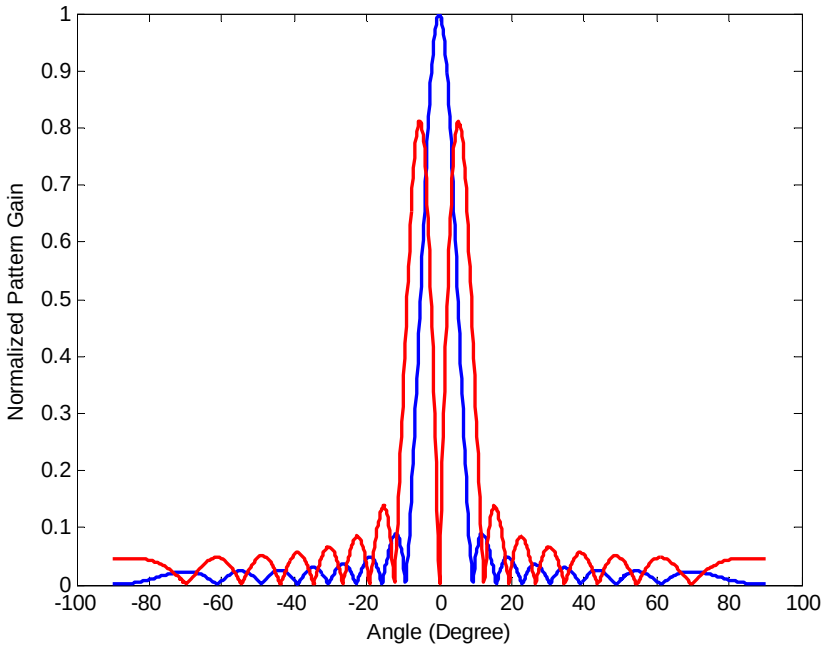

Figure 4-6 Two eigen-beams

As it can be seen from Figure 4-6, two eigen-beams have peaks at other's nulls.

The Table 4-2 shows the labeling of various cases in the figures of following subsections:

Table 4-2 Labeling of the graphs

Case	Labeling
Optimum	Optimum Case
Two Eigen-Beam Undistorted	2EB
Two Eigen-Beam with Hamming Tapering	2EB-HAMMING
Two Eigen-Beam with Kaiser Tapering	2EB-KAISER
Two Eigen-Beam with Taylor Tapering	2EB-TAYLOR
Two Eigen-Beam Antenna Tapering (corresponds to the best tapering among Hamming, Kaiser and Taylor and will be determined later)	2EB-AT
Two Eigen-Beam with Small Phase Distortion	2EB-PD-LOW
Two Eigen-Beam with Large Phase Distortion	2EB-PD-HIGH
Two Eigen-Beam with Small Phase Distortion and Using Sample Matrix Inversion	2EB-PD-LOW-SMI
Two Eigen-Beam with Large Phase Distortion and Using Sample Matrix Inversion	2EB-PD-HIGH-SMI
Two Eigen-Beam with Internal Clutter Motion	2EB-ICM
Two Eigen-Beam with Internal Clutter Motion and Using Sample Matrix Inversion	2EB-ICM-SMI
Adaptive Displaced Phase Center Antenna	ADPCA
One Eigen-Beam	1EB
Three Eigen-Beam	3EB
Combination of Two Eigen-Beams	COMB
Combination of Two Eigen-Beams with Large Phase Error and Using Sample Matrix Inversion	COMB-PD-MAX-SMI

4.4.1. Undistorted (UN) Case

In undistorted case, there is no distortion on the received signal and no tapering in the eigen-beams.

The eigenvalues of the difference matrix of the undistorted case can be seen in Figure 4-7:

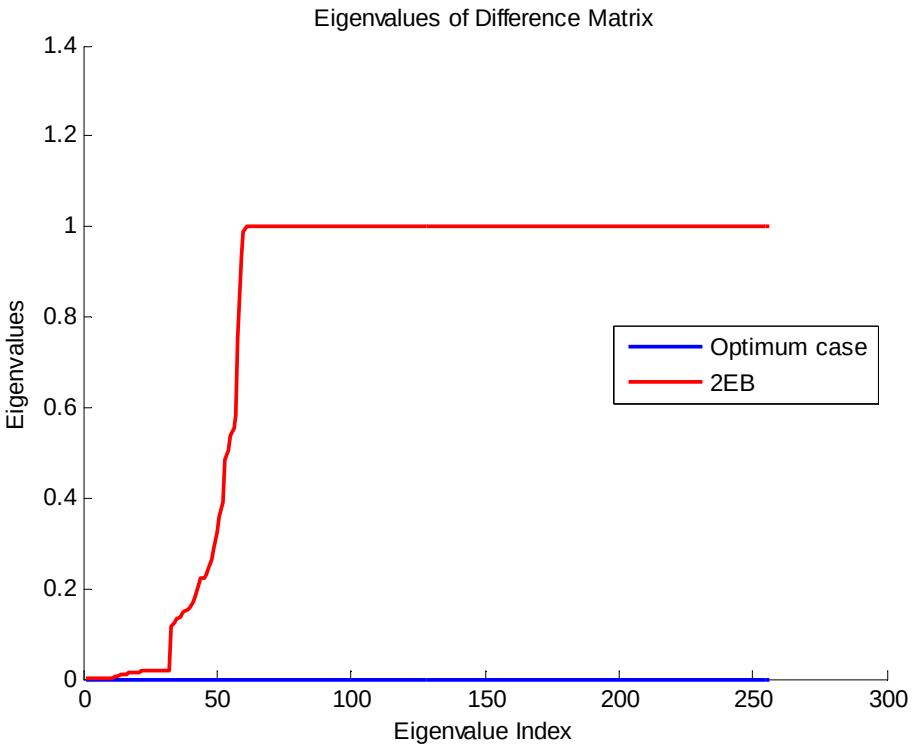

Figure 4-7 Eigenvalues of difference matrix in undistorted condition

The eigenvalues in Figure 4-7 are found by using the clutter and noise covariance matrices defined in (2-20) and (2-29) respectively. In optimum STAP case, all 256 DoFs are nulled in difference matrix, which is expected, because the difference matrix is a zero matrix if optimum STAP is operated, since the optimum STAP has a zero difference with itself.

However, in undistorted case, the number of channels reduced to 2N (2 beams, N pulses), thus we are able to null 2N = 32 many eigenvalues at most.

Thus, SCNR loss values for optimum STAP and undistorted two eigen-beam case can be compared as in Figure 4-8:

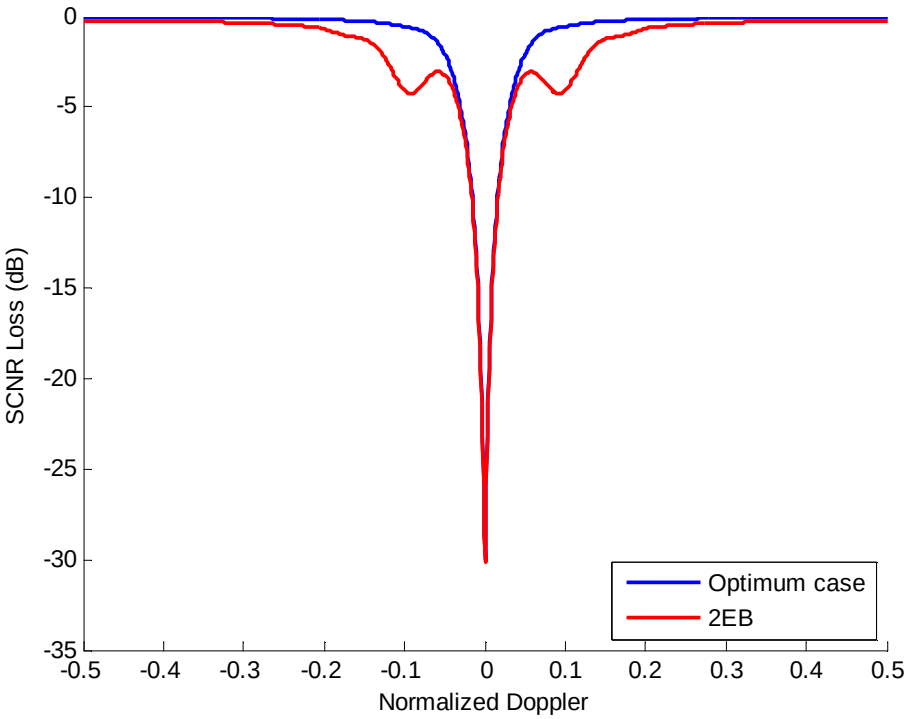

Figure 4-8 SCNR loss in undistorted case

SCNR loss is the difference between SCNR value of a case calculated with (4-7) and the value in (3-11). Optimum STAP defines an SCNR bound to all rank reduction operations. It can be observed that, the performance of undistorted case is close to the theoretical bound in endo-clutter regions (around zero normalized Doppler). Selecting two eigenvectors of antenna covariance matrix as beamforming weights (eigen-beam approach) is the main reason for that closeness, because this choice significantly suppresses the clutter power (or the greatest eigenvalues) of that subspace.

SCNR difference of optimum STAP and undistorted two eigen-beam case can be seen in Figure 4-9:

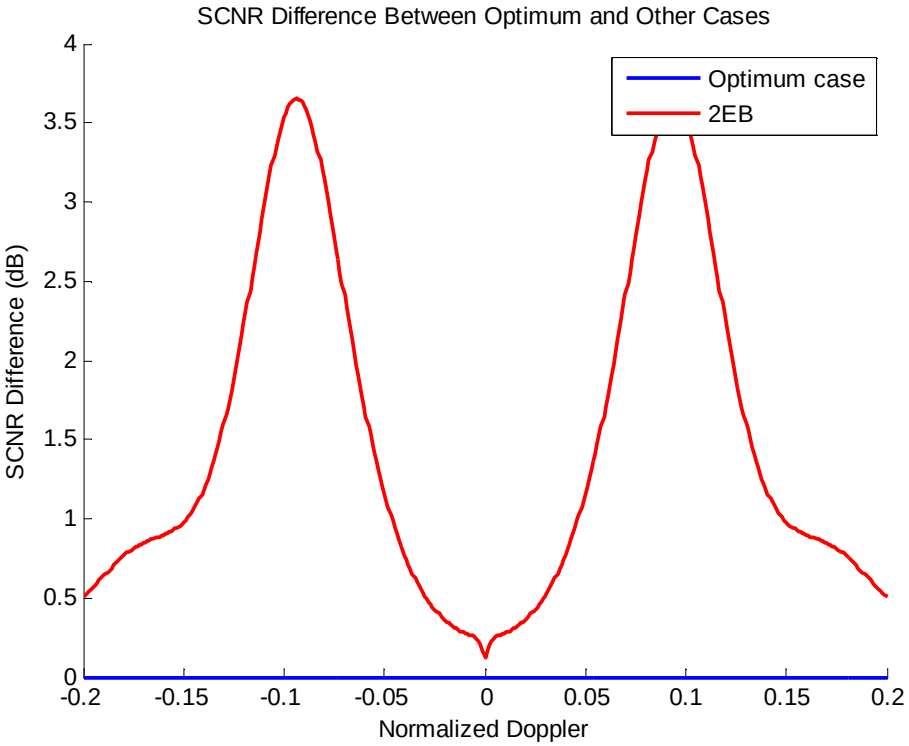

Figure 4-9 SCNR difference between optimum and undistorted cases

It can be seen from Figure 4-9 that, there are high losses around normalized Doppler 0.1 which are due to the local minima of the SCNR curve for two eigen-beam case. These losses can be reduced by using antenna tapering, as discussed in the next section.

4.4.2. Antenna Tapering (AT) Case

In antenna tapering case, a tapering operation is applied to the beam-forming coefficients (i.e. eigen-beams) to smooth the SCNR performance around normalized Doppler 0.1 which is shown in Figure 4-9.

Table 4-3 summarizes the properties of the taperings applied to the eigen-beams:

Table 4-3 Tapering properties

Tapering	**Properties**	
Hamming	-	
Kaiser	Shape parameter = 2	
Taylor	Number of constant level sidelobes = 4	Sidelobe level = -20 dB

The parameters for different tapering methods are chosen by running several simulations with different parameters. Since there are lots of parameter combinations, the results of all simulations are not given here, but only the best results obtained are presented.

Eigenvalues of difference matrices of the tapering methods can be seen from Figure 4-10:

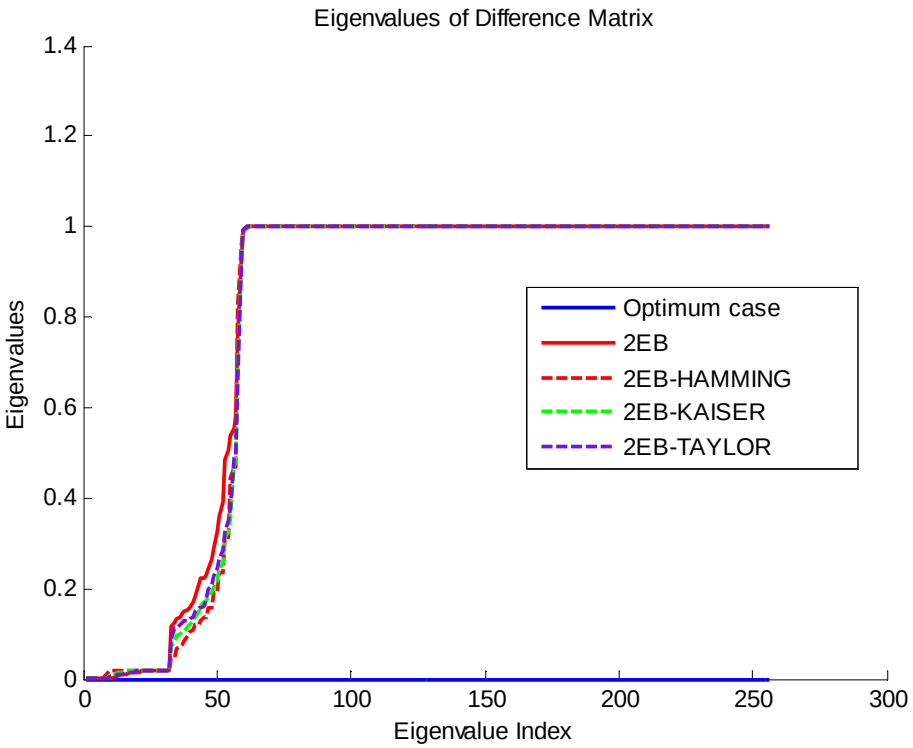

Figure 4-10 Eigenvalues of difference matrices in UN and AT cases

It can be inferred from Figure 4-10 that all the tapering methods have improved the eigenvalue nulling slightly.

A better interpretation is possible by inspecting Figure 4-11:

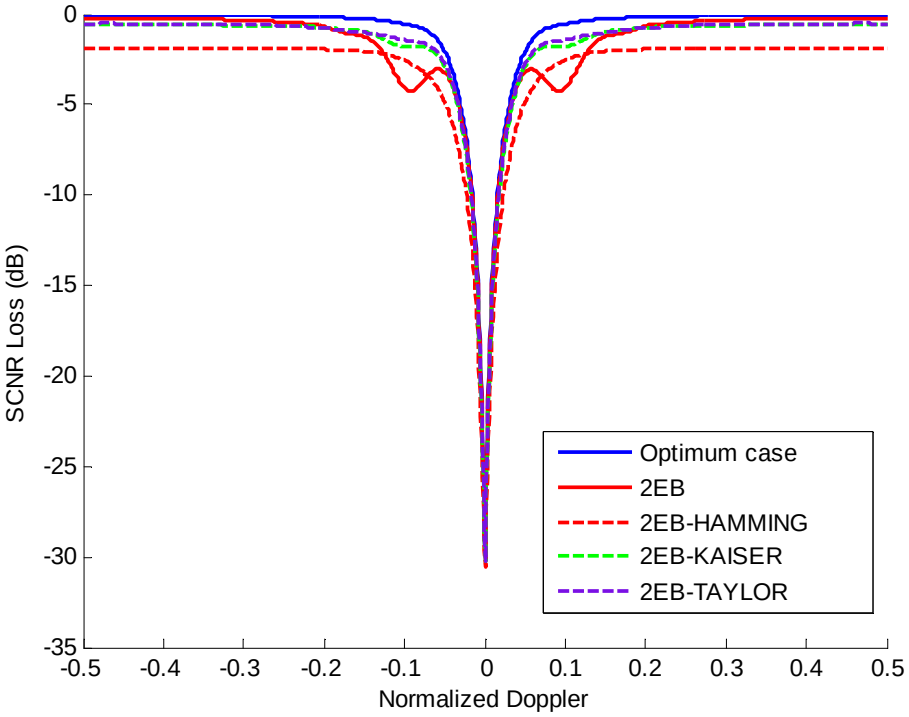

Figure 4-11 SCNR loss in UN and AT cases

As it can be seen from Figure 4-11, for all tapering methods, the SCNR performance in the endo-clutter region slightly decreases; however, a significant gain is achieved in the local minima around normalized Doppler 0.1. Moreover, Hamming tapering seems to cause significant SCNR losses both for endo-clutter and exo-clutter regions. Thus, Hamming tapering will not be considered in the further discussions.

A close look to the endo-clutter SCNR region in Figure 4-12 gives an idea for the best tapering among those that has been investigated:

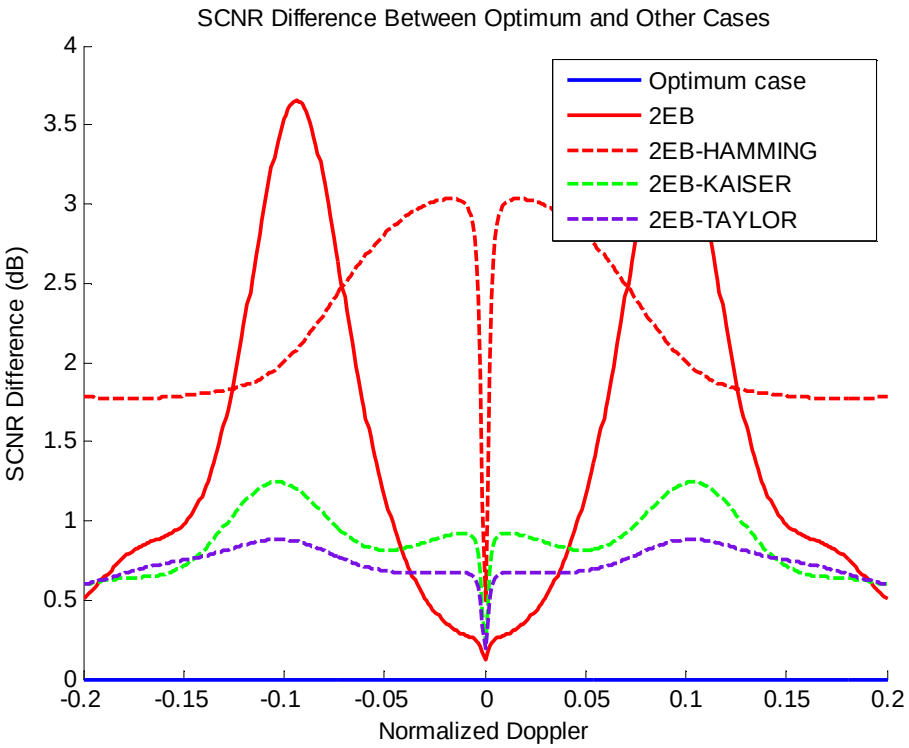

Figure 4-12 SCNR difference between optimum and UN and AT cases

In Figure 4-12, Taylor tapering seems to be better than the Kaiser tapering in nearly most of the normalized Doppler regions. Thus, in the foregoing analyses, eigen-beams with Taylor tapering will be used to compare the performance of different beam-space rank reduction techniques and it will be referred to as 2EB-AT case.

4.4.3. Phase Distortion (PD) Case

In practical implementations, due to the non-ideal cabling, non identical fabrication of beam-former hardwares and different thermal characteristics of the materials, it is impossible to have phase equivalent receiver channels. These practical issues cause frequency dependent

phase distortions on receiver channels. In order to simplify the analyses, the radar is assumed to have a narrowband operation; thus, the phase distortions will be frequency independent (constant during the reception operation).

In the phase distortion (PD) case, the receiver channels are distorted by a Gaussian random phase with unity amplitude, which may degrade the performance of reduced rank STAP operation. The phase distortion is modeled as follows:

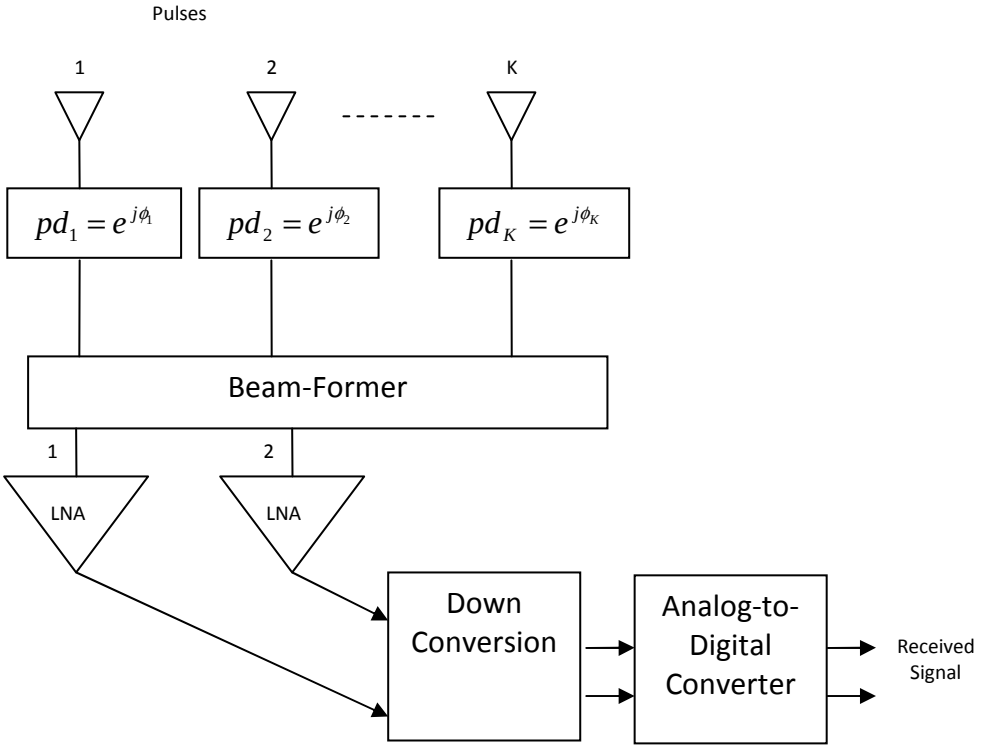

Figure 4-13 Phase distortion model

Here $pd_j = e^{j\phi_j}$ are random constant phases with unity amplitude and ϕ_j are Gaussian random variables with zero mean and certain variances which correspond to certain rms degree of errors. Performance under

two different phase error will be investigated. These errors have 5^o and 50^o rms values and will be referred to as LOW and HIGH phase distortions.

A pre-defined or structured covariance matrix cannot be informed of these phase errors. However, a system which uses sample matrix and Sample Matrix Inversion (SMI) is able to estimate these errors in order to improve the performance. Sample Matrix Inversion is a term which indicates that the clutter plus noise covariance matrix is estimated from the collected data, and its inverse is directly used in detection operation defined in (3-4), [5], [7]. The eigenvalue nulling performances of PD cases under pre-defined covariance matrix and sample matrix conditions are illustrated in Figure 4-14:

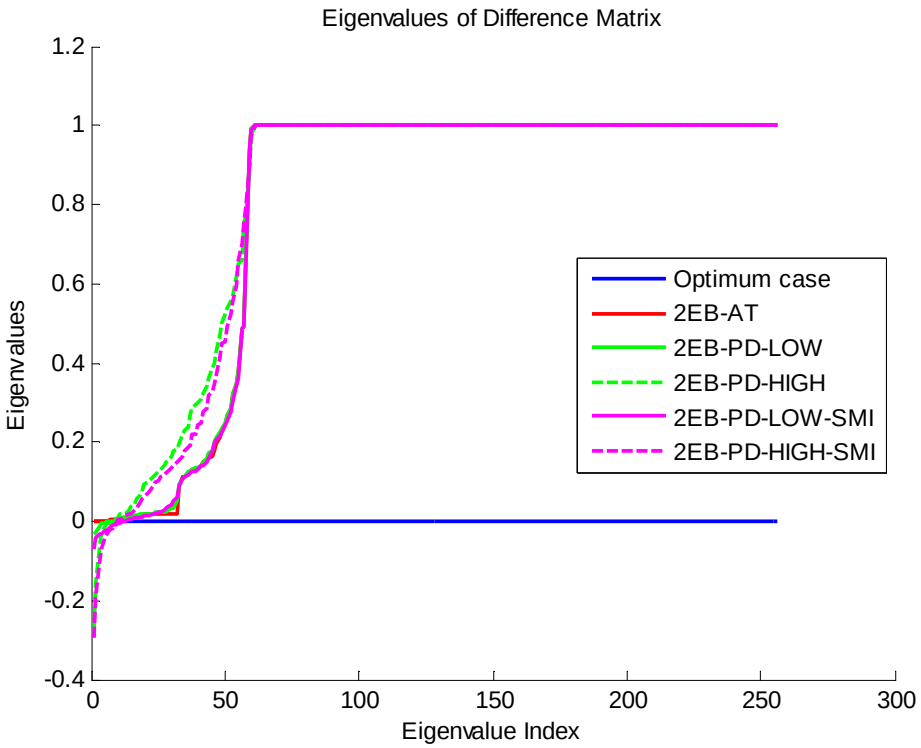

Figure 4-14 Eigenvalues of difference matrices in PD cases

It can be seen from Figure 4-14 that, eigenvalue nulling of low phase error case (5^o) and high phase error case (50^o) is better if SMI is estimated and used as covariance matrix. The phase distortions applied in the simulation are shown in Table **4-4**:

Table 4-4 Phase distortions

	5^o	50^o		5^o	50^o
Channel 1	-1.5230	40.1445	Channel 9	6.9676	28.7421
Channel 2	-8.7700	0.9076	Channel 10	-0.6159	-1.6524
Channel 3	-6.9641	39.6720	Channel 11	-1.8547	28.1665
Channel 4	-3.3450	-61.0013	Channel 12	1.5842	-98.1329
Channel 5	-7.1018	13.9161	Channel 13	-3.1472	17.4780
Channel 6	-8.9707	-31.6199	Channel 14	-4.2940	99.0134
Channel 7	-2.1531	-9.2784	Channel 15	-7.9950	-50.7836
Channel 8	2.6744	114.5373	Channel 16	-5.9756	-71.1882

It is expected to have greater SCNR losses in pre-defined covariance matrix cases. Because, the covariance matrix is defined without the knowledge of the phase distortions and can not correct these distortions. This effect can be seen from Figure 4-15 (one simulation is performed using the phase distortions in Table **4-4**):

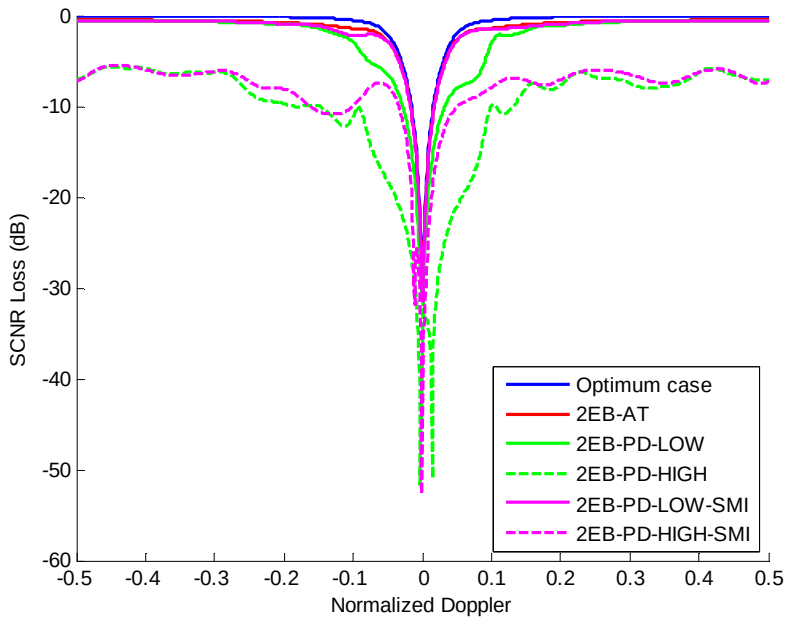

Figure 4-15 SCNR loss in PD cases

The performance of low phase error case with SMI is very close to the performance of ideal two eigen-beam (2EB) case. As can be seen from Figure 4-15, estimating the covariance matrix and using SMI in the calculations increases the performance of reduced rank STAP. Especially there is a significant improvement in endo-clutter performance which can be observed in Figure 4-16:

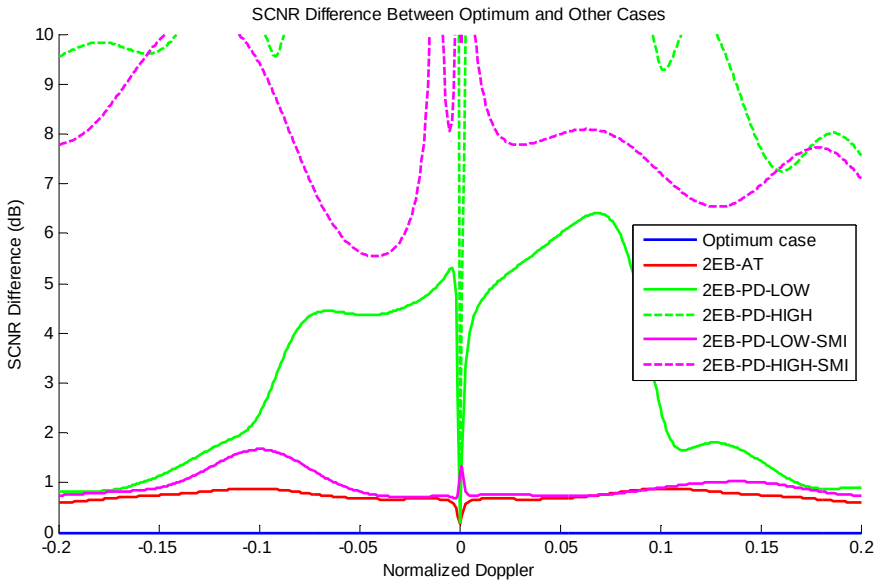

Figure 4-16 SCNR difference between optimum PD cases

Using SMI increases the endo-clutter performance in both low and high PD cases. The endo-clutter performance of the PD-LOW-SMI case is very similar to that of 2EB-AT case, which indicates that two eigen-beam approach can tolerate 5^{o} rms phase distortions. The phase distortion immunity concept is out of the scope of this work and will not be discussed further.

4.4.4. Internal Clutter Motion (ICM) Case

The ground targets can be considered to be stationary and does not have a Doppler spread around the frequency spectrum. However, in a windy environment, the trees, leaves and other elastic objects will move with the randomly directed wind force, which will cause a random Doppler shift in the clutter spectrum. In the Internal Clutter Motion (ICM) case, the Doppler spread caused by the wind will be considered. This spread broadens the clutter spectrum and in [11] it is investigated in detail.

By analyzing the measurements in [11], the authors determine a clutter spectrum function as indicated in (4-31):

$$P_c(f)=\frac{r}{r+1}\delta(f)+\frac{1}{r+1}\frac{b\lambda}{4}e^{-\frac{b\lambda}{2}|f|}. \quad (4\text{-}31)$$

In (4-31), the first term is considered as a DC term and the second one as an AC term. The parameter r represents the power ratio between DC and AC components and can be found from (4-32):

$$10\log(r)=-15.5\log(w)-12.1\log(f_c)+63.2. \quad (4\text{-}32)$$

Here w is wind speed in miles per hour, f_c is the carrier frequency in GHz and the logarithms are base 10. By taking inverse Fourier Transform of the spectrum, auto-correlation function can be obtained as in (4-34):

$$r_c(\tau)=\int_{-\infty}^{\infty}P_c(f)e^{j2\pi f\tau}df, \quad (4\text{-}33)$$

$$r_c(\tau)=\frac{r}{r+1}+\frac{1}{r+1}\frac{(b\lambda)^2}{(b\lambda)^2+(4\pi\tau)^2}. \quad (4\text{-}34)$$

Since the ICM is a temporal decorrelation and has an auto-correlation function, this decorrelation can be modeled as a covariance matrix taper in temporal covariance matrix and its effect changes from pulse-to-pulse (but not channel-to-channel).

$$\mathbf{T_{ij}}=r_c\left((i-j)T_p\right). \quad (4\text{-}35)$$

Here in (4-35), T_{ij} is the ij th entry of temporal covariance matrix taper and T_p is the pulse repetition interval.

Overall space-time covariance matrix taper can be found with (4-36):

$$\mathbf{T_{ST}}=\mathbf{T}\otimes\mathbf{1_{KxK}}, \quad (4\text{-}36)$$

where $\mathbf{T}_{\mathbf{ST}}$ is the space-time covariance matrix taper, $\mathbf{T}$ is the temporal covariance matrix taper, $\mathbf{1}_{\mathbf{KxK}}$ is a matrix of size KxK with all ones and $\otimes$ represents the Kronecker product operation.

The covariance matrix taper is determined with using the parameters in Table 4-5:

Table 4-5 ICM parameters

Parameter Symbol	Parameter	Value
f_c	Operating Frequency	7.5 GHz
w	Wind Speed	15 miles/hour
T_p	Pulse Repetition Interval	100 microseconds

The covariance matrix taper obtained from (4-36) is illustrated in Figure 4-17:

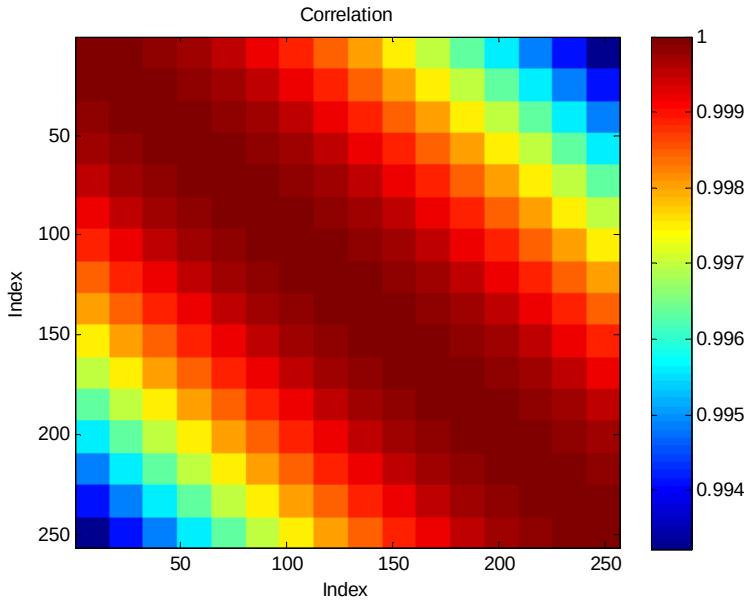

Figure 4-17 ICM covariance tapering matrix

The ICM effect can be observed by applying the operation in (4-36) to the covariance matrix:

$$\mathbf{R}_{\mathbf{ICM}} = \mathbf{R} \circ \mathbf{T}_{\mathbf{ST}}, \tag{4-37}$$

where $\mathbf{R}_{\mathbf{ICM}}$ is the tapered covariance matrix (ICM covariance matrix) and $\circ$ represents the Hadamard product operation.

Similar to phase distortion (PD) case, if a pre-defined covariance matrix is used, without the knowledge of the ICM, the performance will degrade significantly. However, using SMI provides the knowledge of a possible ICM and decreases its effect. The eigenvalue nulling performance of ICM case can be seen in Figure 4-18:

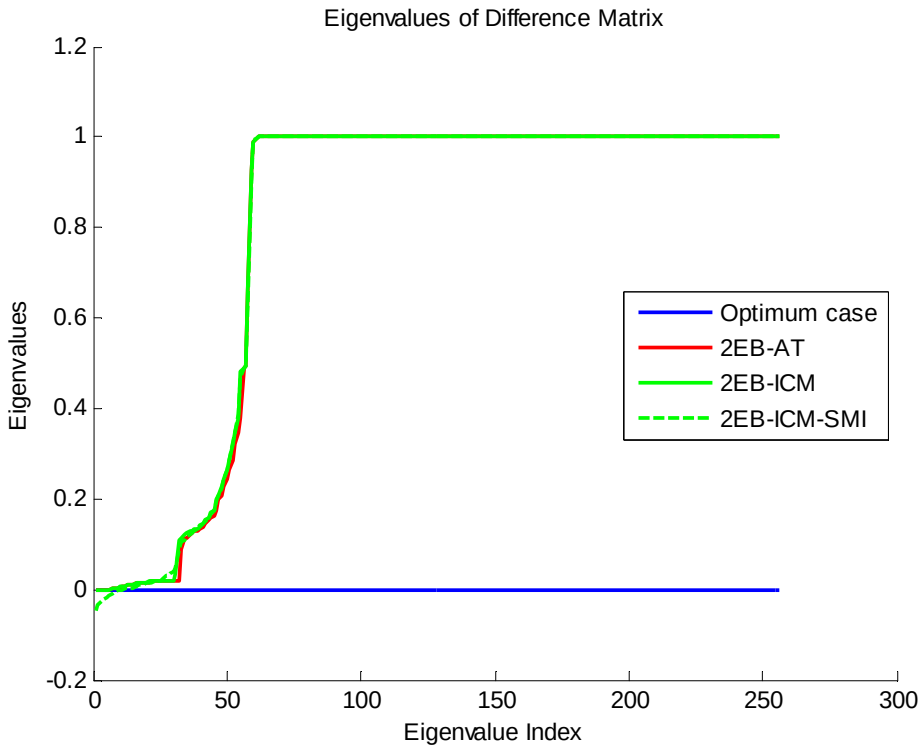

Figure 4-18 Eigenvalues of difference matrices in ICM cases

The eigenvalue nulling in Figure 4-18 seems to degrade slightly, when there is an ICM. SCNR losses in ICM case are illustrated in Figure 4-19:

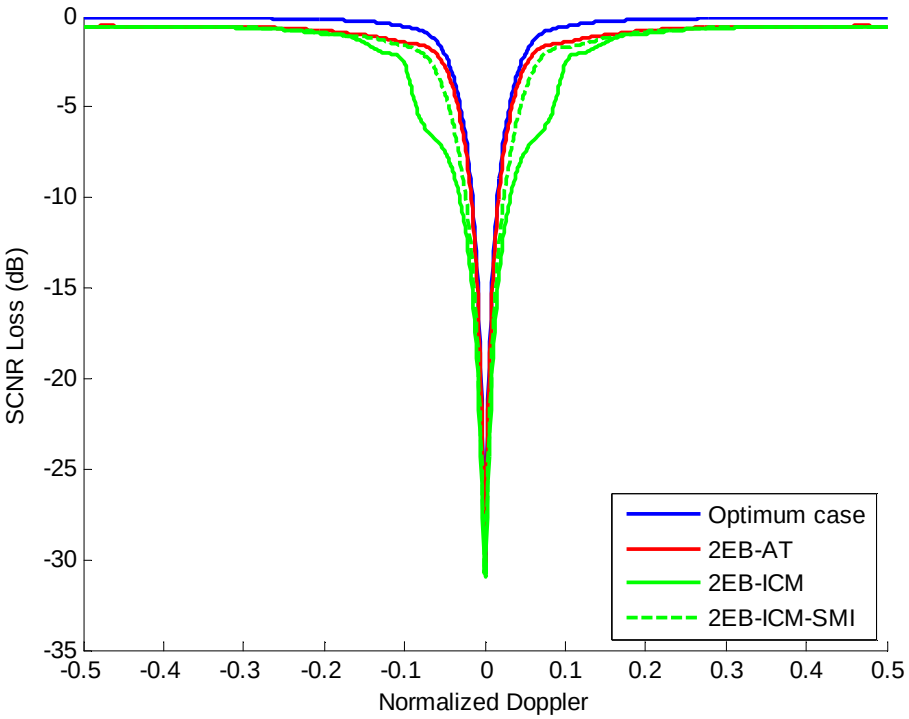

Figure 4-19 SCNR loss in ICM cases

As expected, using a pre-defined covariance matrix caused significant SCNR losses. The performance of ICM with an estimation of SMI is very close to the ideal two eigen-beam case, but they are not equal. Because, internal clutter motions spreads the clutter spectrum further and increases the clutter power in higher Doppler shifts. Thus, even if the SMI is estimated, because of this extra Doppler spread, two eigen-beam performance without the ICM cannot be achieved in ICM case.

A closer look to the endo-clutter SCNR performance in Figure 4-20 supports this conclusion:

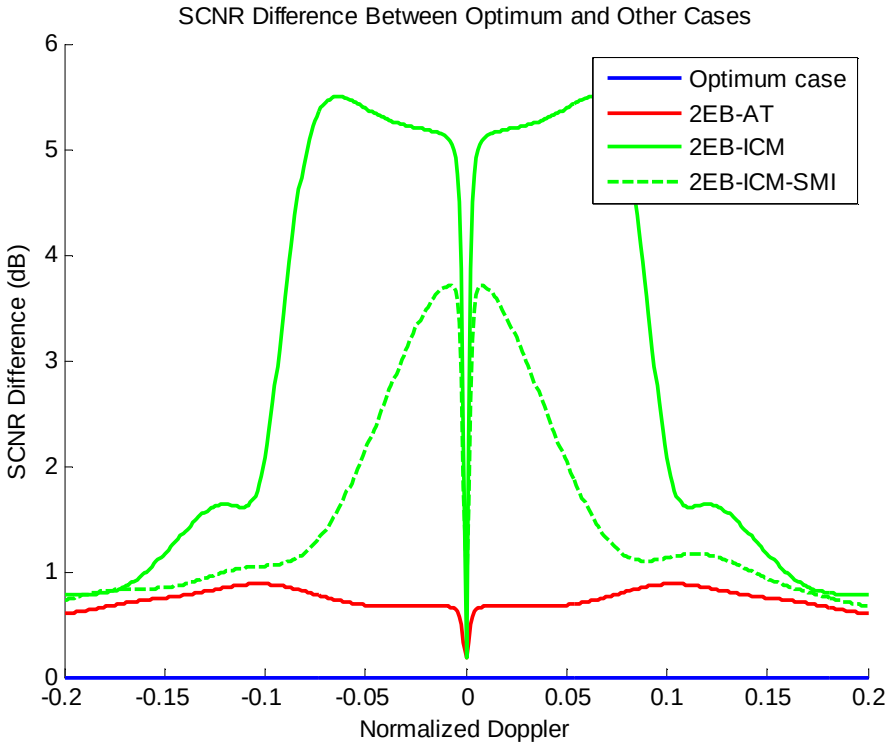

Figure 4-20 SCNR difference between optimum ICM cases

It can be seen from Figure 4-20 that estimating SMI increases the performance in windy conditions; however, 2EB-AT performance is not achieved due to the extra Doppler spread caused by ICM. But after a certain normalized Doppler value (around 0.1) their performances become very similar because the effect of the spread vanishes.

4.5. Performance Comparisons of Eigen-Beams and Other Beam Patterns

In this section, two eigen-beam approach is compared to one eigen-beam and three eigen-beam approaches, in order to find the minimum number of eigen-beams, which is needed to have a reasonable endo-clutter GMTI

performance. In addition, two eigen-beam case will be compared to the ADPCA and other two channel cases to reveal any performance differences between those two channel GMTI techniques.

4.5.1. Comparison to One and Three Eigen-Beam Approaches

In one eigen-beam case (which is a one channel GMTI technique), the eigenvector corresponding to the greatest eigenvalue is selected as the beam-pattern. Similarly, in three eigen-beam case, the eigenvectors corresponding to the three largest eigenvalues are selected as beam patterns. In Figure 4-21 and Figure 4-22, the beam patterns of one and three eigen-beam cases can be observed, respectively:

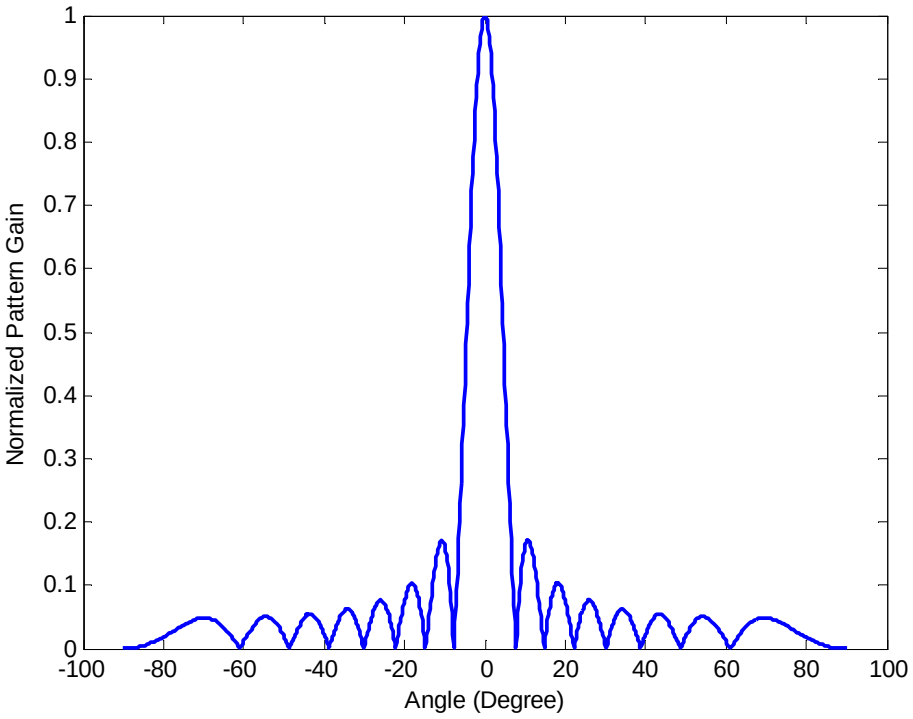

Figure 4-21 Beam pattern of one eigen-beam (1 EB) case

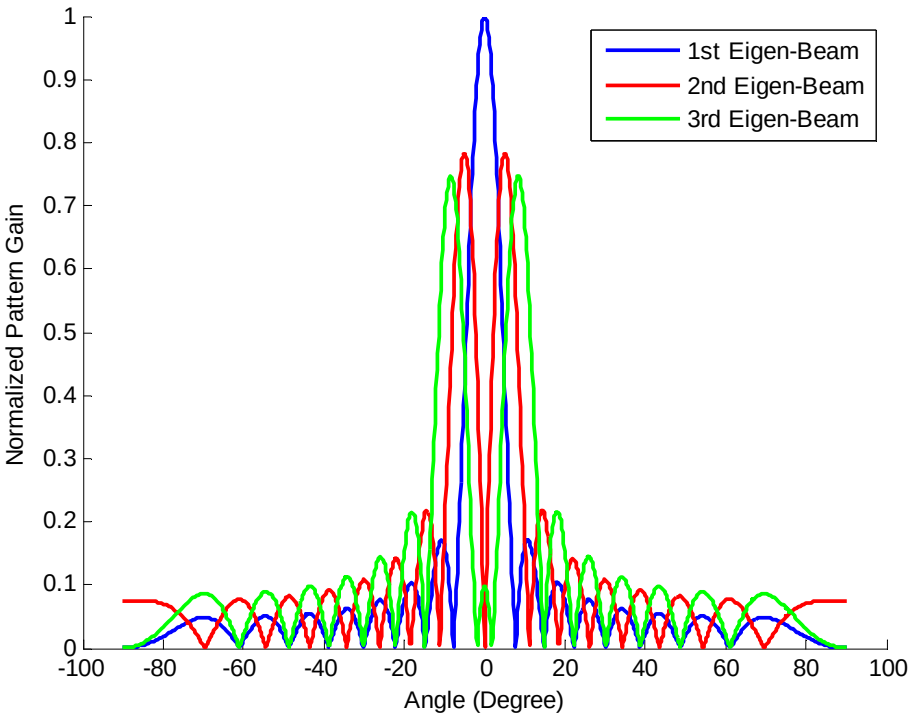

Figure 4-22 Beam patterns of three eigen-beam (3 EB) case

In Figure 4-22, 1st Eigen-Beam refers to the eigenvector with greatest eigenvalue.

Using the patterns defined for one and three eigen-beam case, the eigenvalue nulling performance comparison of eigen-beam cases can be done (under no phase distortion and ICM) as illustrated in Figure 4-23:

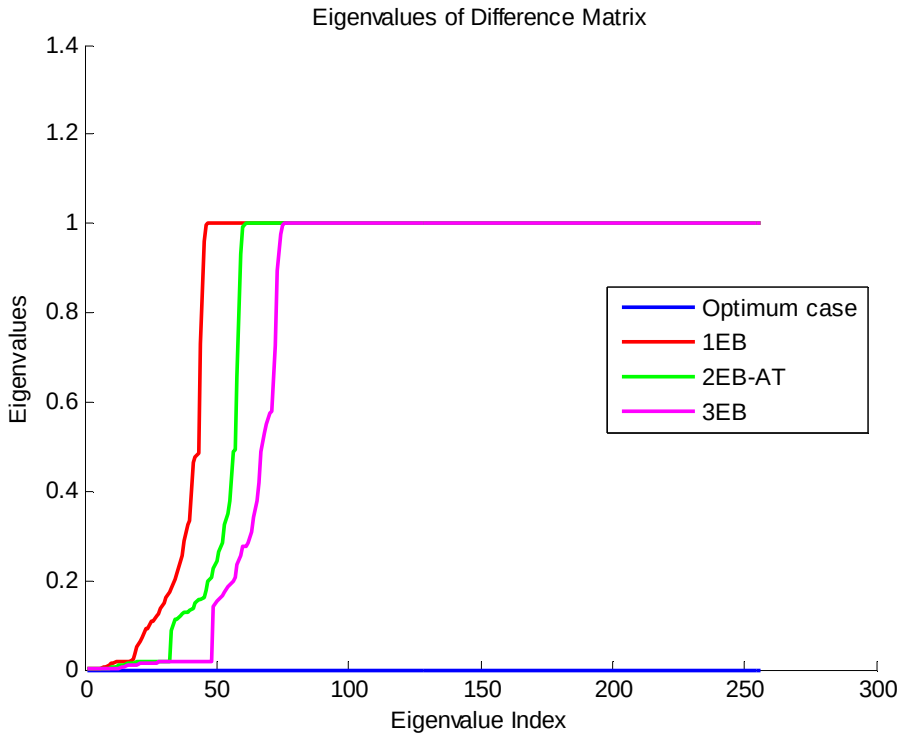

Figure 4-23 Eigenvalue nulling performances of eigen-beam approaches

It can be seen from Figure 4-23 that, eigen-value nulling performance increases as the number of eigen-beams increases. It is shown in (3-34) that the clutter covariance matrix is not of full rank (the number of non-zero eigenvalues is not equal to the number of DoFs). This property implies that for some number of eigen-beams, the endo-clutter performance approaches to the optimum SCNR bound.

We can see the results of this property in Figure 4-24 and Figure 4-25:

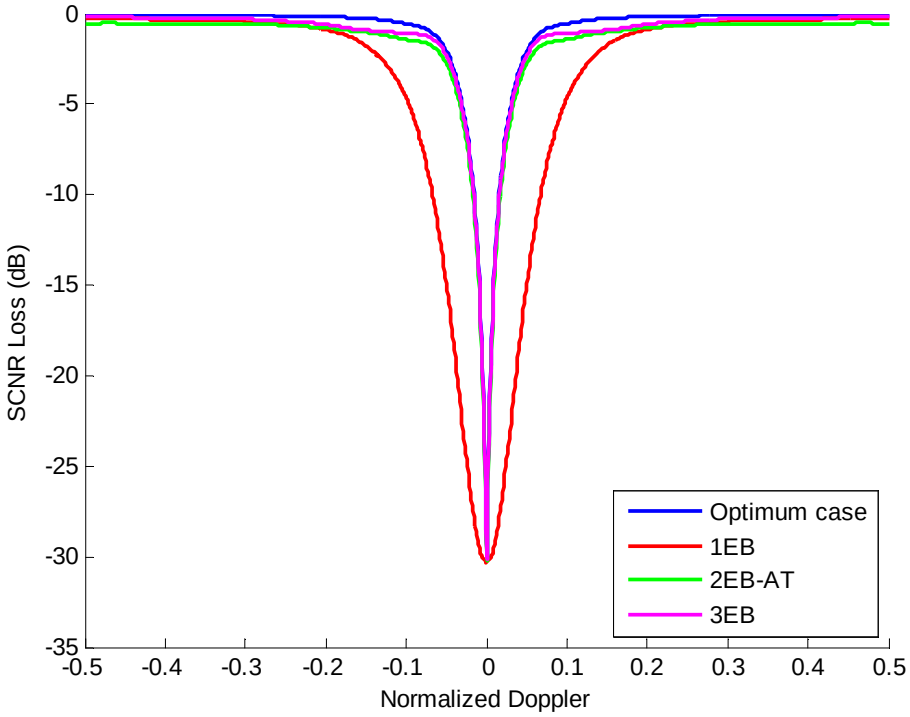

Figure 4-24 SCNR bounds for eigen-beam cases

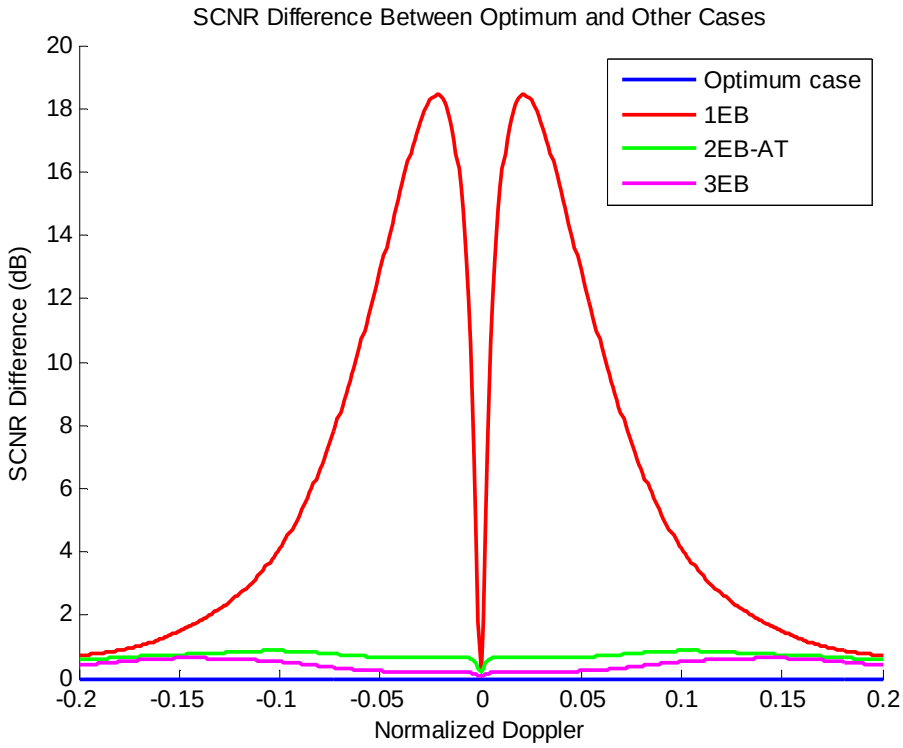

Figure 4-25 SCNR bounds for eigen-beam cases

In Figure 4-25, we can observe that the endo-clutter performance increases significantly, if we use two eigen-beams rather than one. However, increasing it further does not improve the performance high enough to compensate the cost of designing a three channel receiver and signal processor.

4.5.2. Comparison to ADPCA and Other Two Channel Approaches

In ADPCA case, two gain-identical beams (which are displaced in space) are constituted without using the knowledge of eigenvectors.

The antenna pattern used in ADPCA case is shown in Figure 4-26:

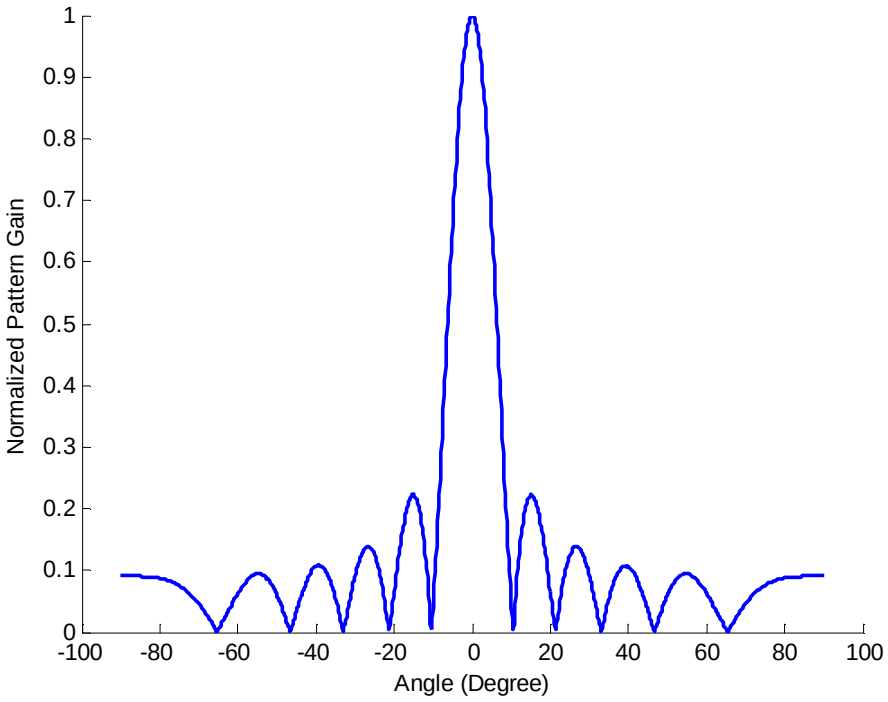

Figure 4-26 Antenna pattern of ADPCA case

Using the beam patterns above, we will get eigenvalue nulling performances illustrated in Figure 4-27:

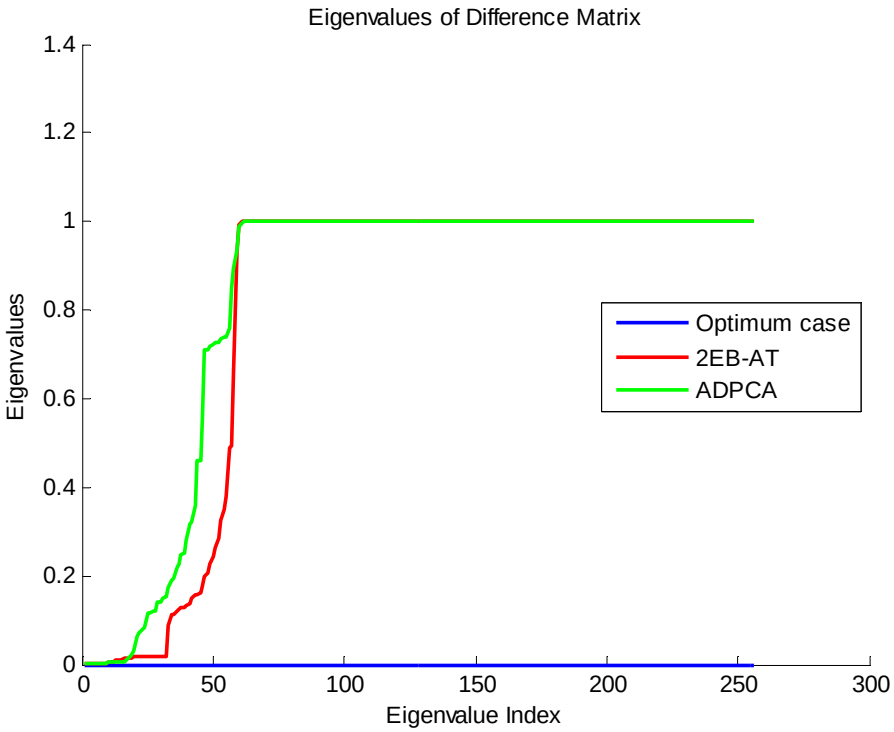

Figure 4-27 Differenece matrix comparison of the two eigen-beams and ADPCA case

It can be seen in Figure 4-27 that ADPCA eigenvalue nulling performance is worse than that of the two eigen-beam case. SCNR bound performances in Figure 4-28 and Figure 4-29 give a more direct idea about these approaches:

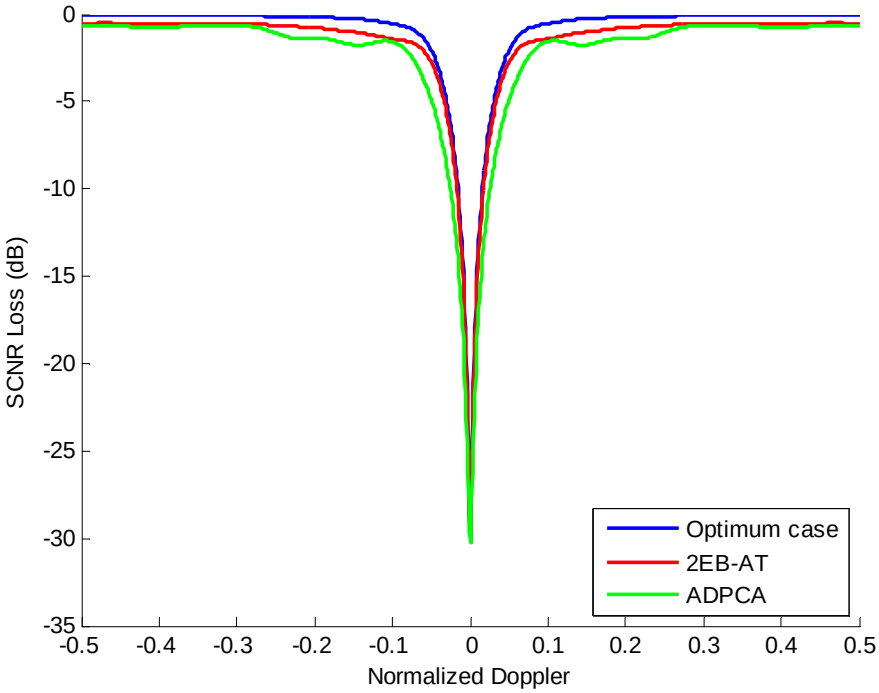

Figure 4-28 SCNR loss comparison

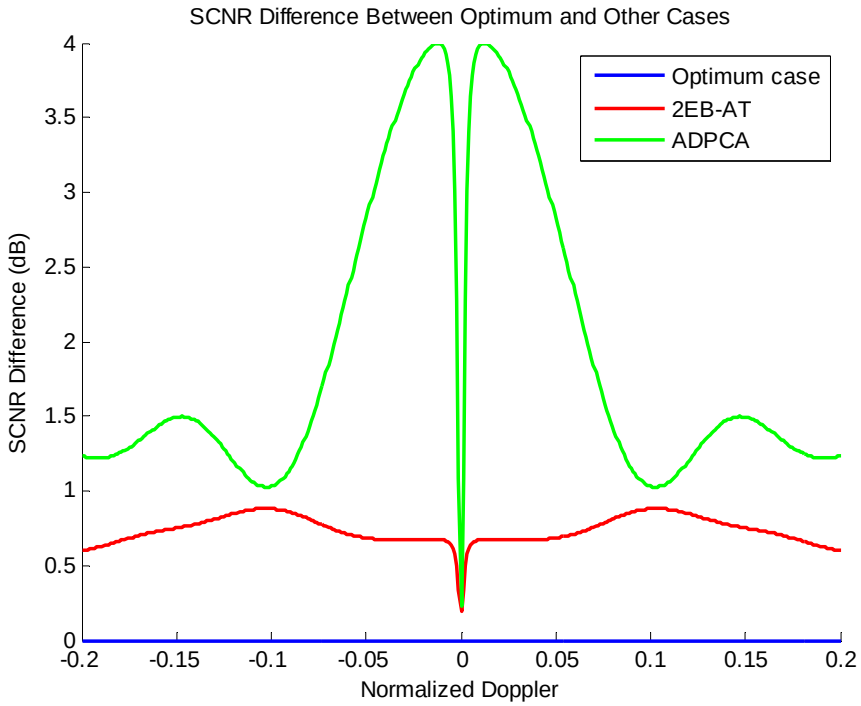

Figure 4-29 SCNR difference comparison between optimum and other cases

In Figure 4-29, endo-clutter performance of two eigen-beam case is better than the ADPCA case, if the patterns of ADPCA are selected without the knowledge of clutter statistics.

Consider a linear combination of the beam-forming weights of two eigen-beam case as defined in (4-38) and (4-39):

$$\mathbf{w}_{\mathrm{ADPCA\_1}} = \kappa\left(\mathbf{w}_1 + \mathbf{w}_2\right), \tag{4-38}$$

$$\mathbf{w}_{\mathrm{ADPCA\_2}} = \kappa\left(\mathbf{w}_1 - \mathbf{w}_2\right), \tag{4-39}$$

$$\kappa = \sqrt{\frac{1}{2}}. \tag{4-40}$$

Here, $\mathbf{w}_{\mathrm{ADPCA\_1}}$ and $\mathbf{w}_{\mathrm{ADPCA\_2}}$ are beam-forming weights in ADPCA case, $\mathbf{w}_1$ and $\mathbf{w}_2$ are beam-forming weights of two eigen-beams and κ is normalizing coefficient which satisfies the constraints defined in Section 4.2.

The ADPCA beam that is constituted with the beam-forming weights in (4-38) and (4-39) is given in Figure 4-30:

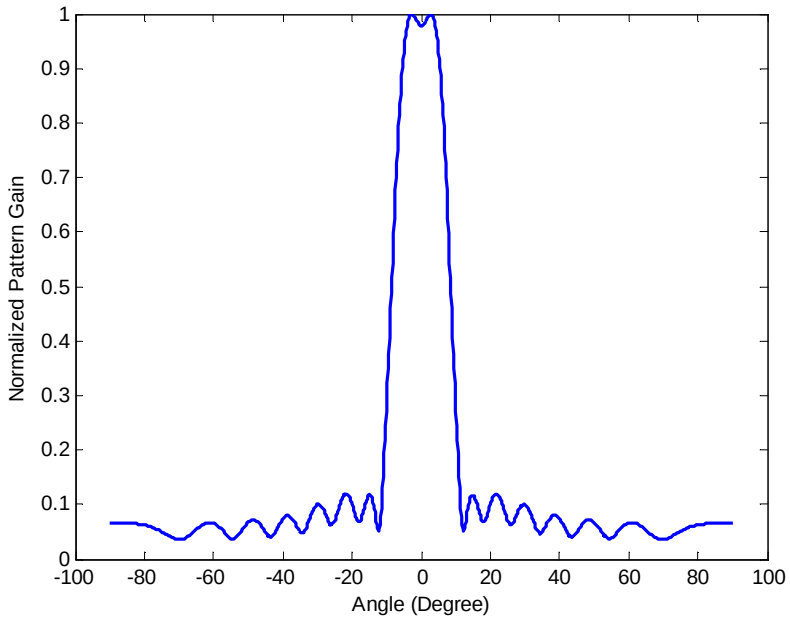

Figure 4-30 Beam pattern of ADPCA obtained with linear combination

Two eigen-beam and ADPCA eigenvalue nulling performance obtained by linear combination patterns are shown in Figure 4-31:

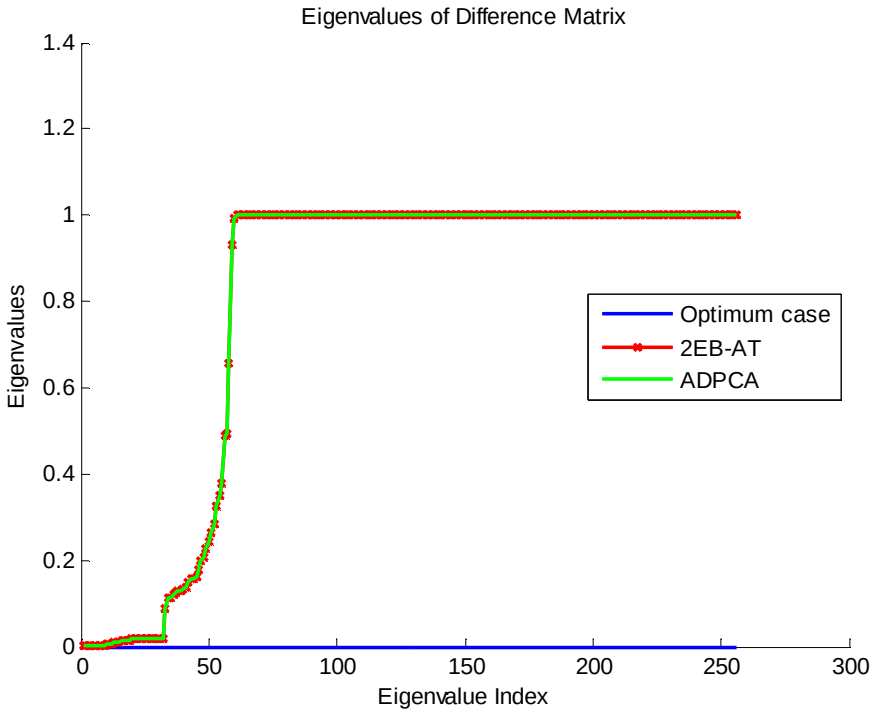

Figure 4-31 Difference matrix comparison

The difference matrix eigenvalues of two eigen-beam and ADPCA cases are very similar to each other.

However, the SCNR graphs in Figure 4-32 and Figure 4-33 will give more information:

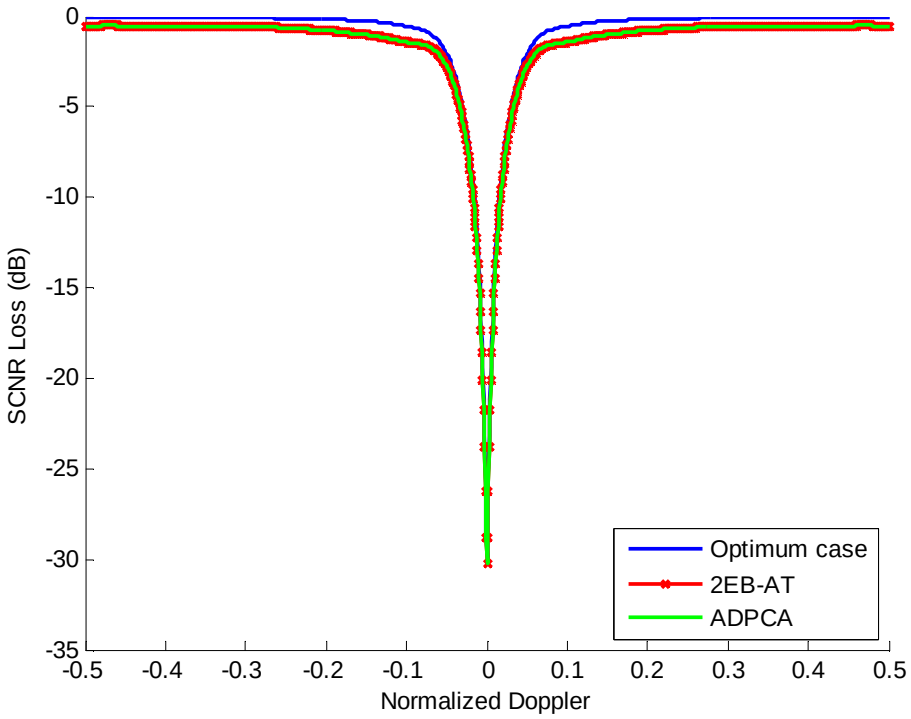

Figure 4-32 SCNR loss comparison

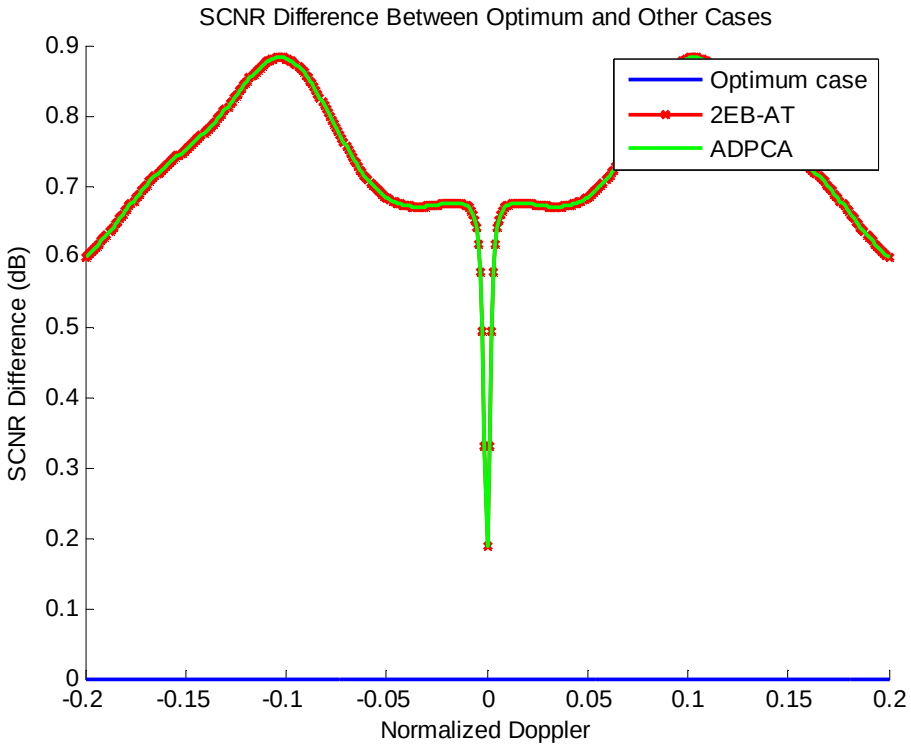

Figure 4-33 SCNR difference comparison

Figure 4-32 and Figure 4-33 show that, by linearly combining the eigen-beams and applying the constraints, the two eigen-beam and ADPCA cases have exactly the same performance both in endo-clutter and exo-clutter conditions.

In addition to ADPCA case, the performance of a general linear combination case can be investigated, whether it gives the same performance or not, by conducting an analytic analyses.

Consider beam-former matrices of eigen-beam (EB) and combination (CB) cases as shown in (4-41) and (4-42), respectively:

$$\mathbf{B}_{\mathbf{EB}} = \begin{bmatrix} \mathbf{w}_1 & \mathbf{w}_2 & \cdots & \mathbf{0}_{\mathbf{Kx1}} & \mathbf{0}_{\mathbf{Kx1}} \\ \mathbf{0}_{\mathbf{Kx1}} & \mathbf{0}_{\mathbf{Kx1}} & \cdots & \vdots & \vdots \\ \vdots & \vdots & \cdots & \mathbf{0}_{\mathbf{Kx1}} & \mathbf{0}_{\mathbf{Kx1}} \\ \mathbf{0}_{\mathbf{Kx1}} & \mathbf{0}_{\mathbf{Kx1}} & \cdots & \mathbf{w}_1 & \mathbf{w}_2 \end{bmatrix}, \tag{4-41}$$

$$\mathbf{B}_{\mathbf{CB}} = \begin{bmatrix} \kappa(a\mathbf{w}_1 + b\mathbf{w}_2) & \kappa(b\mathbf{w}_1 - a\mathbf{w}_2) & \cdots & \mathbf{0}_{\mathbf{Kx1}} & \mathbf{0}_{\mathbf{Kx1}} \\ \mathbf{0}_{\mathbf{Kx1}} & \mathbf{0}_{\mathbf{Kx1}} & \cdots & \vdots & \vdots \\ \vdots & \vdots & \cdots & \mathbf{0}_{\mathbf{Kx1}} & \mathbf{0}_{\mathbf{Kx1}} \\ \mathbf{0}_{\mathbf{Kx1}} & \mathbf{0}_{\mathbf{Kx1}} & \cdots & \kappa(a\mathbf{w}_1 + b\mathbf{w}_2) & \kappa(b\mathbf{w}_1 - a\mathbf{w}_2) \end{bmatrix}. \tag{4-42}$$

Here a and b are arbitrary real numbers and κ is the normalizing coefficient and its value can be found as in (4-43):

$$\kappa = \sqrt{\frac{1}{a^2 + b^2}}. \tag{4-43}$$

We know that since $\mathbf{w}_1$ and $\mathbf{w}_2$ are eigenvectors, they are orthogonal. This orthogonality provides the following property in (4-45):

$$\mathbf{B}_{\mathbf{EB}}^{\mathbf{H}}\mathbf{B}_{\mathbf{EB}} = \begin{bmatrix} \mathbf{w}_1^{\mathbf{H}}\mathbf{w}_1 & \mathbf{w}_1^{\mathbf{H}}\mathbf{w}_2 & \cdots & 0 & 0 \\ \mathbf{w}_2^{\mathbf{H}}\mathbf{w}_1 & \mathbf{w}_2^{\mathbf{H}}\mathbf{w}_2 & \cdots & \vdots & \vdots \\ \vdots & \vdots & \cdots & \mathbf{w}_1^{\mathbf{H}}\mathbf{w}_1 & \mathbf{w}_1^{\mathbf{H}}\mathbf{w}_2 \\ 0 & 0 & \cdots & \mathbf{w}_2^{\mathbf{H}}\mathbf{w}_1 & \mathbf{w}_2^{\mathbf{H}}\mathbf{w}_2 \end{bmatrix}, \tag{4-44}$$

$$\mathbf{B}_{\mathbf{EB}}^{\mathbf{H}}\mathbf{B}_{\mathbf{EB}} = \begin{bmatrix} 1 & 0 & \cdots & 0 & 0 \\ 0 & 1 & \cdots & \vdots & \vdots \\ \vdots & \vdots & \cdots & 1 & 0 \\ 0 & 0 & \cdots & 0 & 1 \end{bmatrix} = \mathbf{I}_{\mathbf{2Nx2N}}. \tag{4-45}$$

Similarly, we can prove that the combination definition in (4-42) also provides two orthogonal beam-former weights.

Consider the dot product in (4-46):

$$\left(\kappa\left(a\mathbf{w_1}+b\mathbf{w_2}\right)\right)^{\mathbf{H}}\kappa\left(b\mathbf{w_1}-a\mathbf{w_2}\right). \tag{4-46}$$

$$\kappa\left(abw_1^H w_1 - a^2 w_1^H w_2 - b^2 w_2^H w_1 + abw_2^H w_2\right) \tag{4-47}$$

$$\kappa\left(ab-0-0+ab\right)=0 \tag{4-48}$$

It can be seen from (4-48), the combination pattern is also orthogonal and the property defined for $\mathbf{B_{EB}}$ in (4-45) is also valid for $\mathbf{B_{CB}}$.

For another property, consider the following matrix multiplication defined in (4-49):

$$\mathbf{B}_{\mathbf{CB}}^{\mathbf{H}}\mathbf{B}_{\mathbf{EB}}=\begin{bmatrix}\mathbf{A}_{\kappa} & \mathbf{0}_{2x2} & \cdots & \mathbf{0}_{2x2}\\ \mathbf{0}_{2x2} & \mathbf{A}_{\kappa} & \ddots & \vdots\\ \vdots & \ddots & \ddots & \mathbf{0}_{2x2}\\ \mathbf{0}_{2x2} & \cdots & \mathbf{0}_{2x2} & \mathbf{A}_{\kappa}\end{bmatrix}, \tag{4-49}$$

$$\mathbf{A}_{\kappa}=\begin{bmatrix}\kappa a & \kappa b\\ \kappa b & -\kappa a\end{bmatrix}, \tag{4-50}$$

$$\mathbf{B}_{\mathbf{CB}}^{\mathbf{H}}\mathbf{B}_{\mathbf{EB}}=\mathbf{B}_{\mathbf{EB}}^{\mathbf{H}}\mathbf{B}_{\mathbf{CB}}. \tag{4-51}$$

The matrix defined in (4-49) is a Hermitian matrix with a block diagonal matrix form. Its inverse is simple to find, which is indicated in (4-52):

$$\left(\mathbf{B}_{\mathbf{CB}}^{\mathbf{H}}\mathbf{B}_{\mathbf{EB}}\right)^{-1}=\begin{bmatrix}\mathbf{A}_{\kappa}^{-1} & \mathbf{0}_{2x2} & \cdots & \mathbf{0}_{2x2}\\ \mathbf{0}_{2x2} & \mathbf{A}_{\kappa}^{-1} & \ddots & \vdots\\ \vdots & \ddots & \ddots & \mathbf{0}_{2x2}\\ \mathbf{0}_{2x2} & \cdots & \mathbf{0}_{2x2} & \mathbf{A}_{\kappa}^{-1}\end{bmatrix}. \tag{4-52}$$

An interesting property of matrix $\mathbf{A}_{\kappa}$ can be used to find the analytic inverse of the matrix $\mathbf{B}_{\mathbf{CB}}^{\mathbf{H}}\mathbf{B}_{\mathbf{EB}}$ which is given in (4-56):

$$\mathbf{A}_{\kappa}^{-1} = \frac{1}{-\kappa^2\left(a^2+b^2\right)}\begin{bmatrix} -\kappa a & -\kappa b \\ -\kappa b & \kappa a \end{bmatrix}, \tag{4-53}$$

$$\mathbf{A}_{\kappa}^{-1} = \frac{1}{-\left(\frac{1}{\sqrt{\left(a^2+b^2\right)}}\right)^2\left(a^2+b^2\right)}\begin{bmatrix} -\kappa a & -\kappa b \\ -\kappa b & \kappa a \end{bmatrix}, \tag{4-54}$$

$$\mathbf{A}_{\kappa}^{-1} = \begin{bmatrix} \kappa a & \kappa b \\ \kappa b & -\kappa a \end{bmatrix} = \mathbf{A}_{\kappa}, \tag{4-55}$$

$$\left(\mathbf{B}_{\mathbf{CB}}^{\mathbf{H}}\mathbf{B}_{\mathbf{EB}}\right)^{-1} = \mathbf{B}_{\mathbf{CB}}^{\mathbf{H}}\mathbf{B}_{\mathbf{EB}}. \tag{4-56}$$

As indicated by (4-55), the matrix $\mathbf{A}_{\kappa}$ is a unitary matrix. It is clear that matrix $\mathbf{B}_{\mathbf{CB}}^{\mathbf{H}}\mathbf{B}_{\mathbf{EB}}$ is also a unitary matrix.

Then we can define the following equalities in (4-57) and (4-58), by using unitary and Hermitian properties:

$$\mathbf{I}_{\mathbf{2Nx2N}} = \mathbf{B}_{\mathbf{CB}}^{\mathbf{H}}\mathbf{B}_{\mathbf{EB}}\left(\mathbf{B}_{\mathbf{CB}}^{\mathbf{H}}\mathbf{B}_{\mathbf{EB}}\right)^{-1} = \mathbf{B}_{\mathbf{CB}}^{\mathbf{H}}\mathbf{B}_{\mathbf{EB}}\mathbf{B}_{\mathbf{EB}}^{\mathbf{H}}\mathbf{B}_{\mathbf{CB}} = \mathbf{B}_{\mathbf{EB}}^{\mathbf{H}}\mathbf{B}_{\mathbf{CB}}\mathbf{B}_{\mathbf{CB}}^{\mathbf{H}}\mathbf{B}_{\mathbf{EB}}, \tag{4-57}$$

$$\mathbf{B}_{\mathbf{CB}}^{\mathbf{H}} = \mathbf{B}_{\mathbf{CB}}^{\mathbf{H}}\mathbf{B}_{\mathbf{EB}}\mathbf{B}_{\mathbf{EB}}^{\mathbf{H}} \tag{4-58}$$

Now we can prove the equivalence in performances of two eigen-beam and combination cases. $\mathbf{R}_{\mathbf{difference\_EB}}$ and $\mathbf{R}_{\mathbf{difference\_CB}}$ are the difference matrices of two eigen-beam case and combination cases, respectively. In order to give the same performance, they must be equivalent; thus starting from the difference matrix of two eigen-beam case in (4-59), we can derive the desired result:

$$\mathbf{R}_{\mathbf{difference\_EB}} = \mathbf{R}^{-1} - \mathbf{B}_{\mathbf{EB}}\left(\mathbf{B}_{\mathbf{EB}}^{\mathbf{H}}\left(\mathbf{R}_{\mathbf{c}} + \sigma_n^2\mathbf{I}\right)\mathbf{B}_{\mathbf{EB}}\right)^{-1}\mathbf{B}_{\mathbf{EB}}^{\mathbf{H}}, \tag{4-59}$$

We can insert two identity matrices without violating any equality and then we can substitute (4-57) and (4-58) instead of identity matrices as shown in (4-60), (4-61) and (4-62):

$$\mathbf{R}_{\mathbf{difference\_EB}} = \mathbf{R}^{-1} - \mathbf{B}_{\mathbf{EB}}\left(\mathbf{I}_{\mathbf{2Nx2N}}\mathbf{B}_{\mathbf{EB}}^{\mathbf{H}}\left(\mathbf{R}_{\mathbf{c}} + \sigma_n^2\mathbf{I}\right)\mathbf{B}_{\mathbf{EB}}\mathbf{I}_{\mathbf{2Nx2N}}\right)^{-1}\mathbf{B}_{\mathbf{EB}}^{\mathbf{H}}, \tag{4-60}$$

$$\mathbf{I}_{\mathbf{2Nx2N}}\mathbf{B}_{\mathbf{EB}}^{\mathbf{H}} = \mathbf{B}_{\mathbf{EB}}^{\mathbf{H}}\mathbf{B}_{\mathbf{CB}}\mathbf{B}_{\mathbf{CB}}^{\mathbf{H}}\mathbf{B}_{\mathbf{EB}}\mathbf{B}_{\mathbf{EB}}^{\mathbf{H}} = \mathbf{B}_{\mathbf{EB}}^{\mathbf{H}}\mathbf{B}_{\mathbf{CB}}\mathbf{B}_{\mathbf{CB}}^{\mathbf{H}}, \tag{4-61}$$

$$\mathbf{R}_{\mathbf{difference\_EB}} = \mathbf{R}^{-1} - \mathbf{B}_{\mathbf{EB}}\left(\mathbf{B}_{\mathbf{EB}}^{\mathbf{H}}\mathbf{B}_{\mathbf{CB}}\mathbf{B}_{\mathbf{CB}}^{\mathbf{H}}\left(\mathbf{R}_{\mathbf{c}} + \sigma_n^2\mathbf{I}\right)\mathbf{B}_{\mathbf{CB}}\mathbf{B}_{\mathbf{CB}}^{\mathbf{H}}\mathbf{B}_{\mathbf{EB}}\right)^{-1}\mathbf{B}_{\mathbf{EB}}^{\mathbf{H}}. \tag{4-62}$$

Using the unitary property of matrices $\mathbf{B}_{\mathbf{EB}}^{\mathbf{H}}\mathbf{B}_{\mathbf{CB}}$ and $\mathbf{B}_{\mathbf{CB}}^{\mathbf{H}}\mathbf{B}_{\mathbf{EB}}$ defined in (4-56), we can write the inverse of $\mathbf{B}_{\mathbf{EB}}^{\mathbf{H}}\mathbf{B}_{\mathbf{CB}}\mathbf{B}_{\mathbf{CB}}^{\mathbf{H}}\left(\mathbf{R}_{\mathbf{c}} + \sigma_n^2\mathbf{I}\right)\mathbf{B}_{\mathbf{CB}}\mathbf{B}_{\mathbf{CB}}^{\mathbf{H}}\mathbf{B}_{\mathbf{EB}}$ as:

$$\mathbf{R}_{\mathbf{difference\_EB}} = \mathbf{R}^{-1} - \mathbf{B}_{\mathbf{EB}}\left(\left(\mathbf{B}_{\mathbf{EB}}^{\mathbf{H}}\mathbf{B}_{\mathbf{CB}}\right)\mathbf{B}_{\mathbf{CB}}^{\mathbf{H}}\left(\mathbf{R}_{\mathbf{c}} + \sigma_n^2\mathbf{I}\right)\mathbf{B}_{\mathbf{CB}}\left(\mathbf{B}_{\mathbf{CB}}^{\mathbf{H}}\mathbf{B}_{\mathbf{EB}}\right)\right)^{-1}\mathbf{B}_{\mathbf{EB}}^{\mathbf{H}}, \tag{4-63}$$

$$\mathbf{R}_{\mathbf{difference\_EB}} = \mathbf{R}^{-1} - \mathbf{B}_{\mathbf{EB}}\left(\mathbf{B}_{\mathbf{EB}}^{\mathbf{H}}\mathbf{B}_{\mathbf{CB}}\right)^{-1}\left(\mathbf{B}_{\mathbf{CB}}^{\mathbf{H}}\left(\mathbf{R}_{\mathbf{c}} + \sigma_n^2\mathbf{I}\right)\mathbf{B}_{\mathbf{CB}}\right)^{-1}\left(\mathbf{B}_{\mathbf{CB}}^{\mathbf{H}}\mathbf{B}_{\mathbf{EB}}\right)^{-1}\mathbf{B}_{\mathbf{EB}}^{\mathbf{H}}, \tag{4-64}$$

$$\mathbf{R}_{\mathbf{difference\_EB}} = \mathbf{R}^{-1} - \mathbf{B}_{\mathbf{EB}}\mathbf{B}_{\mathbf{EB}}^{\mathbf{H}}\mathbf{B}_{\mathbf{CB}}\left(\mathbf{B}_{\mathbf{CB}}^{\mathbf{H}}\left(\mathbf{R}_{\mathbf{c}} + \sigma_n^2\mathbf{I}\right)\mathbf{B}_{\mathbf{CB}}\right)^{-1}\mathbf{B}_{\mathbf{CB}}^{\mathbf{H}}\mathbf{B}_{\mathbf{EB}}\mathbf{B}_{\mathbf{EB}}^{\mathbf{H}}. \tag{4-65}$$

Using the property defined in (4-58) we get the proof in (4-67):

$$\mathbf{R}_{\mathbf{difference\_EB}} = \mathbf{R}^{-1} - \mathbf{B}_{\mathbf{CB}}\left(\mathbf{B}_{\mathbf{CB}}^{\mathbf{H}}\left(\mathbf{R}_{\mathbf{c}} + \sigma_n^2\mathbf{I}\right)\mathbf{B}_{\mathbf{CB}}\right)^{-1}\mathbf{B}_{\mathbf{CB}}^{\mathbf{H}}, \tag{4-66}$$

$$\mathbf{R}_{\mathbf{difference\_EB}} = \mathbf{R}_{\mathbf{difference\_CB}}. \tag{4-67}$$

We have shown in (4-67) that the difference matrices of two cases (two eigen-beam and combination cases) are equal to each other. This implies that they have exactly the same performance.

In order to show this result numerically, let $a = 5$ and $b = 3$. The beam patterns in Figure 4-34 is obtained for that combination:

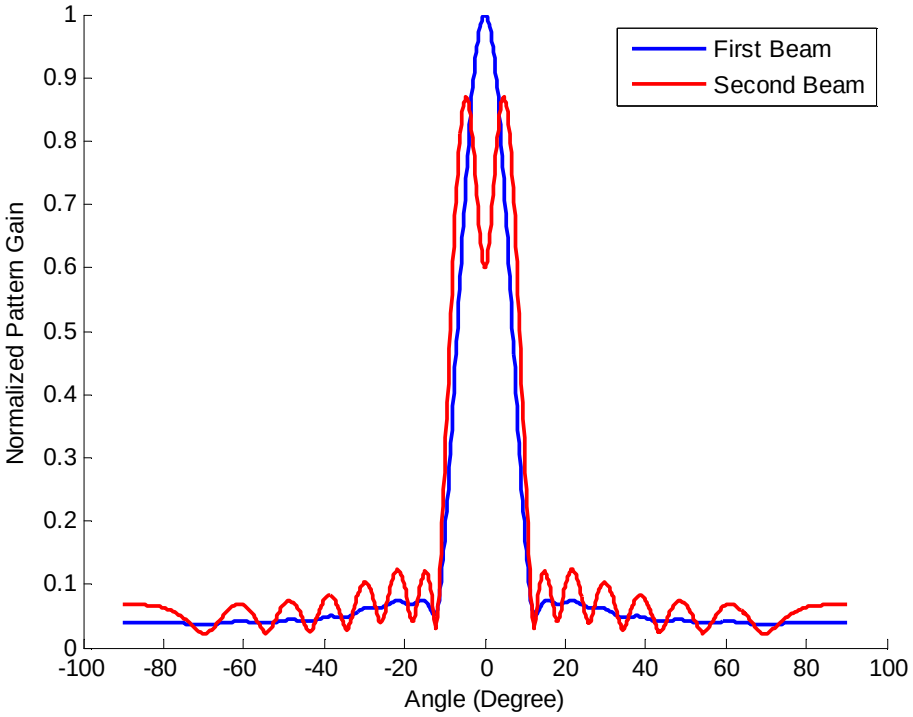

Figure 4-34 Beam patterns for combination (COMB) case

The eigenvalue nulling and SCNR bound performances of two eigen-beam and combination cases are given in Figure 4-35, Figure 4-36 and Figure 4-37:

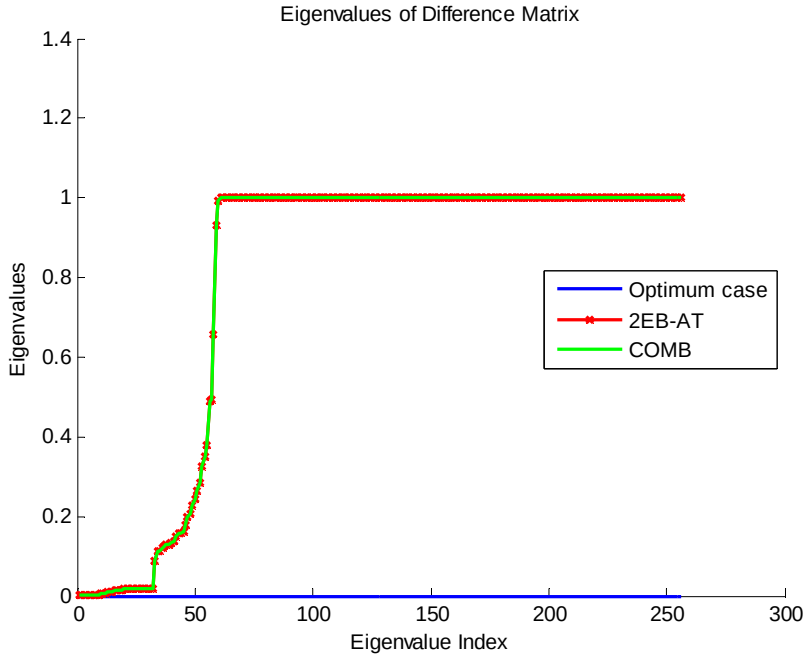

Figure 4-35 Difference matrix comparison in COMB case

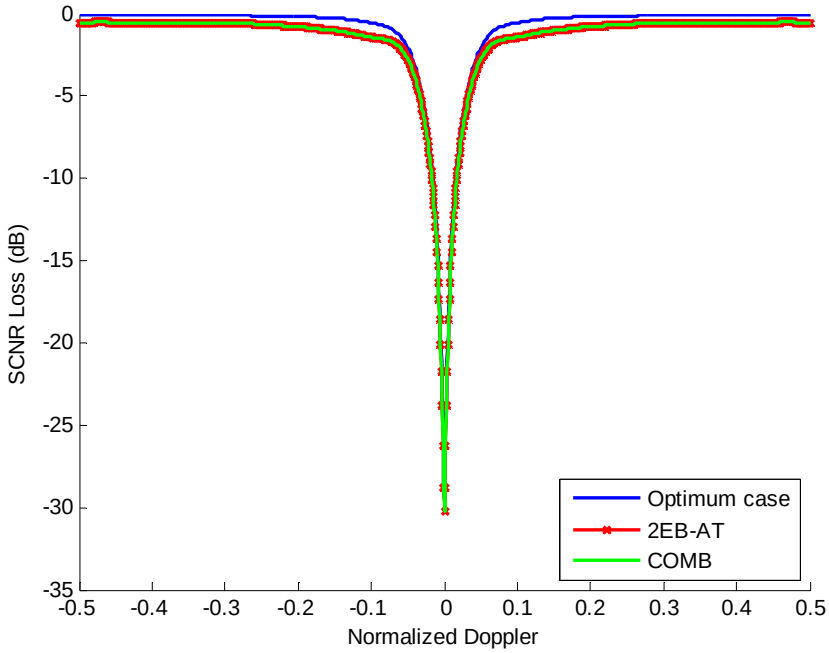

Figure 4-36 SCNR loss comparison in COMB case

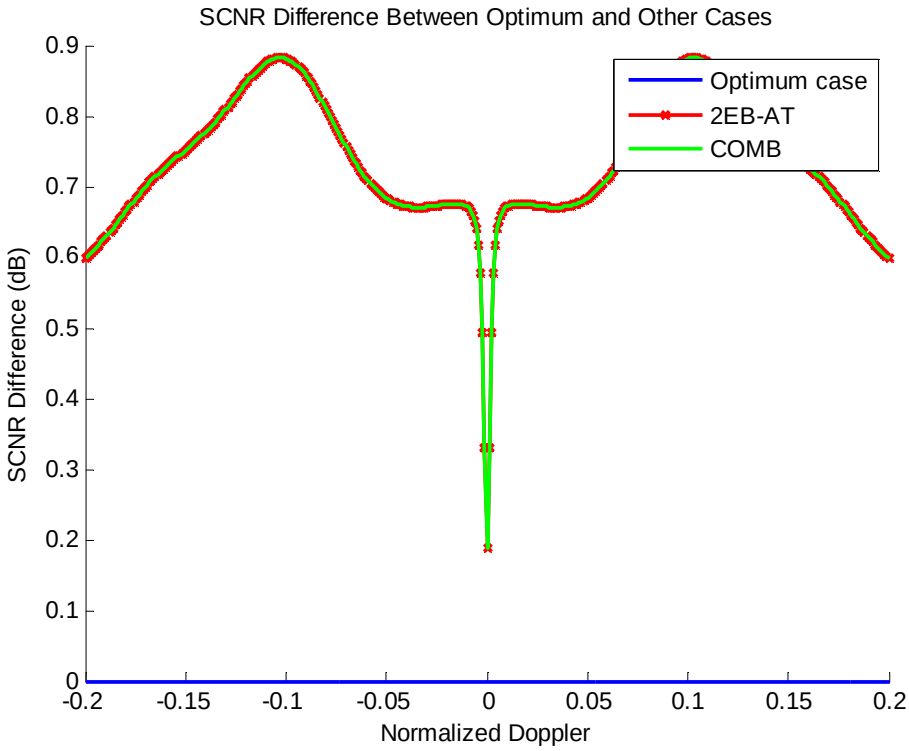

Figure 4-37 SCNR difference comparison in COMB case

As it is indicated in Figure 4-35, Figure 4-36 and Figure 4-37, as long as the constraints are satisfied, all combinations of eigen-beams give exactly the same performance.

Two eigen-beam case and combination case can be compared under non-ideal conditions in order to see whether there is a possible difference or not. Consider the case with 50^{o} rms phase error between channels. In addition, the covariance matrix is estimated from the data itself (SMI case).

The performances of the two eigen-beam and combination case are illustrated in Figure 4-38, Figure 4-39 and Figure 4-40:

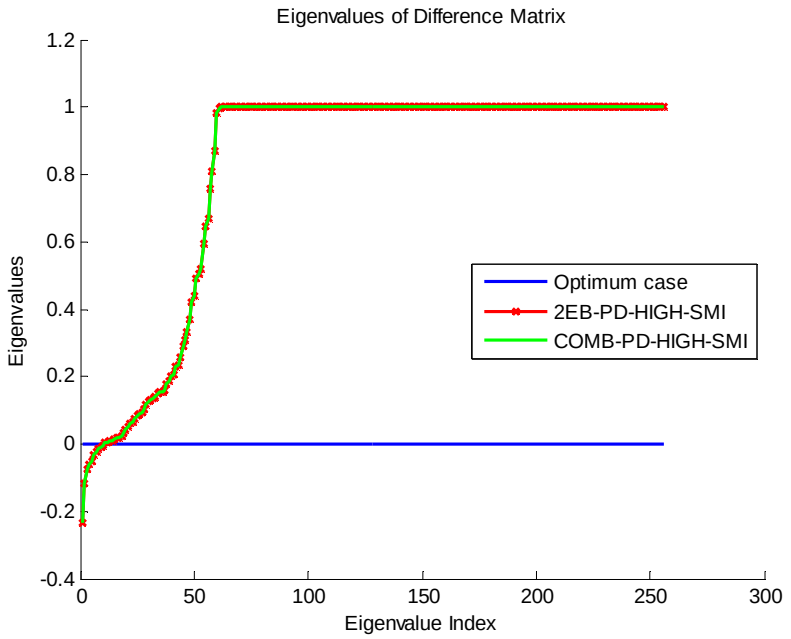

Figure 4-38 Difference matrix comparison under non-ideal conditions

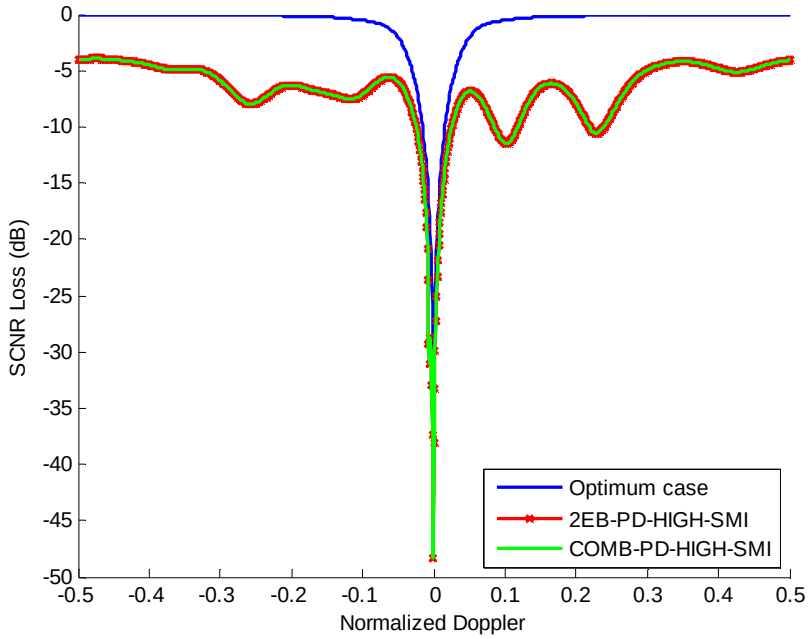

Figure 4-39 SCNR loss comparison under non-ideal conditions

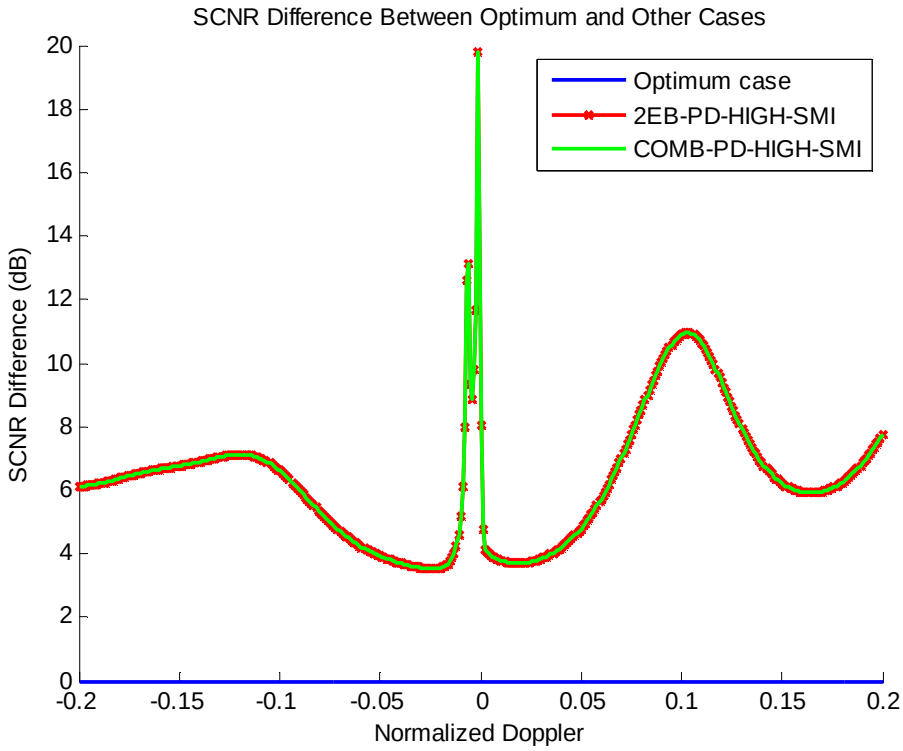

Figure 4-40 SCNR difference comparison under non-ideal conditions

It can be inferred from Figure 4-38, Figure 4-39 and Figure 4-40 that, even if there is a distortion in the receiver channels, the two cases give the same performance even under SMI case. This shows that any arbitrary combinations of eigen-beams give very similar performances under non-ideal circumstances.

CHAPTER 5

CONCLUSION

5.1. Thesis Summary

The objective of this thesis is to derive and propose two channel GMTI signal processing schemes which have good detection performances in the low Doppler (or velocity) region in Doppler spectrum, namely, endo-clutter detection.

For this purpose, basic radar detection and GMTI concepts were introduced. Then, widely used GMTI techniques are discussed in order to emphasize the necessity of developing an adaptive 2D signal processing scheme, which is space-time adaptive processing, to detect endo-clutter targets with a reasonable performance.

In order to understand the performance of STAP approach, signal and statistical models are investigated. These signal and statistical models are then used to determine the SCNR performance of optimum (full STAP) case. As far as the practical implementation issues and signal processing load of full STAP is concerned, the need of a reduced size detection problem is obvious. This need is satisfied by introducing reduced rank STAP, the types of rank reduction, comparison of rank reduction techniques and sub-space processing and eigen-beam concepts.

All the concepts that are introduced throughout the thesis are used in order to propose two eigen-beam technique, which has very similar performance

with full STAP especially in endo-clutter region. Then the performance of two eigen-beam technique is investigated under non-ideal conditions. Afterwards, the minimum number of eigen-beams needed to get satisfactory results is found to support the two eigen-beam approach. Finally, the non-uniqueness of two eigen-beam solution (in terms of detection performance) is emphasized by introducing the linear combination of two eigen-beams.

The main motivation of this thesis is to develop a practical GMTI technique, with two non-adaptive channel, but adaptive Doppler processing. Since the beam constitution (rank reduction) operation is not adaptive, we have to investigate good beam patterns which preserve the maximum amount of information about the full STAP case. By this way, it is aimed to have a good performance in challenging detection regions (slowly moving targets). It is imperative to suppress the clutter signals as much as it can be; thus, eigen-beam concept is introduced, which considers the statistical properties of the clutter in constituting the beams.

5.2. Future Work

Several topics regarding this subject can be investigated to further develop the concepts introduced here. These topics can be as follows:

1. Practical hardware issues concerning the beam-forming operations can be discussed
2. Further investigation of knowledge aided STAP to have an improvement on performance can be made
3. Similar analyses can be performed under non side looking radars

REFERENCES

[1] http://www.fact-archive.com/encyclopedia/History_of_radar, *Last Visited Date 27/06/2010*

[2] http://www.es.northropgrumman.com/solutions/f16aesaradar/assets/gmti.pdf, *Last Visited Date 27/06/2010*

[3] Defence Today, Land Warfare Special Edition, September/October 2006

[4] Richards, Mark A., Ph.D., "Fundamentals of Radar Signal Processing", *McGraw-Hill 2005*

[5] Guerci, J., R., "Space-Time Adaptive Processing for Radar", *Artech House 2003*

[6] Ward, J., "Space Time Adaptive Processing for Airborne Radar" , *Technical Report 1015, MIT Lincoln Laboratory, Lexington, MA, USA, 1998*

[7] Klemm, R., "Principles of Space-Time Adaptive Processing", *The Institution of Engineering and Technology 2006*

[8] Brennan, L. E., and F. M. Staudaher, "Subclutter Visibility Demonstration", *Technical Report RL-TR-92-21, Adaptive Sensors Inc., 1992.*

[9] Ward, J., "Space Time Adaptive Processing for Airborne Radar" , *Technical Report 1015, MIT Lincoln Laboratory, Lexington, MA, USA, 1994*

[10] http://en.wikipedia.org/wiki/Radar, *Last Visited Date 27/06/2010*

[11] Techau, P. M., J. S. Bergin, and J. R. Guerci, ‘‘Effects of Internal Clutter Motion
on STAP in a Heterogeneous Environment,’’ Proc. of 2001 IEEE Radar Conference, *May 2001*

[12] Zhou, S., Giannakis, G., B., “Optimal Transmitter Eigen-Beamforming and Space–Time Block Coding Based on Channel Correlations”, *IEEE Trans. Inf. Theory*, *49(7):1673-1690.*

[13] Teutsch, H., Kellermann, W., “Eigen-Beam Processing For Direction-Of-Arrival Estimation Using Spherical Apertures”, *In Conf. Rec. Joint Workshop for Hands-Free Speech Communication and Microphone Arrays (HSCMA), pages c13–c14, Piscataway, NJ, USA, March 2005.*

[14] Tanık, Y., “İki Anten Kullanan GMTI Performansı”, *ASELSAN Technical Report 2008*

APPENDIX A

DERIVATION OF CLUTTER COVARIANCE MATRIX

Remember that the total response received from i'th channel and in n'th pulse can be written as in (A-1):

$$c_{ni}(\theta) = c(\theta)G_T(\theta)\exp\left(-j2\pi f_D T_p n\right)\exp\left(j2\pi\phi_i\right), \tag{A-1}$$

$$c_{ni}(\theta) = c(\theta)G_T(\theta)\exp\left(-j\frac{2\pi}{\lambda}\left(2V_A T_p n - id\right)\sin(\theta)\right). \tag{A-2}$$

In (A-2), $c_{ni}(\theta)$ is the clutter return in n'th pulse in i'th channel. Covariance of any channel at any time instant can be found with an expectation operation which is shown in (A-3):

$$\mathbf{R}_{\mathbf{c}}(i+nK, m+kK) = E\left\{c_{ni}(\theta)c_{km}^{*}(\theta)\right\}. \tag{A-3}$$

$$\mathbf{R}_{\mathbf{c}}(i+nK, m+kK) = E\left\{\left|c(\theta)\right|^2\left|G_T(\theta)\right|^2\exp\left(-j\frac{2\pi}{\lambda}\left(2V_A T_p(n-k)-(i-m)d\right)\sin(\theta)\right)\right\} \tag{A-4}$$

$$\mathbf{R}_{\mathbf{c}}(i+nK, m+kK) = \int E\left\{\left|c(\theta)\right|^2\right\}\left|G_T(\theta)\right|^2\exp\left(-j\frac{2\pi}{\lambda}\left(2V_A T_p(n-k)-(i-m)d\right)\sin(\theta)\right)d\theta \tag{A-5}$$

In the equation (A-5), we can observe that the $i+nK$'th row and $m+kK$'th column of the covariance matrix of the clutter signal can be found with an expectation and integration operation. Consequently, covariance matrix can be written as in (A-8):

$$\sigma_c^2 = E\left\{ \left|c(\theta)\right|^2 \right\}, \tag{A-6}$$

$$\Delta x = V_A T_p \,, \tag{A-7}$$

$$\mathbf{R_c}\left(i+nK, m+kK\right) = \sigma_c^2 \int \left|G_T(\theta)\right|^2 \exp\left(- j2\pi \frac{2\Delta x(n-k) - (i-m)d}{\lambda} \sin(\theta) \right) d\theta \,. \tag{A-8}$$

σ_c^2 represents the clutter power provided that:

$$\int \left|G_T(\theta)\right|^2 d\theta = 1 \,. \tag{A-9}$$

APPENDIX B

DERIVATION OF OPTIMUM DETECTOR

Likelihood ratio of the hypotheses can be written as in (B-1).

$$\frac{p(\mathbf{r}\mid H_1)}{p(\mathbf{r}\mid H_0)}=\frac{\dfrac{1}{\pi^{KN}\left|\mathbf{R}+\sigma_t^2\mathbf{p}\mathbf{p}^{\mathbf{H}}\right|}\exp\left(-\dfrac{\mathbf{r}^H\left(\mathbf{R}+\sigma_t^2\mathbf{p}\mathbf{p}^{\mathbf{H}}\right)^{-1}\mathbf{r}}{2}\right)}{\dfrac{1}{\pi^{KN}\left|\mathbf{R}_{\mathbf{c}}+\sigma_n^2\mathbf{I}\right|}\exp\left(-\dfrac{\mathbf{r}^{\mathbf{H}}\mathbf{R}^{-1}\mathbf{r}}{2}\right)}\gtrless\xi, \tag{B-1}$$

$$\exp\left(-\frac{\mathbf{r}^H\left(\mathbf{R}+\sigma_t^2\mathbf{p}\mathbf{p}^{\mathbf{H}}\right)^{-1}\mathbf{r}}{2}+\frac{\mathbf{r}^{\mathbf{H}}\mathbf{R}^{-1}\mathbf{r}}{2}\right)\gtrless\xi', \tag{B-2}$$

$$-\mathbf{r}^H\left(\mathbf{R}+\sigma_t^2\mathbf{p}\mathbf{p}^{\mathbf{H}}\right)^{-1}\mathbf{r}+\mathbf{r}^{\mathbf{H}}\mathbf{R}^{-1}\mathbf{r}\gtrless\xi'' \tag{B-3}$$

Matrix inversion lemma can be written as in (B-4):

$$\left(\mathbf{R}+\sigma_t^2\mathbf{p}\mathbf{p}^{\mathbf{H}}\right)^{-1}=\mathbf{R}^{-1}-\frac{\sigma_t^2}{1+\sigma_t^2\mathbf{p}^{\mathbf{H}}\mathbf{R}^{-1}\mathbf{p}}\mathbf{R}^{-1}\mathbf{p}\mathbf{p}^{\mathbf{H}}\mathbf{R}^{-1}, \tag{B-4}$$

Using the matrix inversion lemma, the test will become as I (B-10):

$$-\mathbf{r}^H\left[\mathbf{R}^{-1}-\frac{\sigma_t^2}{1+\sigma_t^2\mathbf{p}^{\mathbf{H}}\mathbf{R}^{-1}\mathbf{p}}\mathbf{R}^{-1}\mathbf{p}\mathbf{p}^{\mathbf{H}}\mathbf{R}^{-1}\right]\mathbf{r}+\mathbf{r}^{\mathbf{H}}\mathbf{R}^{-1}\mathbf{r}\gtrless\xi'', \tag{B-5}$$

$$-\mathbf{r}^H\mathbf{R}^{-1}\mathbf{r}+\frac{\sigma_t^2}{1+\sigma_t^2\mathbf{p}^{\mathbf{H}}\mathbf{R}^{-1}\mathbf{p}}\left(\mathbf{r}^{\mathbf{H}}\mathbf{R}^{-1}\mathbf{p}\right)\left(\mathbf{p}^{\mathbf{H}}\mathbf{R}^{-1}\mathbf{r}\right)+\mathbf{r}^{\mathbf{H}}\mathbf{R}^{-1}\mathbf{r}\gtrless\xi'', \tag{B-6}$$

$$\frac{\sigma_t^2}{1+\sigma_t^2\mathbf{p}^{\mathbf{H}}\mathbf{R}^{-1}\mathbf{p}}\left(\mathbf{r}^{\mathbf{H}}\mathbf{R}^{-1}\mathbf{p}\right)\left(\mathbf{p}^{\mathbf{H}}\mathbf{R}^{-1}\mathbf{r}\right)\gtrless\xi'', \tag{B-7}$$

$$\left|\mathbf{p}^{\mathbf{H}}\mathbf{R}^{-1}\mathbf{r}\right|^2 \gtrless \xi''', \tag{B-8}$$

$$\mathbf{w}^{\mathbf{H}} = \mathbf{p}^{\mathbf{H}}\mathbf{R}^{-1}, \tag{B-9}$$

$$\left|\mathbf{w}^{\mathbf{H}}\mathbf{r}\right|^2 \gtrless \xi'''. \tag{B-10}$$

APPENDIX C

DERIVATION OF SCNR EQUATION AND SCNR BOUND

In order to find signal-to-clutter plus noise ratio after the weighting operation, we have to write the SCNR equation after weighting as in (C-1):

$$SCNR = \frac{E\left\{ \left\| \mathbf{w}^{\mathbf{H}} \alpha \mathbf{p} \right\|^2 \right\}}{E\left\{ \left\| \mathbf{w}^{\mathbf{H}} \mathbf{c} \right\|^2 \right\} + E\left\{ \left\| \mathbf{w}^{\mathbf{H}} \mathbf{n} \right\|^2 \right\}}, \tag{C-1}$$

$$SCNR = \frac{\sigma_t^2 \left| \mathbf{w}^{\mathbf{H}} \mathbf{p} \right|^2}{E\left\{ \mathbf{w}^{\mathbf{H}} \mathbf{c}\mathbf{c}^{\mathbf{H}} \mathbf{w} \right\} + E\left\{ \mathbf{w}^{\mathbf{H}} \mathbf{n}\mathbf{n}^{\mathbf{H}} \mathbf{w} \right\}}, \tag{C-2}$$

$$SCNR = \frac{\sigma_t^2 \left| \mathbf{w}^{\mathbf{H}} \mathbf{p} \right|^2}{\mathbf{w}^{\mathbf{H}} E\left\{ \mathbf{c}\mathbf{c}^{\mathbf{H}} \right\} \mathbf{w} + \mathbf{w}^{\mathbf{H}} E\left\{ \mathbf{n}\mathbf{n}^{\mathbf{H}} \right\} \mathbf{w}}, \tag{C-3}$$

$$SCNR = \frac{\sigma_t^2 \left| \mathbf{w}^{\mathbf{H}} \mathbf{p} \right|^2}{\mathbf{w}^{\mathbf{H}} \mathbf{R}_{\mathbf{c}} \mathbf{w} + \mathbf{w}^{\mathbf{H}} \sigma_n^2 \mathbf{I} \mathbf{w}}, \tag{C-4}$$

$$SCNR = \frac{\sigma_t^2 \left| \mathbf{w}^{\mathbf{H}} \mathbf{p} \right|^2}{\mathbf{w}^{\mathbf{H}} \mathbf{R} \mathbf{w}}. \tag{C-5}$$

Here (C-5) represents the SCNR value after processing the received data with weight vector $\mathbf{w}$. We can manipulate (C-5) in order to find a bound to SCNR, using Schwarz inequality:

$$SCNR = \frac{\sigma_t^2 \left| \mathbf{w}^{\mathbf{H}} \mathbf{p} \right|^2}{\mathbf{w}^{\mathbf{H}} \mathbf{R} \mathbf{w}}, \tag{C-6}$$

$$SCNR = \frac{\sigma_t^2 \left| \mathbf{w}^{\mathbf{H}} \mathbf{R}^{1/2} \mathbf{R}^{-1/2} \mathbf{p} \right|^2}{\mathbf{w}^{\mathbf{H}} \mathbf{R} \mathbf{w}}, \tag{C-7}$$

$$SCNR \le \frac{\sigma_t^2 \left\| \mathbf{w}^{\mathbf{H}} \mathbf{R}^{1/2} \right\|^2 \left\| \mathbf{R}^{-1/2} \mathbf{p} \right\|^2}{\mathbf{w}^{\mathbf{H}} \mathbf{R} \mathbf{w}}, \tag{C-8}$$

$$SCNR \le \frac{\sigma_t^2 \left(\mathbf{w}^{\mathbf{H}} \mathbf{R} \mathbf{w} \right) \left(\mathbf{p}^{\mathbf{H}} \mathbf{R}^{-1} \mathbf{p} \right)}{\mathbf{w}^{\mathbf{H}} \mathbf{R} \mathbf{w}}, \tag{C-9}$$

$$SCNR \le \sigma_t^2 \mathbf{p}^{\mathbf{H}} \mathbf{R}^{-1} \mathbf{p} . \tag{C-10}$$

Eqn. (C-10) represents the SCNR bound that can be achieved by optimum STAP technique.

APPENDIX D

DERIVATION OF DIFFERENCE MATRIX OF ONE PULSE CASE

The difference matrix of the one pulse case (N=1) can be found as in

$$\mathbf{R}_{\mathbf{difference}} = \left(\mathbf{R}_{\mathbf{c}} + \sigma_n^2\mathbf{I}\right)^{-1} - \mathbf{B}\left(\mathbf{B}^{\mathbf{H}}\mathbf{R}_{\mathbf{c}}\mathbf{B} + \sigma_n^2\mathbf{I}\right)^{-1}\mathbf{B}^{\mathbf{H}}, \tag{D-1}$$

$$\mathbf{R}_{\mathbf{difference}} = \left(\mathbf{R}_{\mathbf{c}} + \sigma_n^2\mathbf{I}\right)^{-1} - \mathbf{B}\left(\mathbf{B}^{\mathbf{H}}\mathbf{R}_{\mathbf{c}}\mathbf{B} + \sigma_n^2\mathbf{B}^{\mathbf{H}}\mathbf{I}\mathbf{B}\right)^{-1}\mathbf{B}^{\mathbf{H}}, \tag{D-2}$$

$$\mathbf{R}_{\mathbf{difference}} = \left(\mathbf{R}_{\mathbf{c}} + \sigma_n^2\mathbf{I}\right)^{-1} - \mathbf{B}\left(\mathbf{B}^{\mathbf{H}}\left(\mathbf{R}_{\mathbf{c}} + \sigma_n^2\mathbf{I}\right)\mathbf{B}\right)^{-1}\mathbf{B}^{\mathbf{H}}, \tag{D-3}$$

$$\mathbf{R}_{\mathbf{difference}} = \sum_{i=1}^{K}\frac{1}{\lambda_i}\mathbf{e_i}\mathbf{e_i^H} - \mathbf{B}\left(\mathbf{B}^{\mathbf{H}}\sum_{i=1}^{K}\lambda_i\mathbf{e_i}\mathbf{e_i^H}\mathbf{B}\right)^{-1}\mathbf{B}^{\mathbf{H}}, \tag{D-4}$$

$$\mathbf{R}_{\mathbf{difference}} = \sum_{i=1}^{K}\frac{1}{\lambda_i}\mathbf{e_i}\mathbf{e_i^H} - \mathbf{B}\left(\begin{bmatrix}\lambda_1 & 0\\ 0 & \lambda_2\end{bmatrix}\right)^{-1}\mathbf{B}^{\mathbf{H}}, \tag{D-5}$$

$$\mathbf{R}_{\mathbf{difference}} = \sum_{i=1}^{K}\frac{1}{\lambda_i}\mathbf{e_i}\mathbf{e_i^H} - \mathbf{B}\begin{bmatrix}1/\lambda_1 & 0\\ 0 & 1/\lambda_2\end{bmatrix}\mathbf{B}^{\mathbf{H}}, \tag{D-6}$$

$$\mathbf{R}_{\mathbf{difference}} = \sum_{i=1}^{K}\frac{1}{\lambda_i}\mathbf{e_i}\mathbf{e_i^H} - \frac{1}{\lambda_1}\mathbf{e_1}\mathbf{e_1^H} - \frac{1}{\lambda_2}\mathbf{e_2}\mathbf{e_2^H}, \tag{D-7}$$

$$\mathbf{R}_{\mathbf{difference}} = \sum_{i=3}^{K}\frac{1}{\lambda_i}\mathbf{e_i}\mathbf{e_i^H}\ . \tag{D-8}$$